Investigation of Solar Powered Enhanced Evaporative Cooling System for Vegetables Warehouse Air-conditioning Application

Fitala Bula Godana

A Thesis Submitted to the Department of Mechanical Engineering

School of Mechanical, Chemical and Materials Engineering

Presented in Partial Fulfillment of the Requirement for the Degree of Master of Science in Thermal Engineering

Office of Graduate Studies

Adama Science and Technology University

November, 2022

Adama, Ethiopia

Investigation of Solar Powered Enhanced Evaporative Cooling System for Vegetables Warehouse Air-conditioning Application

Fitala Bula Godana

Advisor**:** Dr. Addisu Bekele

A Thesis Submitted to the Department of Mechanical Engineering

School of Mechanical, Chemical and Materials Engineering

Presented in Partial Fulfillment of the Requirement for the Degree of Master of Science in Thermal Engineering

November, 2022

Adama, Ethiopia

Declaration

I hereby declare that this Master Thesis entitled "Investigation of Solar Powered Enhanced Evaporative Cooling System for Vegetables Warehouse Air-conditioning Application" is my original work. That is, it has not been submitted for the award of any academic degree, diploma or certificate in any other university. All sources of materials that are used for this thesis have been duly acknowledged through citation.

Fitala Bula Godana	________________________	____________________
Name of student	Signature	Date

Recommendation

I, the advisor of this thesis, hereby certify that I have read the revised version of the thesis entitled “Investigation of Solar Powered Enhanced Evaporative Cooling System for Vegetables Warehouse Air-conditioning Application” prepared under my guidance by Fitala Bula Godana submitted in partial fulfillment of the requirements for the degree of Mater of Science in Thermal Engineering. Therefore, I recommend the submission of revised version of the thesis to the department following the applicable procedures.

Major Advisor	Signature	Date

Approval Page of M.Sc. Thesis

I, the advisor of the thesis entitled "Investigation of Solar Powered Enhanced Evaporative Cooling System for Vegetables Warehouse Air-conditioning Application" and developed by Fitala Bula Godana hereby certify that the recommendation and suggestions made by the board of examiners are appropriately incorporated into the final version of the thesis.

____________________	________________	____________
Major Advisor	Signature	Date

We, the undersigned, members of the Board of Examiners of the thesis by Fitala Bula Godana have read and evaluated the thesis entitled "Investigation of Solar Powered Enhanced Evaporative Cooling System for Vegetables Warehouse Air-conditioning Application" and examined the candidate during open defense. This is, therefore, to certify that the thesis is accepted for partial fulfillment of the requirement of the degree of Master of Science in Thermal Engineering.

____________________	________________	____________
Chairperson	Signature	Date
____________________	________________	____________
Internal Examiner	Signature	Date
____________________	________________	____________
External Examiner	Signature	Date

Finally, approval and acceptance of the thesis is contingent upon submission of its final copy to the Office of Postgraduate Studies (OPGS) through the Department Graduate Council (DGC) and School Graduate Committee (SGC).

____________________	________________	____________
Department Head	Signature	Date
____________________	________________	____________
School Dean	Signature	Date
____________________	________________	____________
Office of Postgraduate Studies, Dean	Signature	Date

ACKNOWLEDGMENT

First, I would like to thank the almighty God, for giving me the commitment and courage to Passover different obstacles and challenges and to come up with the accomplishment of this thesis work. Next and for most, I would like to thank and express my deepest gratitude to my advisor, **Dr. Addisu Bekele (Associate Professor, Mechanical Engineering Department)** for his valuable and tireless advices, encourage and great motivation throughout my thesis work. In addition, I would like to express my gratitude to **Dr. Gezhagn H and Dr. Dawit G**, for their unforgettable support during the past two year. I also thanks my family for their continuous support and supervision to make me courageous, patient and be successful in my work. My deepest gratitude also extended to my friends and all those beside me by idea and supporting me for the accomplishment of my work.

ABSTRACT

Vegetables are perishable crops, which have high moisture content. The central rift-valley is an areas which the vegetables produced widely in Ethiopia. The high moisture content nature of the vegetables results high post-harvest losses in the absence of proper storage condition. Most of research and review show that in Ethiopia, the post-harvest loss of vegetables is approximates 50 to 70%. This results a huge income losses to farmers and increases of produces price on the market, which causes the increase of poverty rate in the country. In order to reduce postharvest loss of vegetables the roles of low cost evaporative cooling storage technology is great. In this investigation, an appropriate configuration of evaporative cooling system that enhanced by solid-desiccant pre-dehumidifier and Maisotsenko-cycle pre-cooler were developed for the storage of tomato produces harvested from 2.1 hectare . The performances of each unit of the system were analyzed by developing their respective mathematical models. SIMPLE algorithm were used to solve and simulate the mathematical model of the storage room. For all developed model, a general MATLAB code program is developed. It can be found that the maximum outlet temperature glycol from manifold is 139ºC and obtained at 0.012kg/s. To substitute the gap during night time mass of 236 kg of Erytriol are required. The storage tank has a capability of storing thermal energy for 5 hour. The wet bulb and dew point effectiveness of the M-cycle attained were 1.43 and 0.76 respectively. The system can achieve the required storage and humidity level of 12.5 to 20ºC and 83% respectively within 2 hour of operation.

***Key word**: Enhanced Evaporative Cooling, Desiccant coated heat exchanger, Maisotsenko-cycle, Phase Change Material, Evacuated Tube Solar Collector.*

TABLE OF CONTENTS

LIST OF TABLES

LIST OF FIGURES

ABBREVIATION

Abbreviation	*Description*
PHL	*Post-Harvest loss*
SSA	*Sub-Saharan Africa*
ECSA	*Ethiopian Central Statistics Agency*
DC	*Desiccant Cooling*
DEC	*Direct Evaporative Cooling*
IEC	*Indirect Evaporative Cooling*
SDC	*Solid Desiccant Cooling*
LDC	*Liquid Desiccant Cooling*
HME	*Heat and mass exchangers*
FAO	*Food and agricultural organization*
RH	*Relative Humidity*
EC	*Evaporative Cooling*
PVP	*Photo Voltaic Panel*
ECT	*Evaporative Cooling Technology*
COP	*Coefficient of Performances*
DCHE	*Desiccant Coated Heat Exchangers*
TES	*Thermal Energy Storage*
HPETSC	*Heat Pipe Evacuated Tube Solar Collector*
GDP	*Growth and Developmental Plan*
M-cycle	*Maisotsenko-cycle*
PCM	*Phase Change Material*
HTF	*Heat Transfer Tube*
LMTD	*Logarithmic Mean Temperature Difference*
FPC	*Flat Plate Collector*
PTC	*Parabolic Trough Collector*
CW	*Cold water*
HW	*Hot water*

NOMENCLATURE

Symbol	***Description***	***Units***
$\dot{m}$	*Mass flow rate*	*kg/s*
v	*Velocity*	*m/s*
u	*x-component velocity*	*m/s*
T	*Temperature*	*ºC*
k	*Thermal conductivity*	*W/m.K*
c	*Specific heat capacity*	*kJ/kg.K*
Q	*Heat transfer*	*W*
U	*Overall heat transfer coefficient*	$W/m^2.^oC$
h	*Convective heat transfer coefficient*	$W/m^2.K$
P	*Pressures*	*Pa*
A	*Area*	m^2
I_{SC}	*Solar constant*	W/m^2
H	*Global daily radiation*	W/m^2
H_O	*Extraterrestrial radiation*	W/m^2
H_D	*Diffused daily radiation*	W/m^2
H_B	*Beam daily radiation*	W/m^2
I	*Global hourly radiation*	W/m^2
I_B	*Beam hourly radiation*	W/m^2
I_D	*Diffused hourly radiation*	W/m^2
V	*Volume*	m^3
N_u	*Nusslet number*	-
R_e	*Reynold's number*	-
g	*Gravity*	m/s^2
D	*Diameter*	*m*
L	*Length*	*m*
R	*Heat transfer resistance*	*K/W*
h_{fg}	*Latent heat of fusion*	*kJ/kg*
P_r	*Prandtl number*	m^2/s
N_s	*Daylight length*	*hr*
n_s	*Sunshine hour*	*hr*

GREEK SYMBOLS

Symbols	***Description***	***Units***
ρ	*Density*	kg/m^3
δ	*Declination angle*	^{o}
ϕ	*Latitude*	^{o}
β	*Slope*	^{o}
θ	*Incident angle*	^{o}
θ_Z	*Zenith angle*	^{o}
ω	*Hour angle*	^{o}
σ	*Stefan-Boltzmann constant*	$W/(m^2.K^2)$
μ	*Dynamic viscosity*	*m.s*
ε	*Emissivity*	-
τ	*Transmissivity*	-
α	*Thermal absorptivity*	-
ϵ	*porosity*	*%*
η	*Efficiency*	*%*

SUBSCRIPTS

Subscripts	***Description***
in	*Inlet*
out	*Outlet*
con	*Condenser*
ev	*Evaporator*
g	*Glass*
ab	*Absorber*
w	*Water*
f	*Fluid*
v	*Vapor*
man	*Manifold*
amb	*Ambient*

CHAPTER ONE

INTRODUCTION

1.1 Background of Study

Agriculture is the crucial sector that feed the world and the economy of many country relied on. In Ethiopia, about 84 percent of the country's population engaged in various agricultural activities and high shares of country foreign currency is generated by export of agricultural commodities, which contributes about 42 percent to the country's GDP (growth and developmental plan) (Cochrane & Bekele, 2018). Meki is the study area of this research, which located in the central rift-valley part of Ethiopia. It is a major production area of vegetables (tomato, onion, cabbage and pepper) in the country (Limeneh, 2021).

The main problems that greatly threaten the food security and affect the quantity and nutritional value of the produce is the post-harvest loss (PHL). According to FAO (food and agricultural organization) study, globally each year around 1.3 billion ton of food produced is lost due to post-harvest loss. In Ethiopia the post-harvest losses of horticultural crops is estimated about 15-70% (Urge et al., 2014).

Spoilage due to improper storage of the produce is the main factors that results the post-harvest loss in vegetables. It occurred when the produce stored in uncontrolled temperature and relative humidity condition. In order to preserve the produce for a long period of time and reduce the caused PHL, the produce have to store in a conditioned or controlled atmosphere space. High temperature increase, the chemical reaction inside the produce which shorten the shelf life of the produces. High relative humidity in high temperature condition favor the growth of mold rot for some produce and low humidity condition may result shrink, wrinkle and flaccid due to dehydration in some produce (Kiaya, 2014). An optimum storage temperature range for tomato and cabbage is 13-15ºC and 0-2ºC respectively. And, an optimum storage relative humidity (RH) tomato and cabbage is 85%-90% and 90%-95% respectively (Gross et al., 2016). But, the mean daily maximum temperature of the selected study are (Meki) ranges between 25-29 ºC and the relative humidity varies between 46-79% (Haile et al., 2020).

The adoption of cost-effective and energy efficient storage technology is required for preserving quality, extending shelf life and reducing postharvest losses of perishable horticultural produce. Among these technologies, evaporative cooling (EC) is an efficient and economical technology for reducing temperature and increasing the relative humidity of a given space, through the evaporation process of water (Venu, 2016). The performance of the evaporative cooling is greatly affected by the amount of relative humidity of ambient air. For better performances; an ambient air with relative humidity below 30% is recommended (El-Dessouky et al., 2000). This implies without any enhancement an evaporative cooling can performs better in hot and dry air condition. To extent the application of evaporative cooling in hot and humid ambient condition, evaporative cooling can be enhanced by desiccant system to pre-dry the supply air before entering the evaporative cooling system and by advanced indirect evaporative cooling (Maisotsenko-cycle) to maximize the cooling effects of the system (Lai et al., 2021).

The desiccant system remove the moisture of air through the strong water vapor attraction property of the desiccant material. It can be classified as solid and liquid desiccant system, based on the type of desiccant material used. As compared to liquid desiccant, the solid desiccant has a higher water adsorption rate, simpler structure and no carry-over (Misha. S, 2012). The widely used desiccant materials are silica gel, zeolites, alumina, hydratable salts and mixtures. For most studies, silica gel was selected as the adsorbent material of solid desiccant system due to its thermo-physical properties (Lai et al., 2021). The solid desiccant need the regeneration temperature of 75 to 120ºC and this temperature range delivered by evacuated tube collector that delivering temperature in the range of 100 to 150°C (Alazazmeh & Mokheimer, 2015). Maisotsenko-cycle decrease the minimum temperature from wet-bulb temperature to the dew temperature of the intake air without extra moisture addition into the supply air (Dizaji et al., 2020). Based on the configuration solid desiccant further classified as fixed bed, rotary wheel and desiccant coated heat exchangers (DCHE). In evaporative cooling enhancement by solid desiccant dehumidification, rotary wheel was the most researched types. However, the main drawn back of rotary wheel that used in the solid-desiccant dehumidification was the large wheel size which requires huge electric power to drive it and this limit its application in an area were the access of electricity is scarce. DCHE is the type of heat exchanger were the desiccant material is uniformly and stably coated on the external surface by coating technology and the cooling fluid flows through the tubes (Vivekh et al., 2018). When compared to rotary wheel, DCHE had higher dehumidification performances and need less electric power due to there is no large size moving or rotating parts. Therefore it is possible to apply the enhanced evaporative cooling for storage of vegetable at farm were the access of electricity is limited by using DCHE instead of rotary wheel used in solid desiccant dehumidification. Hence, this research investigated the performance of enhanced evaporative cooling system, for the storage vegetables at farm that produced around Meki.

1.2 Statement of Problem

The post-harvest loss (PHL) is the main challenges to the development and productivity of this sector and it is estimated about 15-70% of the total production of the produce. This affected greatly the income of the producers and economy of the country by resulting both the quantity and quality loss to the produce. Even if there are many factors contributing for the occurrence of PHL, the main causes of PHL is lack of storage and cooling facilities at the farm that used to pre-cool and store the produce before supplied to the market.

If the storage and cooling were used by the producers (farmers), it helps to preserve the produce during supply of the produces for market is difficult (due to lack and difficulties of transportation service) and during the market price fall (to minimize the farmer's income loss) and ensure the constant supply and availability of the produce throughout the year.

In the selected study area (Meki) there is no cooling and storage facilities used and available at farm. Because, the farmers do not afford the available commercial cooling technologies; due to their financial limitation and even they afford it, the usage of these technologies at the farm is difficult due to there is no electricity (power source of this technology) supply system in countryside were the farm located. Hence, evaporative cooling system is the promising cooling and air conditioning technology that control the relative humidity and temperature of process air separately and this study is aimed to investigate the performance of an enhanced evaporative cooling system in order to preserve the vegetables produce at the farm by managing the temperature and relative humidity storage house and reduce the effects of post-harvest loss discussed above.

1.3 General and Specific Objectives

1.3.1 General objective

The main objective of this research is to investigate solar powered enhanced Evaporative cooling system performances, for air-conditioning of vegetables storage warehouse.

1.3.2 Specific objective

The specific objectives are to:

- Investigate the thermal energy demand required by enhanced evaporative cooling system to store 60,480kg of tomatoes.

- Select and size the heat pipe evacuated tube solar thermal collector which required to supply the regeneration temperature ranges of 70 to 110 ºC.
- Select and design the PCM thermal energy storage which required to store and supply the thermal energy during night.
- Investigate numerically the thermal performance of the enhanced evaporative cooling system using SIMPLE algorithm.

1.4 Significance of Study

This study will provide a numerical approach of analyzing the solar powered evaporative cooling, for the application of precooling and storing the vegetable produce whose storage temperature ranges between 12 to 21 º C. By this the post-harvest loss were greatly reduced and have a contribution to the achievement of national food security program and decreasing of the poverty rate in the country. The result of this study can be used as reference for the further improving of the system performances and design.

1.5 Scope and Limitation of Study

This research covers only the numerical analysis and simulation of enhanced evaporative cooling for air-conditioning of tomato storage warehouse in Meki. The performances of evacuated tube, thermal storage and each unit of the cooling system were analyzed. However, this study did not validate the numerical analysis with experimental.

CHAPTER TWO

LITERATURE REVIEW

2.1 Introduction

The main aim of this review is to give the general clue about the previous work done by different scholars; regarding the solar powered cooling system in general and the enhanced evaporative cooling system in specific; in which their application are for the storage of agricultural product (vegetables). In this review, the vegetables potential's Ethiopia has, the availability of solar energy potential of the country, the causes and effects of vegetables post-harvest loss (PHL) and the available solar cooling system are discussed in reference of the social, economic and political aspect of the country.

2.2 Overview of Vegetables Production

Ethiopia has a potential for the production of tropical, sub-tropical and temperate fruit and vegetables; as the climate of the country is favorable for the growth of such vegetable. In addition to favorable climate condition the country has; the high availability of water resources in the country create the favorable condition for the sustainable production of fruit and vegetables. Among the water resources the country has and used for irrigation purpose, rift valley lakes such as Danbal, and Koka; and rivers such as Abay and awash basin are the well-known one.

From vegetable category, tomato is a widely grown vegetable crop in Ethiopia, in which its area coverage and production was 4953 ha and 6.2 ton per ha respectively. Meki scheme showed the highest land productivity for tomato with the magnitude of 10.29 tons/ha (Haileslassie et al., 2016). Oromia is developing the Koka and Meki horticulture farming clusters (Wondim, 2021).

2.2.1 Post-harvest Losses in Vegetables

Post-harvest loss occurs at different stage from production to the consumption process. According to FAO study, globally each year around 1.3 billion ton of food produced is lost due to post-harvest loss (Ayandiji et al, 2011). In SSA (sub-Saharan Africa) the losses of produces at production and storage stage constitute the high portion of post-harvest loss. In Ethiopia this loss ranges between 15 to 70%.

Abera et al. (2020) assessed the post-harvest losses of tomato in selected districts of East Shewa Zone of Ethiopia using a commodity system analysis. From the assessment, an estimated post-harvest loss of tomato in this study area at different chain was 39.31% and poor post-harvest handling, storage and transportation system are the key constraints for this significant loss.

Therefore, when the postharvest losses was reduced by 50%, food availability would be increased by 20% without cultivating an additional hectare of land for increasing crop yield (Ayandiji et al, 2011).

2.2.2 Thermo-physical properties

The thermo-physical properties of the produce must be known to perform the various heat transfer calculations involved in designing of cold storage. These properties include density, specific heat, enthalpy, thermal conductivity, heat of respiration, rate of transpiration and thermal diffusivity and they presented in Table 2.1.

Table 2.1 Thermo-physical properties of tomatoes (ASHRAE, 2006)

Thermo-physical properties	Food Components	Food Component mass fraction (x)	Food Components thermal properties	Thermal properties of tomatoes
Thermal conductivity W/(m.k)	Water	0.93	0.605146212	0.567356227
	Protein	0.012	0.20272325	
	Fat	0.002	0.122663327	
	Carbohydrate	0.051	0.225743641	
	Fiber	0.011	0.20815648	
	Ash	0.005	0.357761157	
Specific heat,KJ/(kg.k)	Water	0.93	4.129405493	3.976084788
	Protein	0.012	2.033007911	
	Fat	0.002	2.013022147	
	Carbohydrate	0.051	1.587393004	
	Fiber	0.011	1.882291553	
	Ash	0.005	1.13065797	
Thermal diffusivity				0.00014097
Heat of respiration, W/kg				0.100703675

2.2.3 Storage condition of vegetables

Fresh vegetables those harvested from plant is the living tissues. However, as time goes they continue to ripen as the result of respiration and transpiration. This process finally takes them to cellular breakdown and senescence which called spoilage of vegetables. Such kind of vegetables spoilage is the main factors that results the post-harvest loss of fruit and vegetables. Even if the senescence of such produce is inevitable, it is possible to lengthen the life time by controlling some parameter in which the produce stored in.

The temperature and relative humidity of the fruit and vegetables storage are the two main factors which affects the life time of fresh fruit and vegetables. As the temperature increase, the chemical reaction inside the produce increases, which shorten the shelf life of the produce. Similarly, fresh fruit and vegetables has high moisture content; due to this they should have to store in high relative humidity condition. When they subjected to low relative humidity storage condition, they loss the moisture content and become wilt (Kiaya, 2014). Therefore, each produce needs an appropriate storage temperature and relative humidity to lengthen its shelf life and these ranges where summarized in Table 2.2.

Table 2.2 Storage temperature and relative humidity of different horticulture produce (ASHRAE, 2006)

Horticulture	Temperature range (^{o}C)	Relative humidity (%)
Apples	0-2	90-95
Orange	0-2	90-95
Cabbage	0-2	90-95
Carrot	0-2	90-95
Onion	0-2	65-75
Garlic	0-2	65-75
Lemon	4-5	90-95
Peppers	10-12	85-90
Potatoes	10-12	85-90
Avocado	13-15	85-90
Bananas	13-15	85-90
Papayas	13-15	85-90
Mangos	13-15	85-90
Tomatoes	13-15	85-90
Water melon	18-21	85-90

2.3 Solar Powered Cooling Technologies

Out of different energy sources that this world relied on, solar energy is the renewable energy sources that freely available on most part of the world. Different technologies where developed for the utilization of this renewable energy. Out of this technologies, solar power cooling technologies are the well-known technologies and attract the attention of the many researchers. Based on the kind of energy used to drive them, there are two types of solar cooling systems. These are, solar thermal cooling system and solar electric cooling system. In solar thermal cooling system, the thermal energy directly collected by solar collector drives the cooling system. In case of solar electric cooling system, the electric energy that is generated by solar photovoltaic panel (PVP) drives the cooling system. These two technology used both in domestic and industrial for the purpose of refrigeration and air-conditioning, thus saving 95% of (Khalid et al., 2009)

2.3.1 Desiccant cooling system

Air can be dehumidified either by cooling it below its dew point temperature and then removing moisture by condensation, or by sorption process using a desiccant material, in which the desiccant removes the moisture from the air (by adsorption process). The dried warm air can be cooled to desired temperature level by another auxiliary cooling system such as evaporative cooler and cooling coil. During adsorption process, the desiccant releases heat and warms the air. If this generated heat removed properly, then the dehumidification process is an isothermal-dehumidification otherwise it can be an isenthalpic-dehumidification. For the next cycle, the moisture adsorbed by desiccant was removed from desiccant (by desorption process). During desorption process, an absorbed moisture is released to outside by increasing the temperature of the desiccant using heat from an energy source such as electricity, waste heat, or solar energy.

Daou et al. (2006) reviewed the desiccant cooling air conditioning system and have found that one of the most significant advantages of desiccant cooling systems is the possibility of their regeneration by free energy such as waste and solar, without any conversion.

Gagliano et al. (2014) investigated the performance of a solar Assisted Desiccant Cooling System and found that the desiccant technology is about 40% more energy saver and it saves about 150% energy than the conventional vapor compression system.

Alahmer et al. (2018) investigated solar cooling technologies. The investigation found that the solid desiccant system is a non-corrosive technology with low maintenance. However liquid desiccant technology dominates over solid desiccant technology in terms of COP.

Dezfouli et al. (2014) investigated a comparison study among four configurations of a solar desiccant cooling system in the hot and humid weather in Malaysia. These configurations are the one-stage ventilation, one-stage recirculation, two-stage ventilation, and two-stage recirculation. Among these configuration, two-stage ventilation has higher COP (coefficient of performances) and produced lower supply air temperature.

Chaudhary et al. (2018) experimentally investigated an integrated solar assisted desiccant cooling system. The result reveals that the dehumidification effectiveness is significantly dropped with rise in inlet temperature and positively affected by increase in the inlet humidity.

Lai et al. (2021) reviewed an evaporative cooling integrated with solid desiccant systems and founds that a two-stage desiccant arrangement has been proven to be able to improve the dehumidification performance with a lower regeneration temperature. And also developing novel desiccant material with a high water adsorption rate and lower regeneration temperature requirement, and adopting internally cooled desiccant wheel arrangement are effective for improving solid desiccant unit performance.

Misha et al. (2012) carried out the reviews on solid/liquid desiccant in drying application and its regeneration methods. From the reviews the desiccant system in drying application has several advantages including continuous drying even during off-sunshine hours, increased drying rate due to hot and dry air, more uniform drying, and increased product quality especially for heat sensitive products.

Narayanan et al. (2011) done comparative study on different desiccant wheel designs. Results shows that at the selected design conditions, the percentage dehumidification rate of parallel flow, simple counter flow and counter flow with cooling section are 16.27% 25.05% and 29.77% respectively. As the results reveal, counter flow desiccant wheel has much better dehumidification performance than parallel flow, whereas the addition of axial cooling section can improve both dehumidification and cooling performance further.

There are two types of desiccant cooling system based on the type of desiccant type they used. These are, solid desiccant and liquid desiccant cooling system, thus uses solid and liquid type of desiccant respectively. According to the configuration solid desiccant further classified as fixed bed, rotary wheel and desiccant coated heat exchangers (DCHE).

A rotary desiccant wheel is advantageous as it can supply air with uniform humidity at the outlet due to continuous rotation can be provided. The main drawn back of this wheel are the large pressure drop due to the complex structure of the desiccant felts, large wheel size which requires huge electric power to drive it and severe noise and less compactness resulted due to rotating wheels.

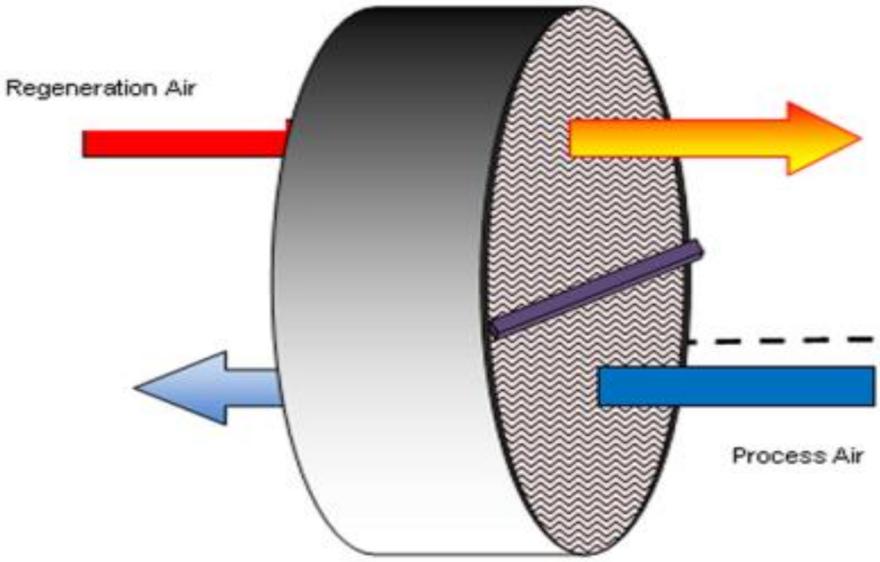

Figure 2.1 Schematic of rotary axial flow desiccant wheel (Narayanan et al, 2011)

DCHE is the type of heat exchanger were the desiccant material is uniformly and stably coated on the external surface by coating technology (dip coating, electrostatic spray and direct synthesis) and the cooling/heating water/air flows through the tubes (Vivekh et al., 2018).

Zhao et al. (2014) experimentally investigated the desiccant dehumidification unit using fin-tube heat exchanger with silica gel coating. They found that rotary wheel has lower pressure and the larger contact area and performs the higher dehumidification efficiency than fixed bed solid desiccant. By this the heat and mass transfer greatly improved.

In rotary wheel and fixed bed since the adsorption heat released by desiccant do not removed simultaneous to dehumidification, it will greatly affect the dehumidification performance and cause higher desorption temperature. However, DCHE internally uses a cooling fluid to remove the adsorption heat released as a result isothermal dehumidification were achieved.

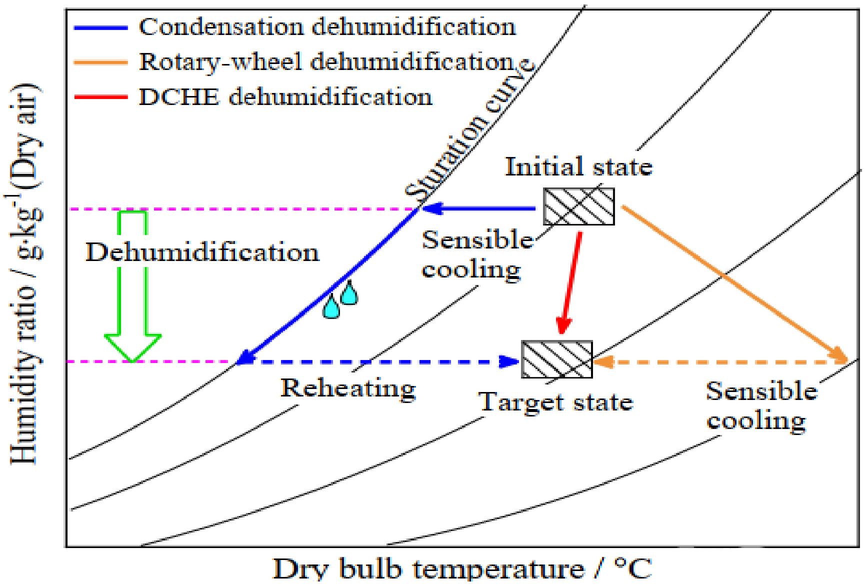

Figure 2.2 Dehumidification principle of three typical dehumidification processes (Zhao et al., 2021)

Bongs et al. (2014) studied an advanced performance of an open desiccant cycle with internal evaporative cooling. The results of the study revealed that when compared to conventional desiccant system a DCHE can increase the dehumidification performance by up to 46%. Sun et al. (2018) experimentally investigated the heat and moisture transfer characteristics of desiccant coated heat exchanger with variable structure sizes. In their investigation performances of three different configuration with different fin pith and depth of DCHE were examined. The result revealed that by decreasing the fin pith and depth decreased, the heat and moisture transfer rate were increased with an increase of the pressure drop.

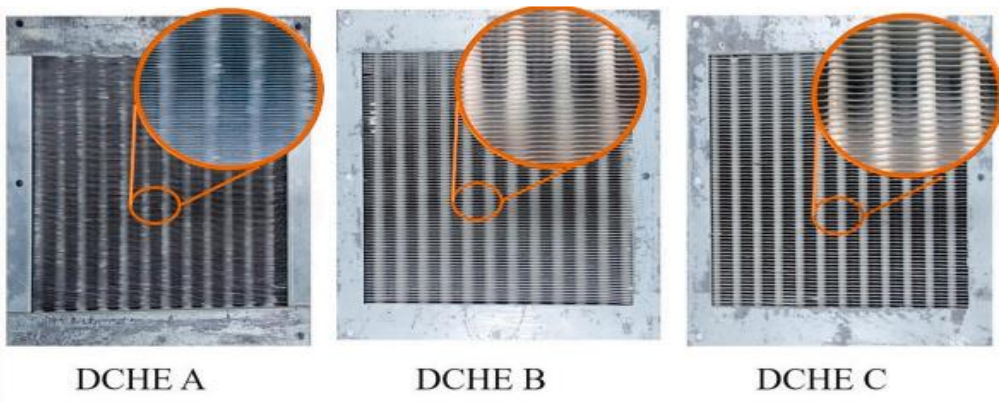

Figure 2.3 Illustration of DCHE-A(fin pitch 2 mm and fin depth 44 mm), DCHE-B (fin pitch 3 mm and fin depth 66 mm), and DCHE-C (fin pitch 4 mm and fin depth 88 mm) (Sun et al., 2018)

2.3.2 Evaporative cooling technology

This technologies provide the cooling condition through the evaporation process of water by some sort of heat energy starting from an ancient time in different part of the world. Based on the ways that the moisture of supplied air handled, two types of Evaporative cooling Technologies (ECT) available. These are Direct Evaporative Cooling (DEC) and Indirect Evaporative Cooling (IEC). In DEC, the air passes over a wet surfaces and has a direct contact. As hot and dry air stream inlet passes through DEC its temperature and relative humidity, decreased and increased respectively. Compared to conventional cooling system, DEC is simple in construction and use, eco-friendly and low energy consumption (Lai et al., 2021). The main drawback of DEC is the minimum theoretical temperature it will achieve is the wet bulb temperature of an inlet air-stream temperature that limit its wide application.

Wet-bulb effectiveness (defined by Equation-2.1) is usually used to evaluate the DEC performance, which represents the ability of DEC to achieve the wet-bulb temperature of the supply air. Similarly, dew point effectiveness (defined by Equation-2.2) is often used to evaluate the IEC performance (Lai et al., 2021).

$$\varepsilon_{wb} = {T_{db,in} - T_{db,out}} \Big/ {T_{db,in} - T_{wb,in}} \quad \text{(2.1)}$$

$$\varepsilon_{dp} = {T_{db,in} - T_{db,out}} \Big/ {T_{db,in} - T_{dp,in}} \quad \text{(2.2)}$$

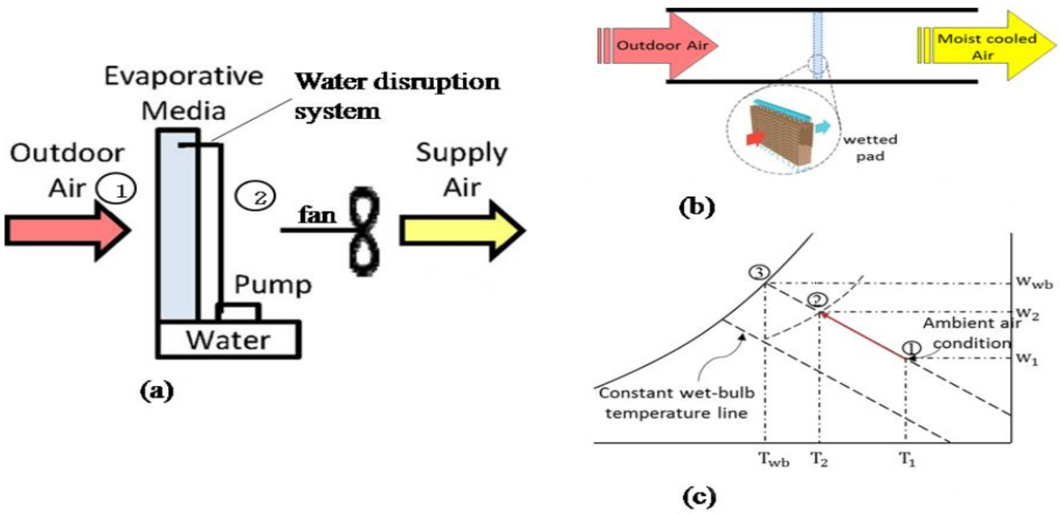

Figure 2.4 (a) Schematic structure, (b) working principle and (c) psychometric chart of a direct evaporative cooling (Amer et al., 2015)

In IEC, the temperature of the inlet air steam decreased without adding the moisture into it. The two main categories of indirect evaporative coolers are wet-bulb temperature and sub wet-bulb temperature IEC systems (Maisotsenko-cycle (M-cycle) based IEC system) (Amer et al., 2015). Wet-bulb temperature IEC system can lower air temperature close to, the wet-bulb temperature of the inlet air; but not above it. It further classified according to the type of heat exchanger as plate-type IEC, tubular-type IEC and heat pipe IEC.

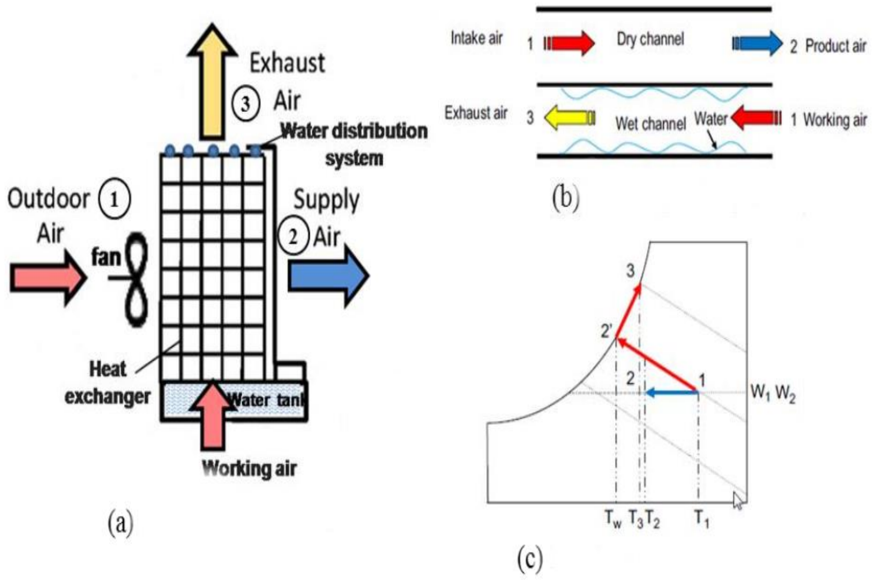

Figure 2.5 (a) Schematic structure, (b) working principle and (c) psychometric chart of wet-bulb temperature indirect evaporative cooling (Amer et al., 2015)

Whereas sub wet-bulb temperature IEC systems can lower the primary air temperature below wet-bulb temperature and approach dew-point temperature of the incoming air. Maisotsenko-cycle (M-cycle) IEC is the advanced system of Indirect Evaporative cooling; thus decreasing the minimum outlet temperature from wet-bulb to dew point temperature of the intake air without adding extra moisture to the air. The ambient condition highly influences the performance of M-cycle IEC, thus its application in humid area is limited. This drawback is avoided if the solid desiccant cooling (SDC) where integrated with it (Lai et al., 2021).

Amer et al. (2015) reviewed an evaporative cooling technologies and they concluded that sub wet-bulb temperature based indirect evaporative cooling (Maisotsenko-cycle) have shown considerable potential towards enhancing the performance and cooling capacity of IEC system for building cooling.

The temperature, relative humidity and velocity of an inlet air and the evaporating surface area was the four main factors that affect the rate of evaporation in evaporative cooling system. Air with a relatively high temperature will be able to stimulate the evaporative process and also be capable of holding a great quantity of water vapors. The rate of evaporation is greatly affected by the velocity of an air. As the humid air particles near the wet surface removed and replaced by dry air particles constantly, the rate of evaporation would increase. Evaporating surface area also favor he evaporation rate; therefore the greater the surface area from which the water evaporates, the greater the rate of evaporation. Since relative humidity is a measure of the air ability to absorb additional water vapor at specific air temperature, the air with low relative humidity can capable of taking additional moisture favor the higher rate of evaporation (Libertya et al., 2013).

Lai et al. (2021) reviewed an evaporative cooling integrated with solid desiccant systems. This review reveal that the evaporative cooling technology (ECT) has been proven to be an energy-efficient alternative for vapor-compression air-conditioning systems, especially in hot and dry climates. ECT includes direct evaporative cooling (DEC) and indirect evaporative cooling (IEC), including M-cycle IEC technologies. M-cycle IEC reduces supply air temperature significantly. However, it was found that the performance of an M-cycle IEC was not satisfactory when the ambient relative humidity (RH) was 70% or above.

Ismanizam et al. (2018) reviewed the desiccant evaporative cooling systems in hot and humid climates. This review reveals that at constant flow rate, the two-stage dehumidification process had higher moisture removal capacity than the single-stage cycle system. The regeneration temperature (above 70°C) is needed to remove the humidity content from the ambient air in hot and humid condition where latent load is high.

Mahmood et al. (2016) investigated an overview of the Maisotsenko cycle (M-cycle) – A way towards dew point evaporative cooling. The M-Cycle uniquely combines the thermodynamic processes of heat transfer and evaporative cooling to enable the product temperature to approach the ambient air dew-point temperature. The study showed that regardless of ambient air temperature the M-Cycle system can achieve the air conditioning load efficiently for various applications when the ambient air humidity is not so high (less than 11.2 g/kg of dry air). The COP of the Maisotsenko cooling tower increases with the increase in ambient air temperature which distinguishes its applicability in hot climates.

Anisimov and Pandelidis (2011) investigated numerically heat- and mass-transfer processes in indirect evaporative air conditioners through the Maisotsenko cycle. They found that the wet bulb and dew-point effectiveness is not an adequate efficiency factor for indirect evaporative air coolers. One of the most influential parameters on cooling effectiveness is the relative humidity of the incoming air stream. It is important to make the incoming air delivered to the heat exchanger as dry as possible.

Cui et al. (2014) studied the fundamental formulation of a modified LMTD method to study indirect evaporative heat exchangers by introducing a configuration of M-cycle IEC. From the result of the study less than 1.5 m/s of inlet air velocity and less than 1.5 of the air ratio between product air and working air are recommended.

Xu et al. (2017) experimentally investigated the supper performance of dew point air cooler by considering the guideless irregular and corrugated surface structure of heat and mass exchange with Coolmax fabric. The experimental results showed that the system had a better cooling performance compared to an existing commercial dew point cooler when a working air ratio of 0.44. The wet-bulb effectiveness and dew-point effectiveness reached 100–109.8% and 67–79.3%, respectively, and COP significantly increased to 52.5.

Tariq et al. (2018) numerically investigated the regenerative counter flow evaporative cooler using alumina nanoparticles in wet channel. In the investigation, the M-cycle developed by adding alumina nanoparticles into the water to improve the heat and mass transfer inside the wet channel. They found that the cooling capacity and energy efficiency ratio increased by 18% and 19%, respectively when the ambient temperature is 45 ºC. Similarly, the cooling capacity and energy efficiency ratio as high as 54% and 22% respectively when the inlet air velocity increased to 1.6 m/s.

Sajjad et al. (2021) reviewed on recent advances in indirect evaporative cooling technology. The review reveals that the major design parameters include system configuration, inlet airflow conditions, channel geometry, and evaporative material. Due to higher cooling effectiveness, cooling capacity, and system compactness, counter-flow arrangement is more effective than the cross-flow arrangement. At a higher inlet air temperature and a lower humidity ratio (i.e. less than 11.35 g/kg), the system provides a higher cooling effectiveness. Feed water temperature has insignificant effect on evaporative cooler performance and the velocity of intake air stream must be small (less than 1.5 m/s) for higher cooling performance. Working intake air ratio must be in range of 0.3 to 0.65 to compromise between cooling capacity and cooling effectiveness. Fabric material has more cooling potential for indirect evaporative cooler due to high heat and mass transfer ability, low cost, contamination resistance, and low pressure drop characteristics. Evaporative cooling systems can be a potential solution of thermal management in various non-human applications such as agricultural storage, poultry, and livestock.

Moshari et al. (2016) done numerical investigation of wet-bulb effectiveness and water consumption in one-and two-stage indirect evaporative coolers. In this study, the three-configuration shown on figure 2.4-4 (Type A, Type B and Type C) were developed for two-stage IEC/IEC and the wet-bulb effectiveness were investigated in various climatic conditions (hot-dry, hot-semi humid, hot-humid, moderate-dry and moderate- humid). Numerical results reveals that, the average wet-bulb effectiveness of two stage is higher than that of the one stage IEC.

Nkolisa (2017) evaluated a low-cost energy-free evaporative cooling system for postharvest storage of perishable horticultural products produced by smallholder farmers of umsinga in Kwazulu-natal. The results shows that the developed low cost evaporative cooling system was able to decrease temperature, increase relative humidity and had a cooling efficiency of 67.17%. The evaporative cooler was also able to maintain color, respiration rate, firmness, mass, total soluble solids and titratable acids of the tomatoes for 20 days compared to room temperature.

Babaremu et al. (2019) investigated the significance of active evaporative cooling system in the shelf life enhancement of vegetables (Red and Green Tomatoes) for minimizing post-harvest losses. The result of the study has shown that the evaporative cooling technology improved and prolonged the shelf life of tomatoes. The cooler was able to reduce the emission of the ripening hormone from the tomatoes as this inhibited and delayed the rate of further ripening of the stored tomatoes in the evaporative cooling system with relative comparison to the samples stored in the ambience.

Taye et al. (2011) developed the direct evaporative cooling system for the preservation of fresh vegetables in Nigeria. Ambient air temperatures and relative humidity during the test periods ranged over 26-32°C and 18-31% respectively. They found that the evaporative cooling system chamber temperature and relative humidity depression from ambient air temperature varied over 16-26°C and 33-88% respectively.

2.3.3 Enhanced evaporative cooling system

According to the review of Lai et al. (2021), the evaporative cooling technology is greatly influenced by the dry-bulb and dew-point temperature difference. As a result, the performance of ECT is less in hot and humid air condition. To overcome this limitation, different integrated system where proposed. Out of the integration of solid-desiccant with evaporative cooling system is one of the promising system. The dehumidification process and the evaporative cooling process are responsible to remove the moisture and handling the sensible heat of the air respectively. There are many investigations done on the integration of solid desiccant with evaporative cooling systems.

Khalid et al. (2009) investigated numerically and experimentally the solar assisted, pre-cooled hybrid desiccant cooling system for four different configurations under Pakistan climates. The results revealed that even if without the assistance of the auxiliary cooling unit all of the configuration did not fully provide a cooling load, the fourth configuration (applied IEC for pre-cooling and DEC for post-cooling of the air) achieved the highest COP.

Goldsworthy and White (2011) numerically investigated the optimization of a desiccant cooling system design with indirect evaporative cooler. The result revealed the integrated system reduced energy consumption and greenhouse emission. When the regeneration temperature was 70 ºC, supply and regeneration airflow ratio was 0.67 and the extraction air ratio of IEC was 0.3, the electrical COP could be greater than 20.

Parmar and Hindoliya (2012) studied the performance of solid desiccant-based evaporative cooling system under four different climatic zones (hot and dry, warm and humid, moderate and composite climates). The result shows that the maximum system thermal COP achieved were 4.98; at 0.55 flow rate ratio of regeneration air and process air. They suggested that the increase of the regeneration air to process air ratio led to an increase of the regeneration heat load requirement and a reduction in system thermal COP.

More than 50% of the total energy consumption of a solid desiccant-based evaporative cooling system was consumed by the regeneration process of the desiccant wheel and this energy consumption were reduced and also a higher coefficient of performance were achieved when a multi-stage desiccant was implemented (Lanbo Lai, 2021).

Dezfouli et al. (2014) simulated four configurations (one-stage ventilation, one-stage recirculation, two-stage ventilation and two-stage recirculation) of solar desiccant cooling system using evaporative cooling in tropical weather in Malaysia. The result of simulation revealed that when the initial air condition is 30 ºC, 0.0200 kg/kg, the supply air were 17.6 ºC and 0.0096 kg/kg. Due to its higher efficiency, the two-stage ventilation system was recommended to use in hot and humid conditions.

Lin et al. (2017) experimentally and numerically studied the cross-flow dew point evaporative cooler (M-cycle IEC) with and without dehumidification. The result of the study revealed that when the ambient air humidity ratio changed from moderate to humid the wet-bulb effectiveness of the M-cycle IEC decreased from 1.25 to 0.86. The cooling capacity the system enhanced by 70% when an integration of dehumidification and evaporative cooling used.

Shahzad et al. (2018) studied experimentally the solid desiccant system integrated with cross flow Maisotsenko cycle evaporative cooler. The finding of the study revealed that Maisotsenko cycle enhanced evaporative cooler system was 62.96% more efficient than the conventional evaporative cooler in terms of thermal COP, but its cooling capacity was 39.29% less due to the extraction air from the dry channel to the wet channel.

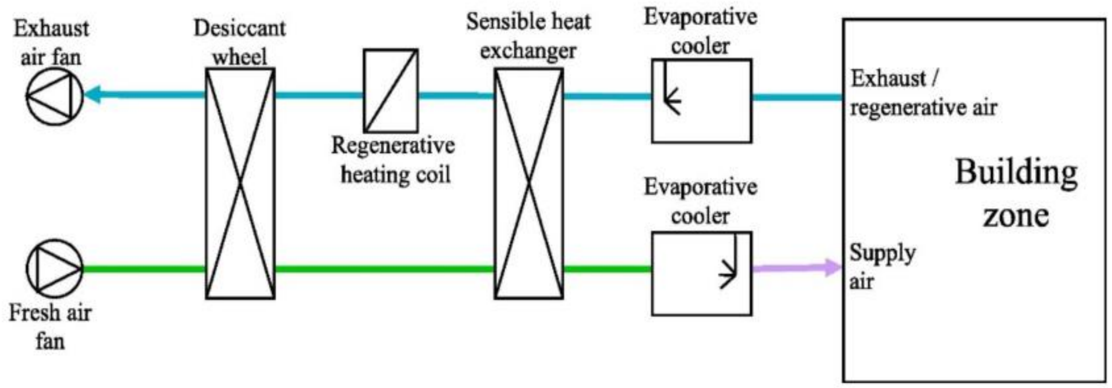

Figure 2.6 Schematic diagram of solid desiccant-based evaporative cooling (Frog et al., 2020)

2.3.4 Evaporative cooling system for vegetables storage

Sipho and Tilahun (2021) investigated the development of a solar powered indirect air cooling combined with direct evaporative cooling system for storage of fruit and vegetables in sub-Saharan Africa, and the result showed that the system maintained a 13-41% higher RH and achieved 7-16°C temperature gradient with ambient.

Samuel (2013) investigated the development of an active evaporative cooling system for short-term storage of fruits and vegetable in a tropical climate. The result of the study reveals that the maximum temperature drop observed was 13ºC and the relative humidity of the cooler was observed around 85.6% – 96.8%.

Olunloyo et al. (2019) developed and assessed the direct evaporative cooling facility for storing fruit and vegetables. They used river sand as the cooling pad and tomato as a test produce. From an assessment, it found that the maximum temperature drop and relative humidity increase achieved by the developed DEC was 1.5ºC and 2%RH respectively.

Deoraj et al. (2015) investigated an evaporative cooler for the storage of fresh fruits and vegetables. Cedar, teak and coconut fiber are the three different types of cooling pad used to test the performances of evaporative cooling. The result revealed that the maximum saturation effectiveness and temperature difference was 64.42% and 5ºC for cedar.

2.4 Solar Thermal Collector

Solar thermal collectors are devices those convert solar radiation into thermal energy. Solar thermal systems are used to produce hot water or working fluid. Now a day different types of solar thermal collectors used for different application. Based on the concentration types of the collector, solar thermal collector can be classified into concentrating and non-concentrating types of solar thermal collector.

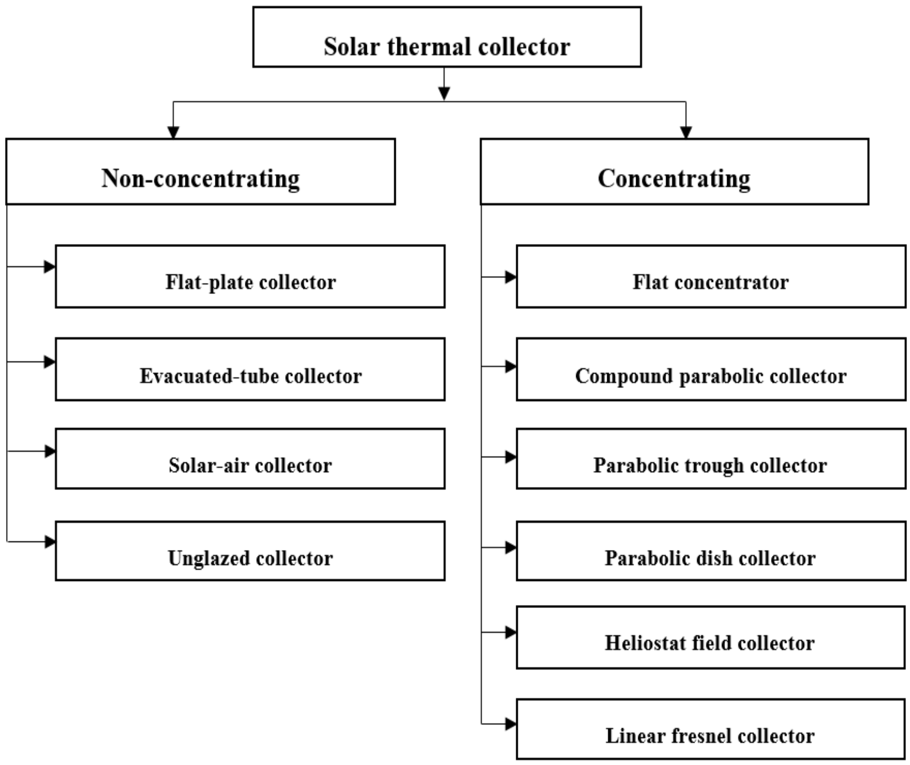

Figure 2.7 Classifications of solar thermal collector

Table 2.3 Solar thermal collector's operational temperature range (Olfian et al., 2020)

Types of solar thermal collector	Operational temperature range (ºC)	About collector
Flat plate collector (FPC)	20-80	-Used in domestic hot water - Low efficiency and outlet temperatures because of heat loss via cover of glass in collector and lack of sun tracking.
Evacuated tube collector (ETC)	50-200	- Their performance during cold weather is more than FPC. - Efficiencies for 500 and 1000 W/m2 are 0.44–0.82 and 0.62–0.82, respectively
Compound parabolic collector (CPC)	60-240	- Efficient in collect and concentrate distant light sources, with some acceptance angle. - Efficiencies for 500 and 1000 W/m2 are 0.45–0.73 and 0.58–0.72, respectively
Parabolic trough collector (PTC)	400-500	- Ability to use hybridization and energy storage by thermal energy storage.
Parabolic dish collector (PDC)	>1500	-This collector equipped with an active tracking system which able to pointing the sun consistently.

The solar thermal cooling technologies performance change based on the hot water temperature. Solar Collector temperature ranges serving different Cooling Cycles is shown below.

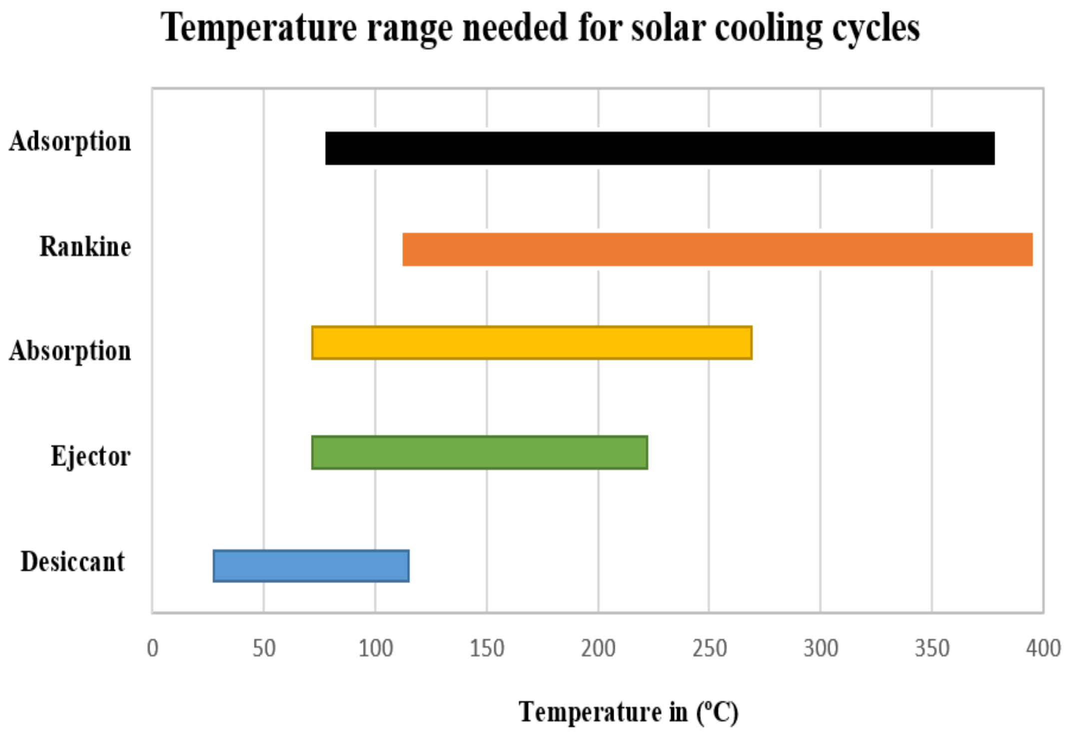

Figure 2.8 Solar Collector temperature ranges serving different Cooling cycles (Alazazmeh et al., 2015)

From Figure 2.8 and Table 2.3, it is concluded that evacuated tube solar thermal collector is preferred for the supply of the required regeneration temperature.

An evacuated tube collector is made of parallel evacuated glass pipes. Each evacuated pipe consists of two tubes, one is inner and the other is outer tube. The inner tube is coated with selective coating while the outer tube is transparent. Light rays pass through the transparent outer tube and are absorbed by the inner tube. Both the inner and outer tubes have minimal reflection properties. The inner tube gets heated while the sunlight passes through the outer tube and to keep the heat inside the inner tube, a vacuum is created which allows the solar radiation to go through but does not allow the heat to transfer (Sabiha et al., 2015).

The main drawbacks of flat plate collector are convection heat loss through glass cover from collector plate and absence of sun tracking. These drawbacks are overcome by evacuated tube collector, due to the presence of vacuum in annular space between two concentric glass tubes, which eliminates sun tracking by its tubular design.

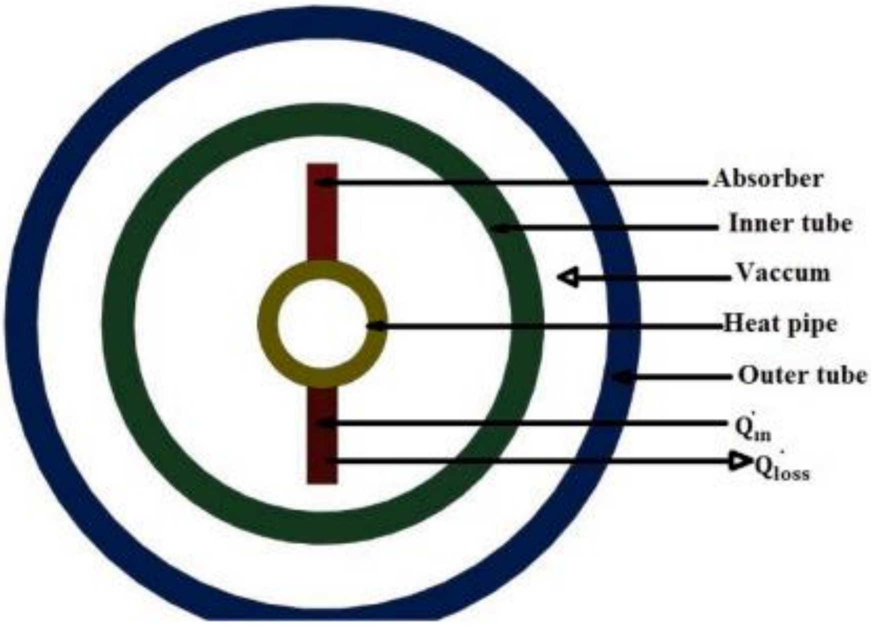

Figure 2.9 Cross-sectional view of evacuated tube solar collector (Kumar et al., 2021)

Sabiha et al. (2015) investigated the progress and latest developments of evacuated tube solar collectors. From an investigation it is concluded that the cylindrical shape of the evacuated tube collector helps to track the sun passively throughout the whole day. When the climate is cold, windy and cloudy, the performance of flat plate collector were reduced. But performance of evacuated tube collectors are unaffected. Due to this evacuated tube collector can gain higher temperatures easily and are able to preserve heat even when the outside weather is cold.

Olfian et al. (2020) reviewed the development on evacuated tube solar collectors and they concluded that when compared with the flat plate collectors, the thermal efficiency of evacuated tube solar collector is high at the temperature range above 80 ºC. Three categories of evacuated tube solar collectors are investigated and it was found that the thermosiphon and U-pipe models are suitable for low-temperatures applications (T < 100 ºC) while the heat pipe model is appropriate for medium and high-temperatures ones (100 ºC <T).

Kumar et al. (2021) reviewed on advances of evacuated tube solar collector using Nano fluids and PCM. By their review, they concluded that the evacuated tube solar collector with heat pipe provides good efficiency and heat pipe ETSC with reflector can further enhance efficiency. When the Nano fluids were introduced as a working fluid, the efficiency of the working fluid increased and the temperature output have been. The evacuated tube collector were highly efficient with PCM than without PCM.

2.5 Thermal Heat Storage

There are three forms that the thermal energy can be stored by. These are latent heat, thermochemical reaction and sensible heat form. When compared to sensible heat storage, latent heat storage provides better storage capacity with minimum volume requirement due to usage of phase change materials (Mohamed, 2017).

Low thermal conductivity (between 0.2 and 0.7 W/m K) of commonly used phase change materials in thermal energy storage is requiring the use of complex heat exchanger geometries to obtain required heat transfer rates from latent heat storage containers. To overcome problem metal fins techniques (carbon cloths, shape stabilized PCMs with graphite, microencapsulated-PCM slurries) and direct contact latent heat storage systems can be used (Da-Cunha, 2016).

Based on the ways of the contact between the heat transfer fluid (HTF) and the PCM, thermal energy storage technologies can be classified as direct-contact type and indirect-contact type according. The indirect-contact type can be classified as PCM in a large container, PCM in a modular unit made of metals, and PCM around an assistant heat. In this type a PCM placed in a large container and the pipeline for the HTF flow is embedded inside the PCM. In modular unit type of indirect contact, PCM is contained in small units and arranged in rows around the HTF pipeline in a container (Li, 2019).

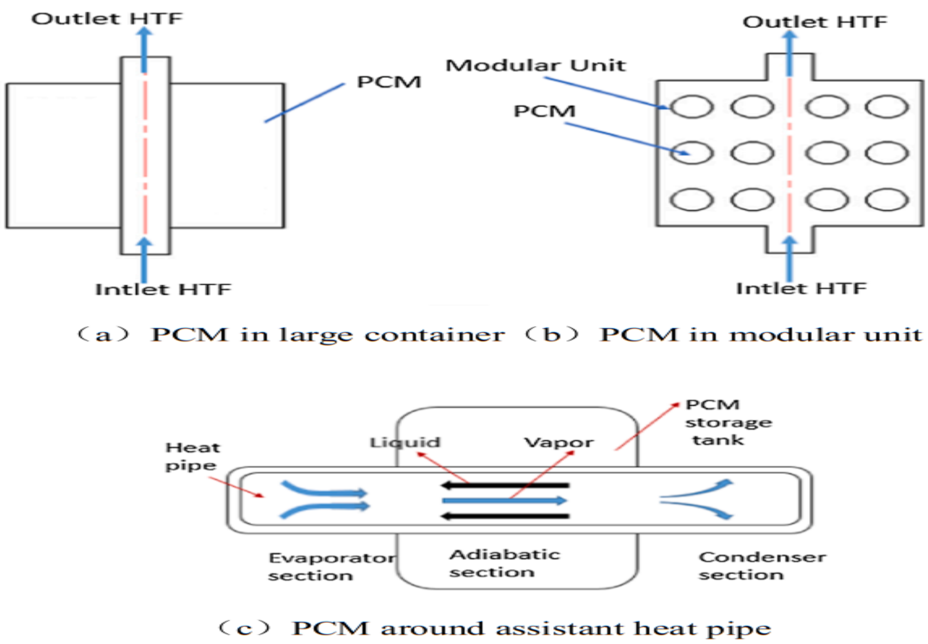

Figure 2.11 Classification of indirect-contact cold storage technologies (Li, 2019)

When the source of energy is a solar energy, the shape and size of phase change material tank have a significant effect on the melting time of the PCM. Broadly, rectangular and cylindrical containers were used in TES. The cylindrical containers further classified in to pipe, cylindrical, and shell and tube model. For the better performances next to shell and tube configuration, the pipe model with the PCM at the shell side and the heat transfer fluid flowing through the center is preferred (Amer et al., 2018).

Malik et al. (2020) investigated solar thermal energy storage system using potash alum as a PCM. They modeled and simulated latent energy storage tank using COMSOL software. The result of an investigation shows that thermal energy can be stored for up to 7 hours at a maximum temperature of 92 ºC and minimum temperature of 81 ◦C after sunset.

Zhao and Tan (2015) numerical investigated a shell-and-tube latent heat storage unit with fins for air-conditioning. In their investigation they used water for the charging loop and air for the discharging loop heat transfer fluid and also RT22 as the storage medium which had a phase change temperature range of 19–23ºC. The result of the study revealed that the effectiveness of the proposed cold storage system was higher than 0.5 and the proposed PCM showed an increase in COP value of approximately 25.6.

Nakaso et al. (2008) numerically investigated an extension of heat transfer area using carbon fiber cloths in latent heat thermal energy storage tanks. They investigated the thermal storage capacity using a paraffin wax with a melting temperature of 49 ºC. The result of the study shows that the system could provide a constant 25 kW thermal power output for 16 h and 32 min.

2.6 Desiccant, Evaporative Cooling Pad and Phase Change Materials

2.6.1 Desiccant materials

The novel properties of desiccant materials for dehumidification are the maximum moisture content uptake, water adsorption isotherm curves, and thermal conductivity. Silica gel, lithium bromide, zeolites, and various metal oxides are the most widely used desiccant materials. According to an International Union of Pure and Applied Chemistry, the adsorption isotherm curves (which represents the equilibrium water adsorption of desiccant materials) were classified into eight types. Equilibrium water adsorption measures the maximum moisture uptake of the desiccant material relative to the moisture content capacity as a function of relative pressure. Type V are the better-suited adsorption isotherm curves followed by type IV and II for DCHE (Venegas et al., 2021).

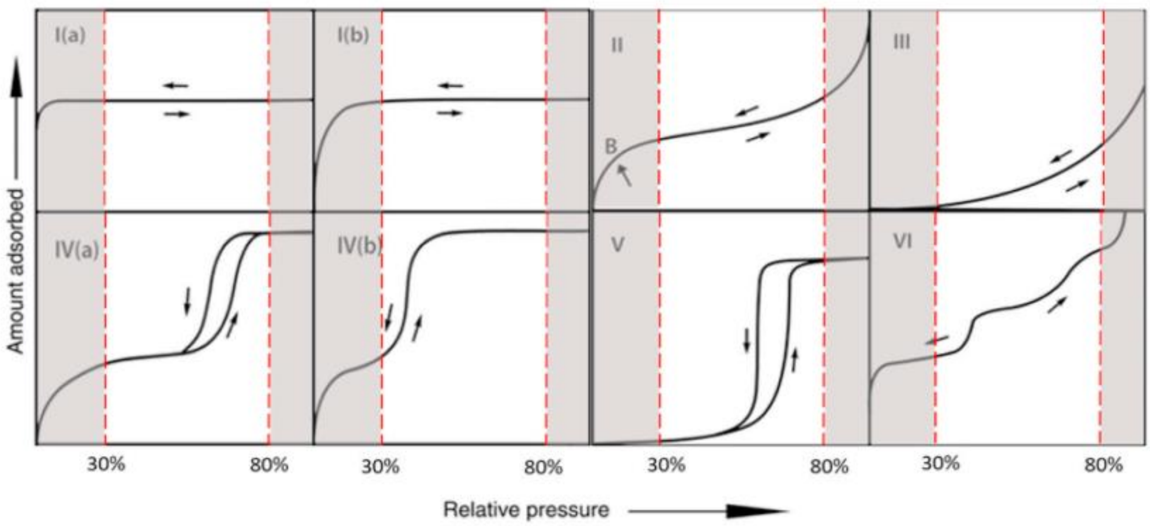

Figure 2.12 International Union of Pure and Applied Chemistry adsorption isotherm curves classification, adapted and modified (Venegas et al., 2021)

Table 2.4 Solid desiccant materials characteristics (Venegas et al., 2021)

Materials	Maximum water uptake (kg/kg dry air)	Adsorption isotherm curves types	Additional notes
Silica, Alumina, and mixed salts aerogels	1.15–1.35	V	Water mass diffusion coefficient 0.89 × 10− 10 [m2/s] (potassium hydroxide); 13.74 × 10− 10 (hydrogen peroxide) [m2/s]
MIL 101 with graphite oxide composite	1.58–1.6	V	Saturation at 6600 [s], 1.5 [kg/kg], 298 K, 70%RH
Cr-soc-MOF-1	1.95	V	Adsorption capacity maintained up to 100 cycles. Apparent surface area 4549 [m2/g]
Chitosan based composite	1.21–1.5	III-V	Regeneration temperature 80 ºC,Total desorption from 1.5 [kg/kg] in 15–20 min at 80 ºC
Aluminum fumarate	0.45	V	No loss of water uptake capacity up to 40 cycles

When silica gel is doped with boron and subjected to neutron irradiation, it can have its adsorptive capacity increased by as much as 23 % (Eduardo & Nóbrega, 2014).

Nakabayashi et al. (2011) investigated and developed a desiccant material of low regeneration temperature. A Wakkanai siliceous shale was impregnated with $CaCl_2$, lithium chloride, or sodium chloride. The water vapor adsorption increases at relative humidity between 50% and 70% when natural shale is impregnated with sodium chloride. At the regeneration temperature of 40ºC, new filter has the capability of adsorbing and desorbing 60g/h water vapor. Where, a silica gel filter adsorbs and desorbs only 10 g/h of water vapor.

2.6.2 Evaporative cooling pad materials

The DEC (direct evaporative cooling) supply air temperature is always higher than the theoretical value and system effectiveness is significantly affected by the cooling pad material under the same inlet air conditions (Lai et al., 2021).

Velasco-Gómez et al. (2020) investigated experimentally cotton fabric based new evaporative cooling pad material. The experimental result shows that the saturation efficiency could reach 100%. This indicates that the outlet air temperature could be cooled to the wet-bulb temperature. The maximum temperature difference was obtained as 19.2 ºC under a hot and dry inlet condition.

Khosravi et al. (2020) experimentally investigated the performance analysis of direct and desiccant assisted evaporative cooling systems using five different evaporation materials with two operation modes. Out of them wood chips were found as the best cooling pad material in direct evaporative cooling mode and founds that the wood chips reduced the air temperature by 10.6 ºC on average and has wet-bulb effectiveness of 81%.

Dogramaci et al. (2019) experimentally studied the potential of using eucalyptus fibers as evaporative cooling pad material. The study reveals that the maximum air temperature drop, the highest cooling efficiency and the highest coefficient of performance of the fiber was 11.3 ºC, 71% and 4.05 respectively. They also recommended that the velocity of an inlet air was 0.6 m/s.

Jain and Hindoliya (2011) experimentally investigated the performance of new evaporative cooling pad materials. They compared coconut fibers and Palash fibers cooling pad materials with conventional commercial products. The results revealed that the temperature difference between the inlet and outlet air could reach 14.9ºC and 16.23ºC for coconut fibers and Palash fibers respectively. In terms of, Palash fibers has higher wet-bulb efficiency than coconut fibers.

2.6.3 Phase-change materials

Phase change materials (PCM) are a group of materials which exchange an amount of thermal energy as latent by a phase transformation and used in latent heat storage applications. It can be classified as organic, inorganic and eutectics according to their chemical nature. Organic PCM mainly paraffin or non-paraffin's such as esters, fatty acids, alcohols and glycols or polymers. Inorganic PCM includes salt hydrates and metals. Were as eutectics PCMs is a mixture of the two. Below 100ºC, organic compounds and salt hydrates are the most interesting materials. Eutectic mixtures with Urea seem promising around 100 ºC, and in the range from 130 ºC up to 1250 ºC eutectic mixtures of inorganic salts appear the most promising PCMs (Elias & Stathopoulos, 2019).

Phase transition temperature in the desired operating, range high latent heat of phase transition per unit volume, high specific heat to contribute in sensible thermal storage, high thermal conductivity of both phases, limited volume change on phase change, low vapor pressure at the operating temperatures, high density, chemical stability, non-corrosive to the construction materials and non-toxic, non-flammable and non-explosive for safety are the desired properties of the phase change materials (Elias & Stathopoulos, 2019). The thermos-physical properties of selected PCM were summarized in (ANNEX A Table A 6-8).

2.7 Heat and Mass Exchanger

Adam et al. (2021) analyzed an indirect evaporative cooler performance under various heat and mass exchanger dimensions and flow parameters. In this analysis mathematical model was developed and simulations were conducted based on different conditions that influence the outlet air temperature, cooling capacity, coefficient of performance, and wet-bulb effectiveness of the system. Specifically, the effect of heat and mass exchanger dimensions and flow parameters on indirect evaporative cooler performance were studied. The result of the analysis showed that the length of the duct should be between 0.6m and 1m, the width of the channel between 0.3m and 0.5m, and the channel gap between 3mm and 6mm to reach optimal operating conditions in climates with moderate humidity. The cooling capacity and efficiency were improved as the working air velocity increased (when the working air velocity increased from 1 m/s to 5 m/s, the product air temperature difference increased from 9.5 ºC to 12.8ºC. However, an increase in the product air velocity has a negative effect on the cooling performance; as a result, less than 1m/s of product air velocity were recommended. Higher inlet air temperature and relative humidity also lower the cooling performance. It is recommended that the flow rate ratio should be in the range 0.3 to 0.5, and wet channel with a bigger gap size than the dry channel helps to obtain this flow rate range.

Chien et al. (2021) experimentally investigated the heat and mass transfer of evaporative cooler with elliptic tube heat exchangers. The results of an investigation revealed that as the air Reynolds number increases the air liquid interaction and mass transfer coefficient were boosted, and also results the better liquid film heat transfer coefficient and mass transfer coefficient. The rise in the wet-bulb temperature of the outside air elevated the hot water temperature and the sprinkler temperature which lead to a better mass transfer coefficient.

2.8 Literature Summary and Research Gap

2.8.1 Literature summary

As revealed by literature review the evaporative cooling system control the temperature and relative humidity of dry by the humidification process. Enhancement of this system needed when maximum possible control over outdoor air temperature and relative humidity were targeted. According to extensive review by Lai et al. (2021), enhancement of evaporative cooling were researched extensively by different scholars. It enhanced by advanced indirect evaporative cooling M-cycle to achieve the maximum temperature drop. But M-cycle performed effectively when the process air (ambient air) relative humidity is low (below 30%RH) and its application were limited in humid air area (Lai, 2021). To extend the application range of M-cycle in humid area, enhancement of the cooling system by desiccant dehumidification system (for the sake of incoming process air dehumidification before M-cycle) developed. Lin et al. (2017) experimentally and numerically studied the cross-flow dew point evaporative cooler (M-cycle IEC) with and without dehumidification and they found that the cooling capacity the system enhanced by 70% when an integration of dehumidification and evaporative cooling used.

The two major categories of desiccant dehumidification was solid and liquid desiccant. Solid desiccant further classified as fixed bed, rotary wheel and desiccant coated heat exchangers (DCHE). Due to there is a possibility of carry out of desiccant material's particles with supply air stream, the application of liquid desiccant type dehumidification were limited for space conditioning. As result the rotary wheel solid dehumidification system were researched and developed widely for building and storage air-conditioning application, because rotary desiccant wheel is advantageous as it can supply air with uniform humidity at the outlet due to continuous rotation. The main drawn back of this wheel are the large pressure drop due to the complex structure of the desiccant felts, large wheel size which requires huge electric power to drive it and severe noise and less compactness resulted due to rotating wheels. This limit the full applications of rotary wheel solid desiccant dehumidification in area were electric supply that run the wheel's motor. Whereas, in DCHE dehumidification the desiccant material is uniformly and stably coated on the external surface by coating technology and the cooling/heating water/air flows through the tubes and remove the adsorption heat released to achieve isothermal dehumidification (Vivekh et al., 2018). When compared to conventional desiccant system a DCHE can increase the dehumidification performance by up to 46% (Bongs et al., 2014).

Desiccant materials needs to be generated external thermal energy generator during desorption process. According to Alazazmeh et al., (2015), the required regeneration temperature for most of desiccant materials ranges between 30 and 130ºC depending on the types of desiccants. Evacuated tube solar thermal collector were preferred for the supply of the required regeneration temperature due to the presence of vacuum in annular space between two concentric glass tubes eliminates sun tracking by its tubular design in which the flat plate solar collectors lack and its operational temperature range is between 50-200 ºC (Olfian et al., 2020). When the source of energy is a solar energy, thermal energy storage were require in order to supply the required regeneration temperature during sun set time.

Compared to another type of thermal energy storage system, latent heat storage provides better storage capacity with minimum volume requirement due to usage of phase change materials (Mohamed et al., 2017). Due to low thermal conductivity (between 0.2 and 0.7 W/m K) nature of commonly used phase change materials is requiring the use of complex heat exchanger geometries to obtain required heat transfer rates from latent heat storage containers. Since the shape and size of phase change material tank have a significant effect on the melting time of the PCM, shell and tube configuration preferred for better performances of TES (Amer et al., 2018). According to the desired properties of the phase change materials investigated by Elias & Stathopoulos (2019), paraffin wax were preferred over others PCM.

As revealed from literature review, the configuration or arrangement of units, the cooling pad and the type of desiccant material used where greatly influence the performances of the system.

2.8.2 Research gap

There are many investigations that carried out on the enhancement techniques of evaporative cooling system in terms of configuration modification, cooling pad development and desiccant materials selection. These enhancement techniques were targeted to develop an evaporative cooling system that can perform effectively and efficiently in wide range of ambient air temperature and relative humidity. Solid-desiccant dehumidification using rotary wheel integrated with M-cycle cooling using finned tube heat and mass exchanger are the extensively investigated mode of evaporative cooling system enhancement for an applications of building air-conditioning (Lai, 2021). The above mentioned integrated system can perform better in hot-dry and hot-humid ambient air condition.

However, one of the main drawn back of rotary wheel that used in the solid-desiccant dehumidification was the large wheel size which requires huge electric power to drive it and this limit its application in an area were the access of electricity is scarce. There is a limitation of an investigation on ways of overcome the above stated drawn back of rotary wheel of solid-desiccant dehumidification.

Whereas DCHE (desiccant coated heat exchanger) is the type of heat exchanger were the desiccant material is uniformly and stably coated on the external surface by coating technology (dip coating, electrostatic spray and direct synthesis) and the cooling water flows through the tubes to remove the adsorption heat released were the isothermal dehumidification were achieved by (Vivekh et al., 2018). When compared to rotary wheel, DCHE had higher dehumidification performances and need less electric power due to there is no large size moving or rotating parts.

Hence, taking this gap into consideration, this study aimed to investigate the performances of evaporative cooling that can be enhanced by solid-desiccant (using DCHE) and M-cycle (using finned tube heat and mass exchanger) in general and for application of vegetable storage at farm in particular.

CHAPTER THREE

METHODOLOGY, DATA COLLECTION AND MATERIALS

3.1 Methodology

In order to accomplish the objectives of this study different research methodology, materials and data are employed. Literature review and data collection is the main secondary and primary sources of data accessing for this study. Based on these data, the thermos-physical property of the tomato is determined and also the cooling load of the produce and the solar potential of the study area are estimated. The enhanced evaporative cooling system also designed based on the gathered data and the phase change and desiccant material also selected. The overall methodology of this study is shown on Figure 3.1.

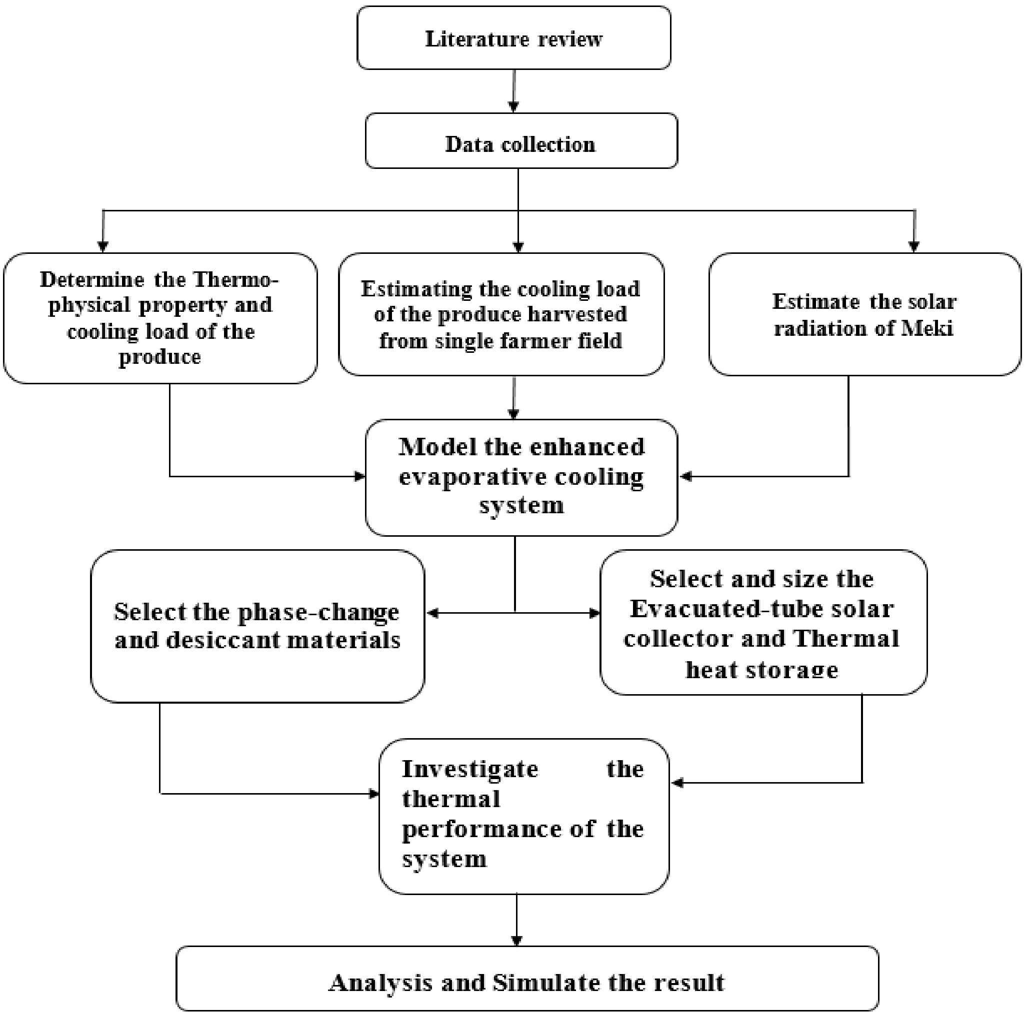

Figure 3.1 Flow diagram of research methodology

3.1.1 Working process of the system

For this investigation, the proposed enhanced evaporative cooling, comprising three main unit/subsystem. These are regeneration unit (comprising cooling tower, phase-change material thermal energy storage and the evacuated tube solar collector), dehumidification unit (comprising desiccant-coated heat exchanger), and M-cycle IEC unit. Due to simultaneous removal of sorption heat generated by circulating cooling water during dehumidification process, the desiccant-coated heat exchanger provide the dry and relatively cool air to M-cycle IEC unit. The whole system's circuit were given on Figure 3.2.

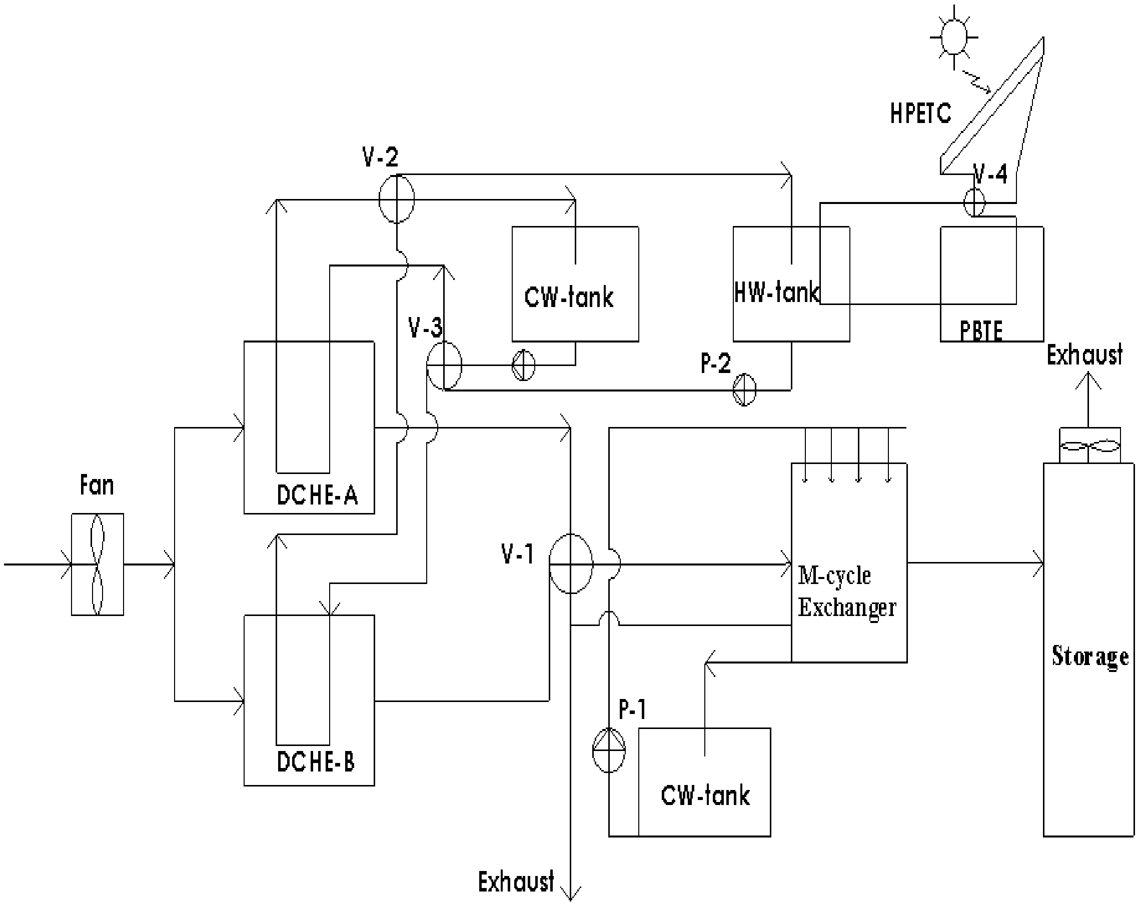

Figure 3.2 System's circuit

In the regeneration unit, two DCHE were used in parallel to dehumidify an incoming ambient air isothermally. An isothermal dehumidification achieved by simultaneously removing the adsorption heat by the cold water from cooling tower. To obtain continuous dehumidification two identical DCHE (DCHE-A & DCHE-B) used and periodically switched. While one DCHE dehumidify an air, another gets regenerated. Figure (3.3) shows the working mode were DCHE-A is dehumidifying an incoming air and cold water circulating through it to remove the adsorption heat released. Simultaneously, DCHE-B were regenerated by regeneration air and hot water circulating through it providing the desiccant regeneration temperature.

As the adsorption ability of the DCHE-A completely approaches to saturation, it's time to switch over the working mode of two DCHEs through reversing valve as shown on Figure 3.4. That means DCHE-B is dehumidifying an incoming air and cold water circulating through it to remove the adsorption heat released. Simultaneously, DCHE-A were regenerated by regeneration air and hot water circulating through it providing the desiccant regeneration temperature. The aforementioned process is recycled again and again for continuous dehumidification.

An ambient air (1) enter to the DCHE-A unit acting as dehumidifier (during which cooled water from cooling tower circulating through it and removing adsorption heat) and supply dehumidified dry air (2) to M-cycle HME. Simultaneously, an ambient air (1) enter to the DCHE-B unit being regenerated (during which hot water from heat storage circulating through it and providing the regeneration temperature) and exhausted to an ambient as humid air (6). The supply dry air (2) sensible cooled further by the M-cycle HME (3). A fraction of this cooled dry air (3) diverted to the wet-channel inside M-cycle HME and the humidified air exhausted to atmosphere (7). The remaining cooled dry air (3) supplied to the storage room. The return air (8) from storage room exhausted to an ambient.

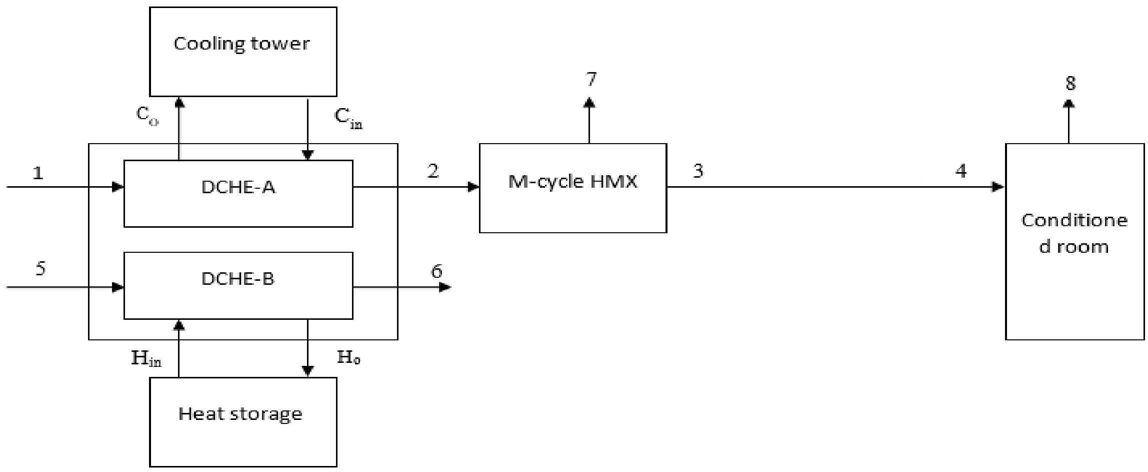

Figure 3.3 schematic diagrams of one-stage enhanced evaporative cooling system configuration (shows regeneration and dehumidification process in DCHE-B and DCHE-A respectively)

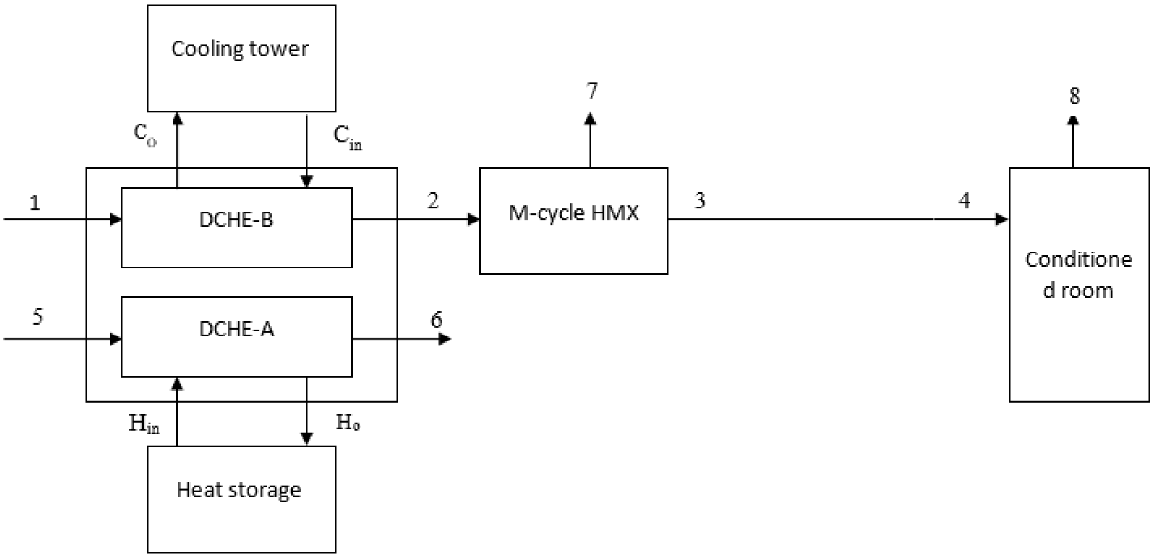

Figure 3.4 schematic diagrams of one-stage enhanced evaporative cooling system configuration (shows regeneration and dehumidification process in DCHE-A and DCHE-B respectively)

3.1.2 Desiccant coated heat exchanger

The DCHE consisting the finned tubes, in which the fins are coated with desiccants and either cooled or hot water circulating through the tubes depending on the mode of operation. The cooled water circulating through the tubes during dehumidification process by removing the adsorption heat from desiccant and the hot water circulating through the tubes during regeneration process by providing the desorption heat to desiccant.

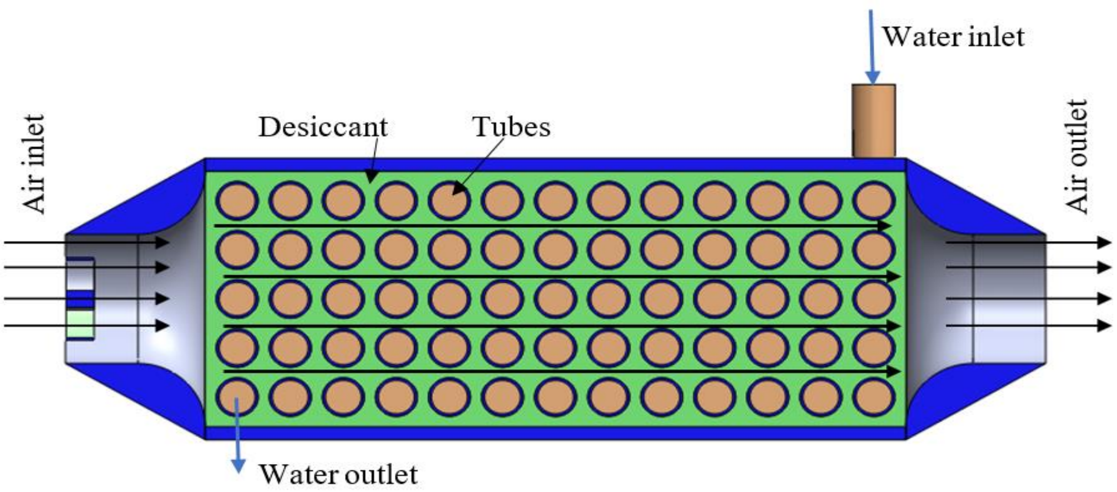

Figure 3.5 Sectioned view of DCHE

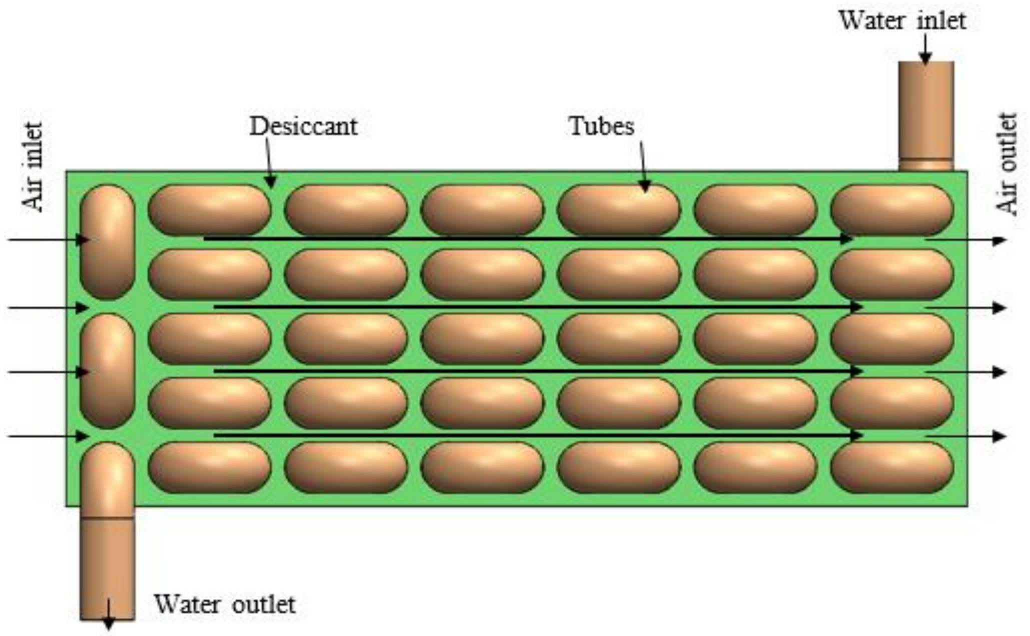

Figure 3.6 Front view of DCHE without casing

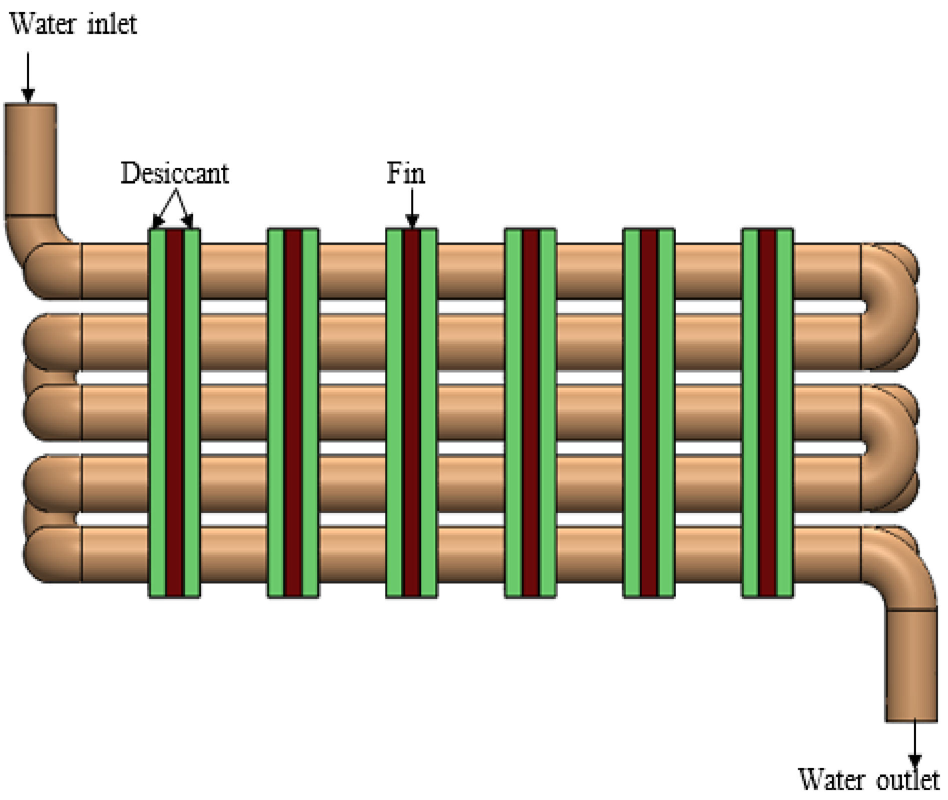

Figure 3.7 Right view of DCHE without casing

3.1.3 M-cycle

The M-cycle heat and mass exchanger consisting two parallel channels (dry and wet channels). The entire remaining dry air from DCHE enters the dry channels and a fraction of it diverted to the wet channel as it flow along the length of dry channel through uniformly distributed holes (that holed on the interface of wet and dry channel) and sensible cooled by wet channel airflow. Due to this structure, the wet-channel airflow becomes pre-cooled, which maximize the cooling efficiency of this heat and mass exchanger.

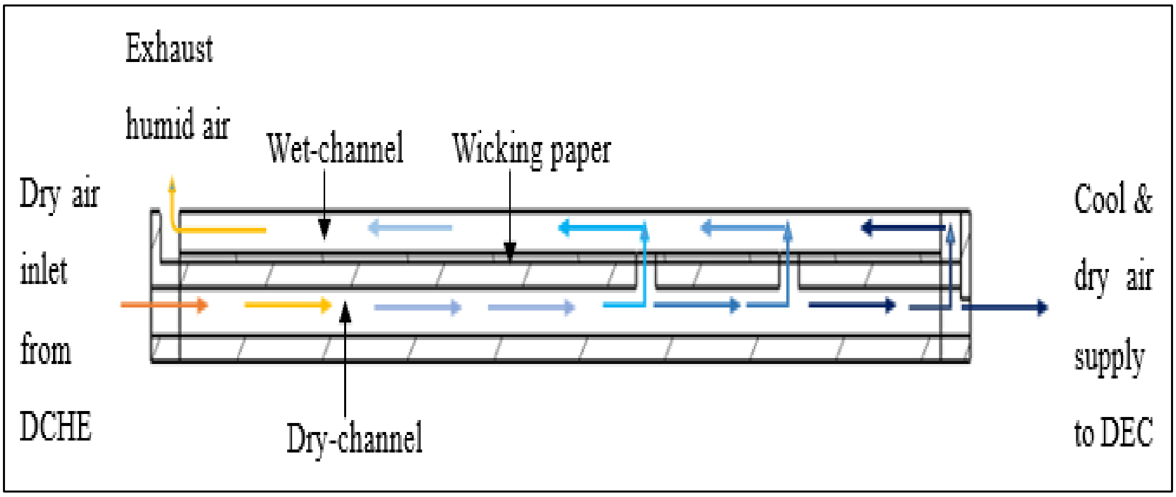

Figure 3.8 Flow schematics of M-cycle HME

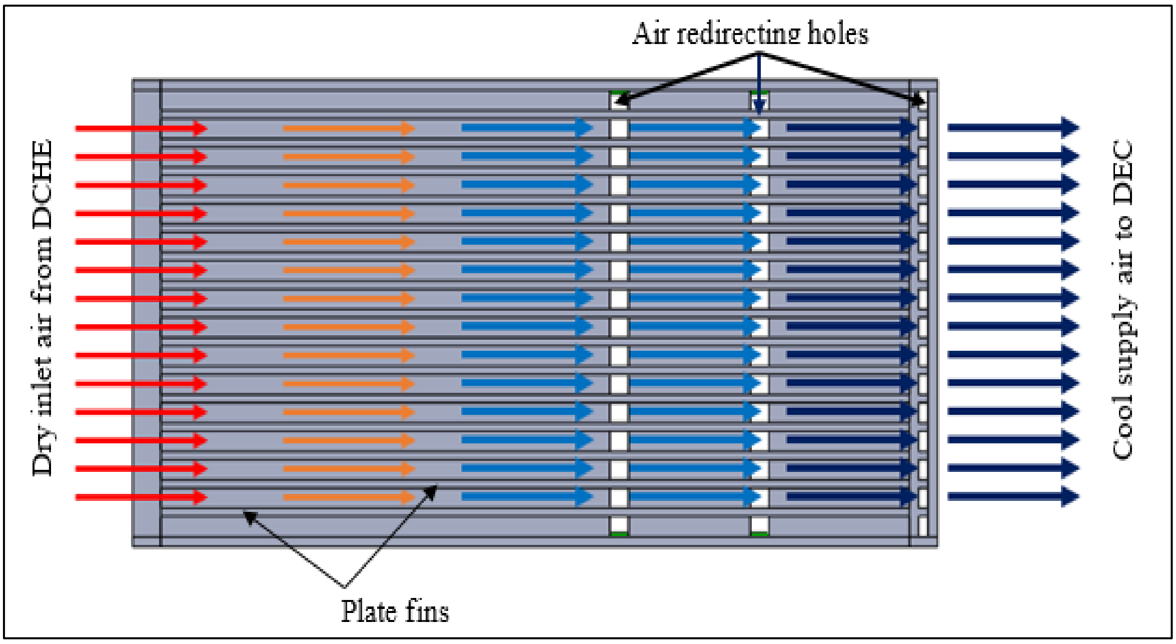

Figure 3.9 Flow schematics of Dry-channel (bottom view)

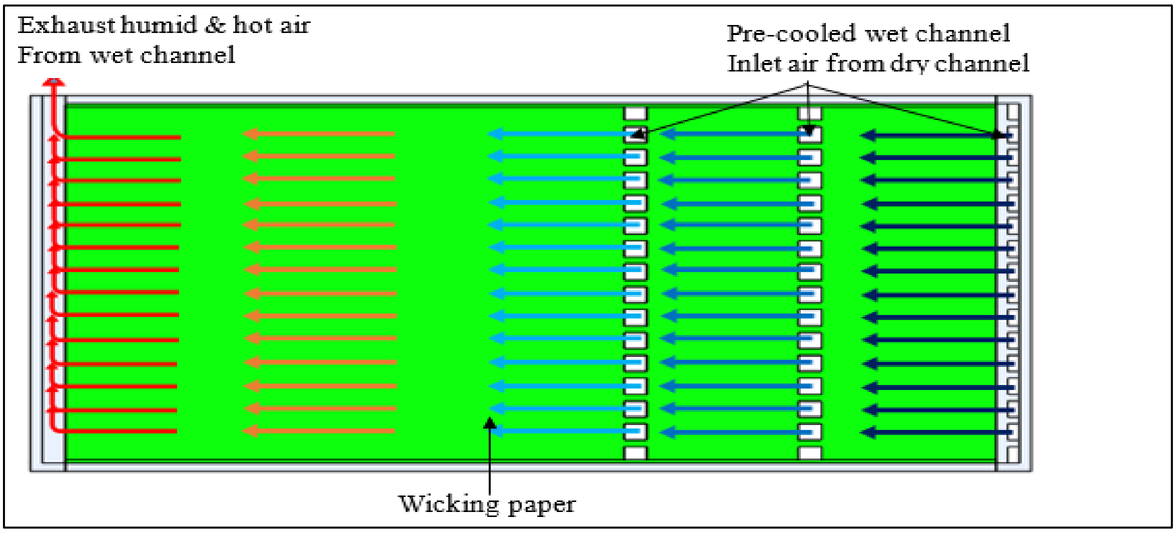

Figure 3.10 Flow schematics of Wet-channel (Top view)

3.1.4 Psychrometric chart.

Process (1-2) is an isothermal dehumidification process in DCHE. Process (2-3) is the sensible cooling process in M-cycle IEC. Process (3-4) is the humidification process in direct evaporative cooler where the humidity and the temperature of the air increased and decreased respectively. The condition at point 4 is the required air condition for storage. During the process of (4-8) the exhaust air from the room heated by both sensible and latent heat from the product.

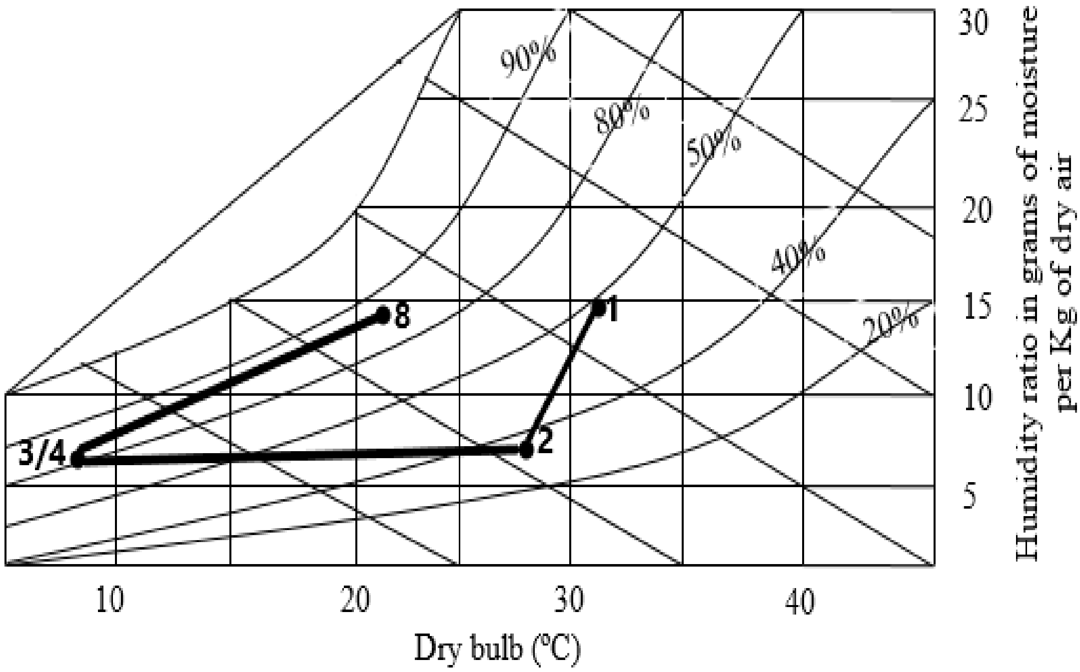

Figure 3.11 Psychometric process of one-stage enhanced evaporative cooling system configuration

3.1.5 SIMPLE Algorithm

The SIMPLE stands for Semi-Implicit Method for Pressure-Linked Equations. The algorithm essentially a guess-and-correct procedure for the calculation of pressure field. This algorithm were given on Figure 3.12

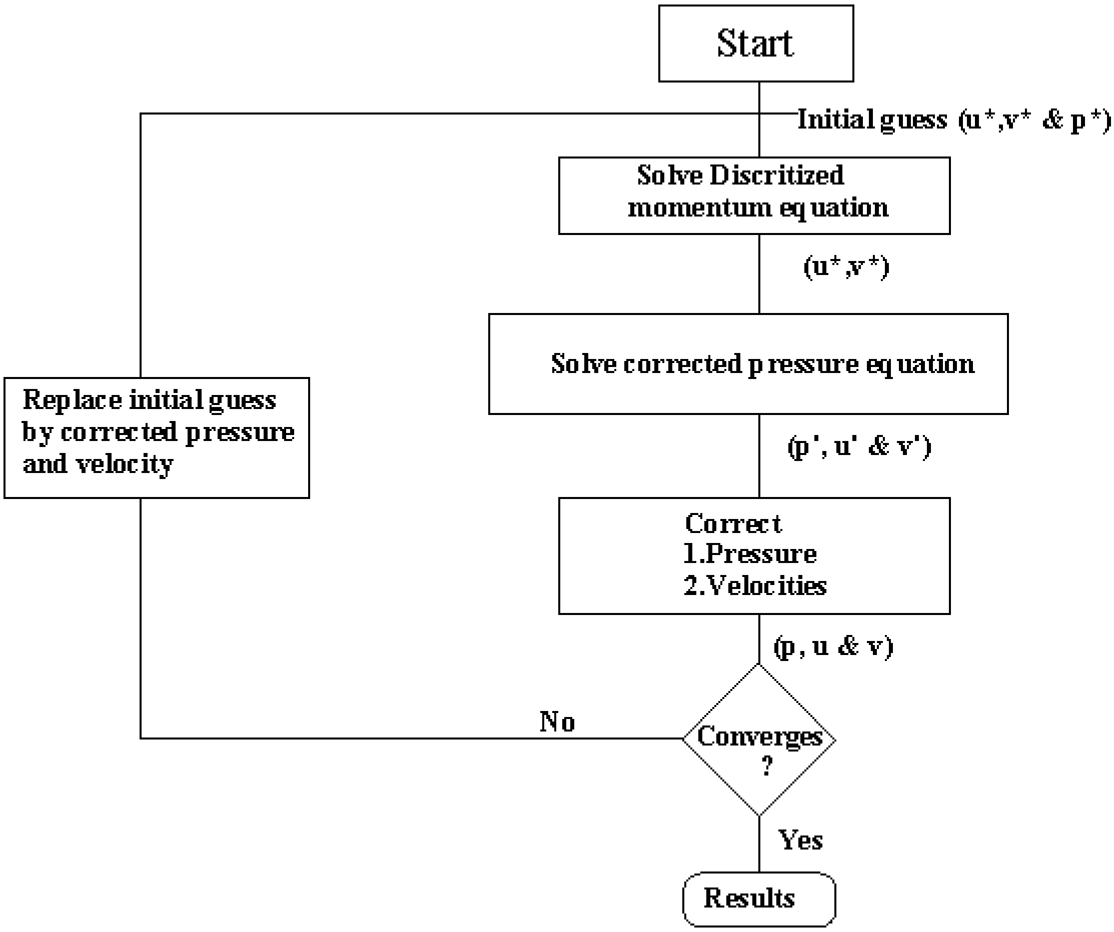

Figure 3.12 SIMPLE Algorithm

3.2 Data Collection and Analysis

Extensive literature review is considered as the secondary data sources in order to identify the properties of the produce, the previous work contribution and obtain standard data's about the available technologies. In addition to this the solar radiation and climate data of Meki can be collected from the Adama metrology station.

3.2.1 Case study area description

This study was conducted in Oromia region, East Shewa zone at Meki irrigation schemes. Due to available enough water resources, and suitable landscape with conducive environment this area is good for vegetables production especially of tomato. The main water sources this area is Meki river (for upper irrigation scheme) and Ziway lake (for down irrigation scheme).

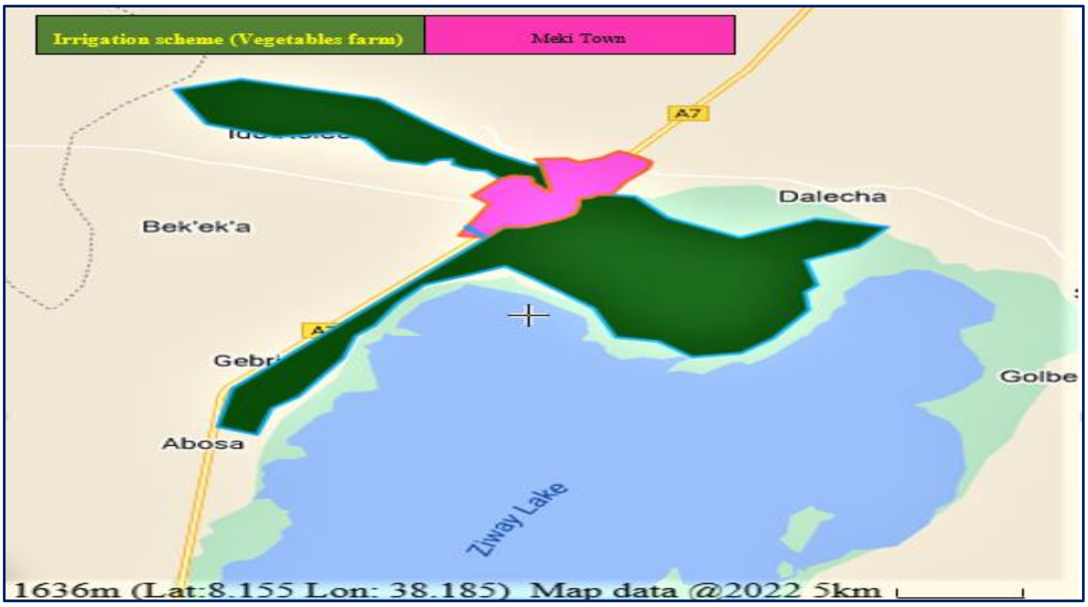

Figure 3.13 Map of the study area of Meki irrigation scheme

3.2.2 Solar data collection

The solar and climate condition data's of the study area (Meki) were collected from Ethiopian metrological service. The average hourly and monthly data of relative humidity, specific humidity, ambient temperature, wind speed and surface pressure of five years measured at 2m height are summarized on the figures shown below.

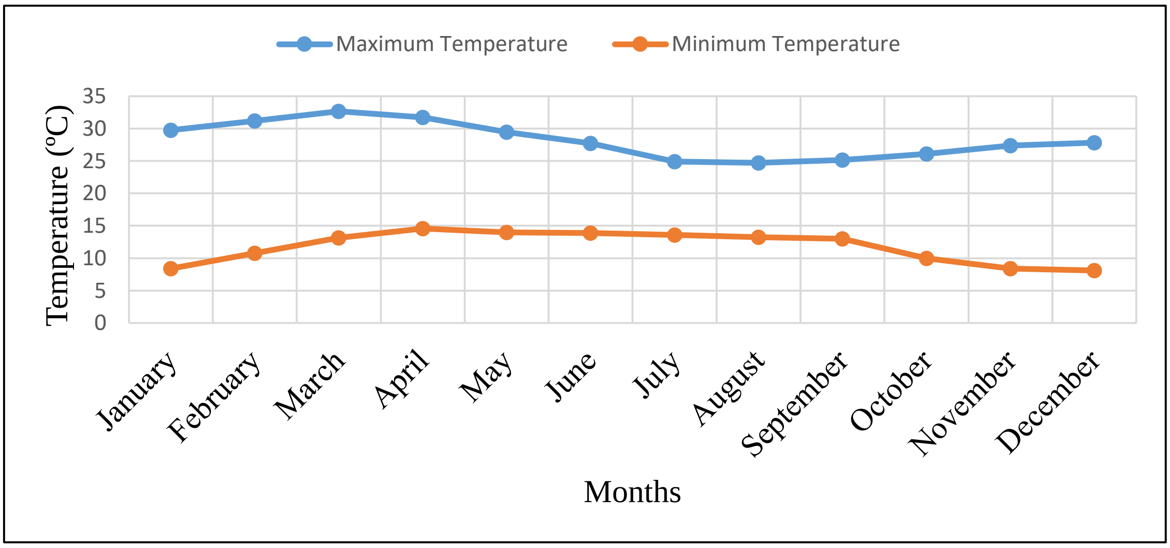

Figure 3.14 The five years average monthly maximum and minimum Temperature of Meki (Adama metrology station)

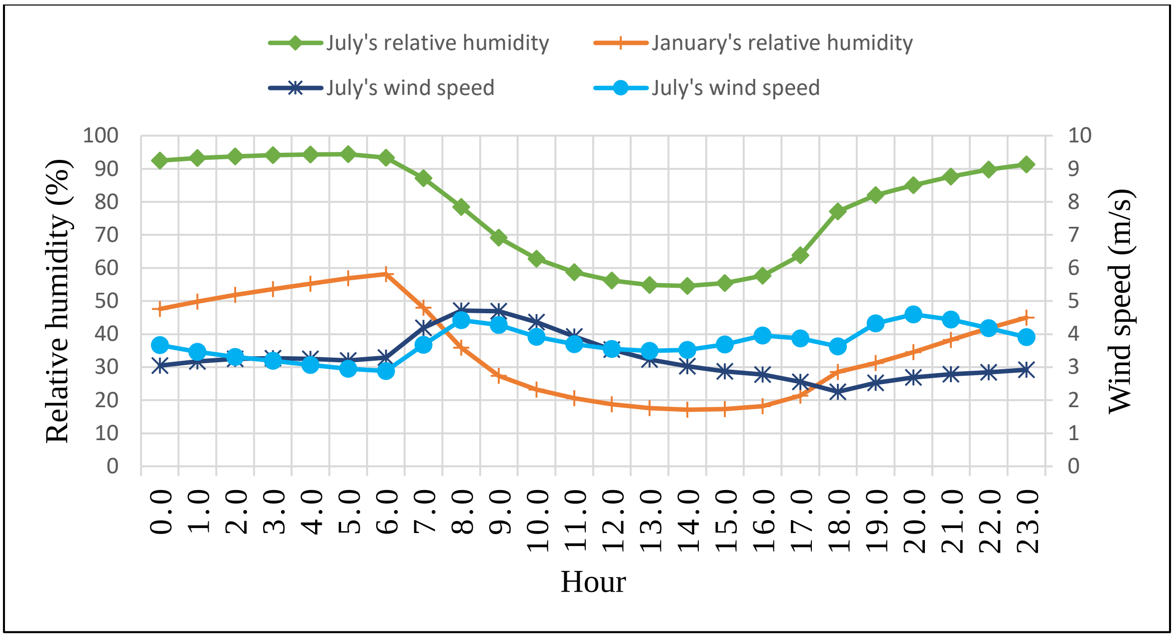

Figure 3.15 The five years January's and January's average hourly climate condition of Meki (Adama metrology station)

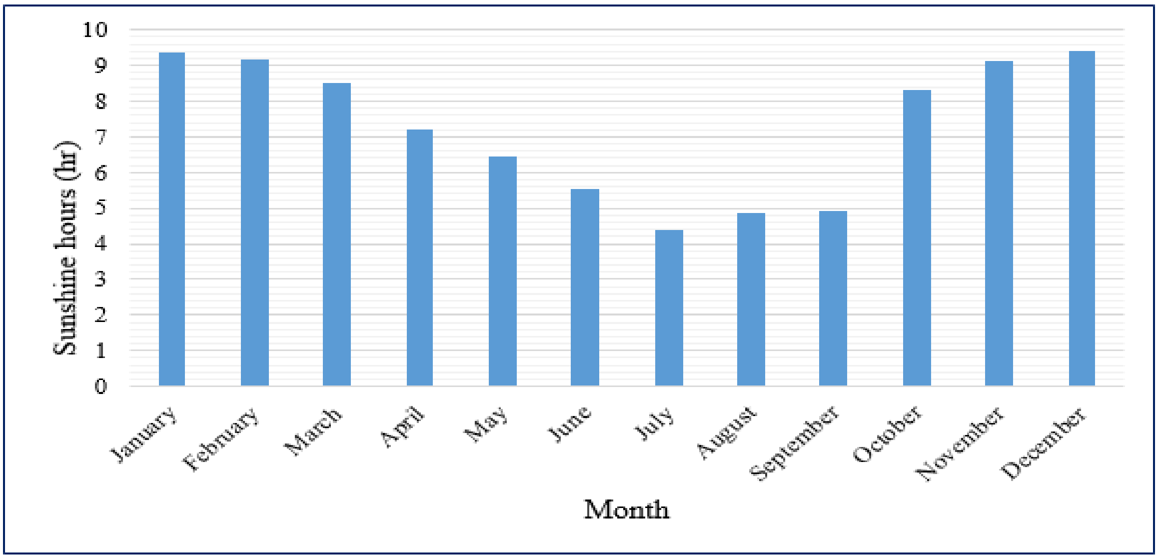

Figure 3.16 Sunshine hour for the representative day of each month in Meki, for an average climatic condition of five years (Adama metrology station)

3.2.3 Production data collection

A questioner was designed and used to collect primary data from tomato producers about the tomato production (area and yield) and harvesting (number of harvesting cycle physical characteristics of harvesting crate). Two stage sampling technique was used to select vegetables producers. Two (from upper irrigation scheme) and Three (from down irrigation scheme) tomato producing kebeles were identified. Then based on random sampling a total of 72 farmers were selected and considered from five kebeles. The summary collected data's is given below.

Table 3.1 Tomato's production data at farms around Meki

Kebele	Number of selected farmer	Production area (ha)	Yield(kg)	Maximum yield per cycle per ha
Haxe	3.0	20.0	1440000.0	28800.0
Giraba	3.0	22.0	1531200.0	27840.0
Bekele-girisa	22.0	38.0	2014000.0	21200.0
Wolda-kalina	22.0	36.0	1944000.0	21600.0
Wolda-maqdala	22.0	35.0	1925000.0	22000.0
Total	72.0	151.0	8854200.0	
Average area per farmer	2.1			
Average yield per hectare	58637.1			
Maximum yield per cycle per hectare	28800.0			

3.3 Materials

Table 3.2 Materials

Types	Materials
Phase change materials	Erytritol
Solid desiccant	Silica gel
Evaporative pad	Palash fibers

3.4 Analysis tools

Table 3.3 Tools

Software's type	Used for
Math lab	Performances analysis
Excel	Data analyzing
Microsoft's word	Document preparing
Microsoft's power point	Document presenting

CHAPTER FOUR

SOLAR RADIATION DATA AND COOLING LOAD ESTIMATION

4.1 Estimation of solar radiation potential

4.1.1 Solar geometries

In order to estimate the solar radiation of study area, different solar geometry and solar angular dimensions were required. The following are the basics solar geometries (Duffie, 2013).

i. Latitude (ϕ): - It is the angular location in reference of equator toward either north or south. Measurement toward north and south is considered as positive and negative respectively. Meki is located at a latitude of 8.1552 due north.

ii. Slope (β): - It is the angle between the plane of the surface and the horizontal.

iii. Declination angle (δ): - The angular position of the sun at solar noon to the plane of the equator, north positive. It given by,

$$\delta = 23.45 sin\left(\frac{360(284+n)}{365}\right) \quad (4.1)$$

Where, n is the representative day of month.

iv. Hour angle (ω): - The angular displacement of the sun east due to rotation of the earth on its axis at 150 per hour, (morning negative, afternoon positive).

$$\omega = 15(solar\ time - 12) \quad (4.2)$$

v. Zenith angle (θ_Z): - The angle between the vertical and the line to the sun or the angle of incidence of beam radiation on a horizontal surface.

$$\theta_Z = cos\phi cos\delta cos\omega + sin\phi sin\delta \quad (4.3)$$

vi. Angle of incidence(θ): - The angle between the beam radiation on a surface and the normal to that surface.

$$\theta = cos^{-1}\big(cos\phi cos\omega(cos\phi cos\beta + sin\phi sin\beta) + sin\delta(sin\phi cos\beta - cos\phi sin\beta)\big) \quad (4.4)$$

vii. Sunset hour (ω_s): - The sunset hour angle is the negative of the sunrise hour angle.

$$\omega_s = cos^{-1}(-tan\phi tan\delta) \quad (4.5)$$

viii. Sunrise hour (N_s): - The total duration in hours of the Sun's movement from sunrise to sunset.

$$N_S = \frac{2}{15}\left(cos^{-1}(-tan\phi tan\delta)\right) \qquad (4.6)$$

4.1.2 Prediction of extraterrestrial radiation on a horizontal surface

The extraterrestrial radiation is a radiation which available outside the atmosphere and it is predicted by equation (9) (Duffie, 2013).

$$H_O = \frac{24*3600}{\pi} I_{SC}\left(1 + 0.033cos\frac{360n}{365}\right)\left(cos\phi cos\delta sin\omega_S + \frac{\pi\omega_S}{180} sin\phi sin\delta\right) \qquad (4.7)$$

Where, I_{SC} is in watts per square meter and Ho is in joules per square meter per day.

4.1.3 Prediction of monthly average daily global radiation on a horizontal surface

Angstrom relation were used to estimate the monthly average daily global radiation on horizontal surfaces (Duffie, 2013).

$$H = H_O\left(a + b\left(\frac{\bar{n}_S}{\bar{N}_S}\right)\right) \qquad (4.8)$$

Where,

$$a = -0.11 + 0.235cos\phi + 0.323\frac{\bar{n}_S}{\bar{N}_S} \qquad (4.9)$$

$$b = 1.449 - 0.533cos\phi - 0.694\frac{\bar{n}_S}{\bar{N}_S} \qquad (4.10)$$

$\bar{N}_S$ is monthly average daily hours of bright sunshine (sunshine hour) and $\bar{n}_S$ is monthly average of the maximum possible daily hours of bright sunshine.

4.1.4 Prediction of monthly average daily diffuse and beam radiation on a horizontal surface

The monthly average daily diffuse radiation were calculated from the monthly average daily global radiation on horizontal surfaces (Duffie, 2013).

$$H_D = H\left(0.931 - 0.814\frac{\bar{n}_S}{\bar{N}_S}\right) \qquad (4.11)$$

The monthly average daily beam radiation is given by,

$$H_B = H - H_D \qquad (4.12)$$

The monthly average solar radiation of the study area (Meki) is given on Figure 4.1. March is the hottest month of the year with 22.7MJ/m2/day. This indicated the maximum sensible load for the room can result in this month (March).

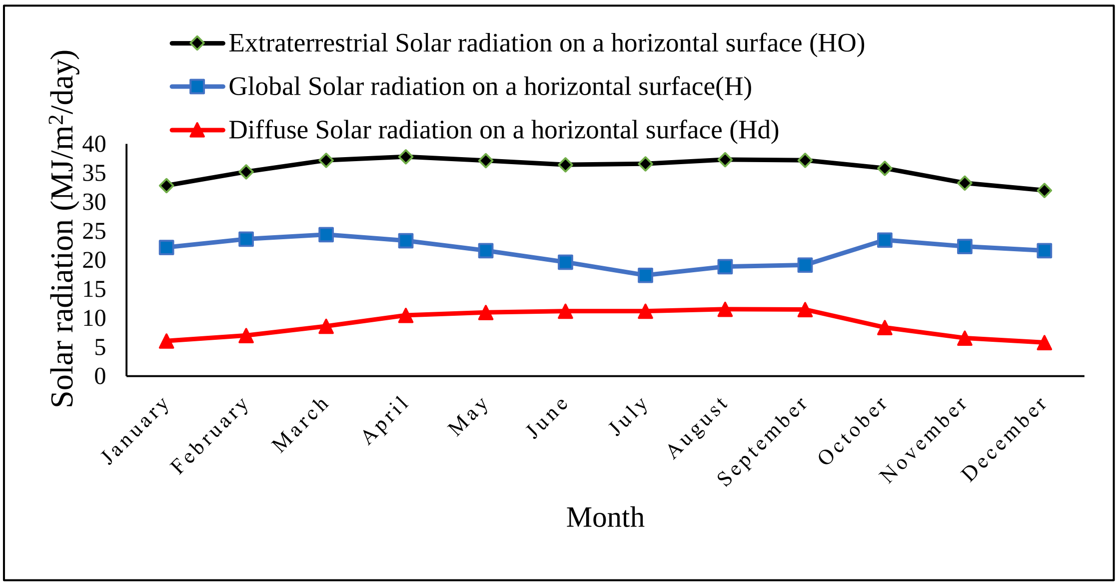

Figure 4.1 Monthly average Extraterrestrial, global, and diffuse radiation on a horizontal surface in Meki

4.1.5 Prediction of monthly average hourly global, diffuse and beam radiation on a horizontal surface

The monthly average hourly global radiation on a horizontal surface can be calculated from the the monthly average daily global radiation on a horizontal surface (Duffie, 2013).

$$I = H\frac{\pi}{24}(a1 + b1cos\omega)\left(\frac{cos\omega - cos\omega_S}{sin\omega_S - \frac{\pi\omega_S}{180}cos\omega_S}\right) \quad (4.13)$$

$$a1 = 0.409 + 0.5016sin(\omega_S - 60) \quad (4.14)$$

$$b1 = 0.6609 - 0.4767sin(\omega_S - 60) \quad (4.15)$$

$$I_D = H_D\frac{\pi}{24}\left(\frac{cos\omega - cos\omega_S}{sin\omega_S - \frac{\pi\omega_S}{180}cos\omega_S}\right) \quad (4.16)$$

$$I_B = I - I_D \quad (4.17)$$

Where, I, I_D and I_B are the monthly average hourly global, diffuse and beam radiation on a horizontal surface respectively and given in joules per square meter per hour.

4.1.6 Prediction of total radiation on sloped surfaces for isotropic sky

$$I_T = I_B R_B + I_D\left(\frac{1+\cos\beta}{2}\right) + I\rho_g\left(\frac{1-\cos\beta}{2}\right) \quad (4.18)$$

Where, I_T are the monthly average hourly total radiation on a horizontal surface and given in joules per square meter per hour.

$$R_B = \frac{\cos\theta}{\cos\theta_Z} \quad (4.19)$$

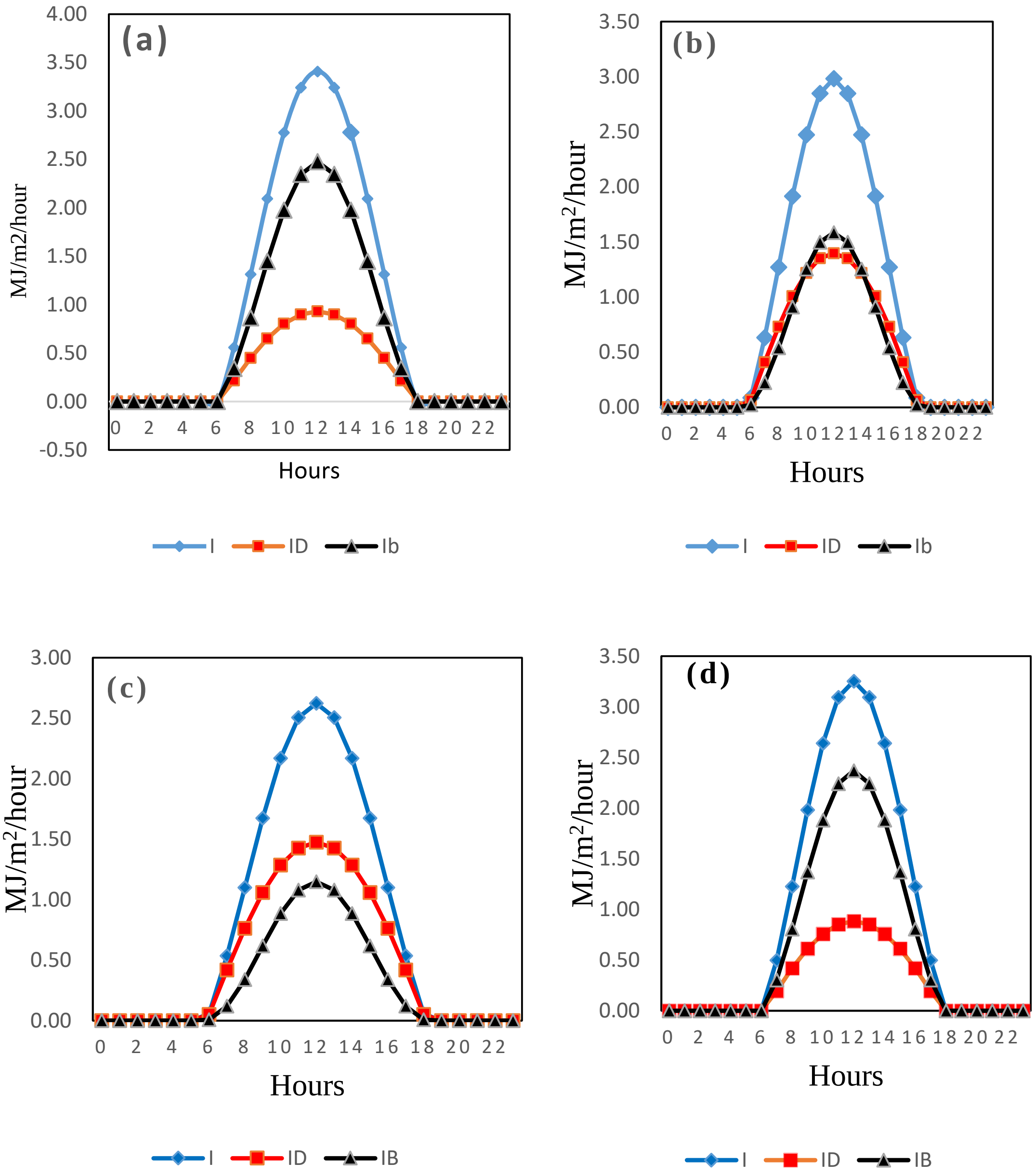

Figure 4.2 Hourly global (I), diffuse (ID) and beam (IB) radiation on a collector surface (30º tilted) for (a) February, (b) May, (c) August and (d) November

Hourly variation of ambient: - The hourly variation of ambient temperature is required to analysis the thermal performances of the thermal solar collector. Since this temperature is not available in the metrological service, it can be computed from daily maximum and minimum data's of ambient temperature. The correlation used to compute the hourly distribution of ambient temperature from minimum and maximum daily temperature is given by (Kalogirou, 2004).

$$T(t) = T_{max} - \frac{(T_{max} - T_{min})}{2}\left[1 - \sin\frac{(\pi t - 9\pi)}{2}\right] \quad (4.20)$$

The hourly temperature of an ambient air estimated from the daily mean maximum and daily mean minimum temperatures. Figure 4.3 gives this hourly distribution an ambient air temperature. From the figure, the maximum 31.5ºC results at 14:30 hour and the minimum 10.5ºC results at 6:00 hour.

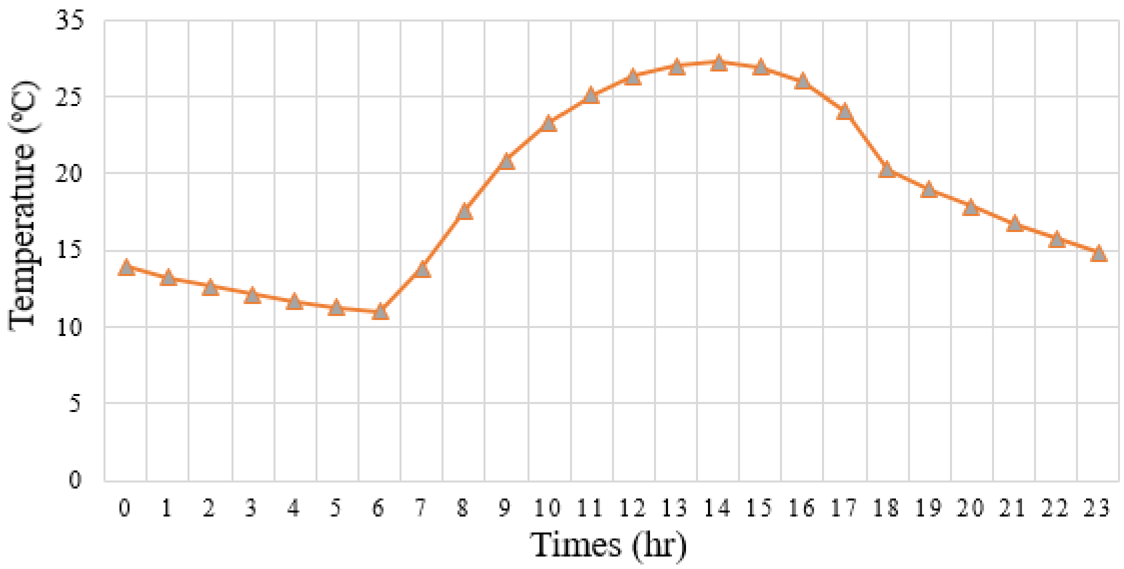

Figure 4.3 Hourly variation of ambient temperature of Meki in (℃) for March

4.2 Cooling Load Calculation

In order to slow down the deterioration of the produce, the temperature of the storage room should lowered and maintained to certain storage temperature level by removing a heat from the room continuously. The cooling load represents an amount of heat should be removed from the room to attain the desired storage temperature. It used to determine the cooling capacity of the cooling equipment. The main loads those accounts for cooling load are, transmission load (heat transferred through roof, wall and floor of storage room), product load (heat transferred from the produce to the room by respiration and field heat), internal load (heat transferred from people, lighting, equipment and machines to the room) and infiltration load (heat transferred to the room due to air exchange and ventilation) (Krishnakumar, 2017). The equations and detail description of these load were summarized in ANNEX-C, Table-C1.

Assumption:

- The heat transfer through floor is negligible

A. Transmission (wall) load

$$Q_W = \left[\frac{(10.584+0.0847v_i+0.0235v_o)}{(4.87+0.02467v_i+0.0086v_o)}\right](T_o - T_i) \quad \text{…………………………….………… (4.21)}$$

B. Product field load

$$Q_p = 66.797\left(T_f - T_i\right) \quad \text{……………………………………………………..…. (4.22)}$$

C. Respiration heat load

$$Q_R = 1.692\,\frac{kWh}{day} \quad \text{…………………………………………………….…… (4.23)}$$

D. Service load: The serqvice load includes load of people, equipment, filtration and lighting. These loads accounts 10% of the cumulative loads of wall and product loads.

$$Q_S = 0.1\left(Q_W + Q_R + Q_p\right) \quad \text{…………………………………………….…… (4.24)}$$

Therefore, to accounts for error it is recommended to use a safety factor in calculation. The recommended range of safety factor is between 1.1 and 1.5. In this calculation 1.3 safety factor were used. Then the total cooling load can be:

$$Q_{Total} = 1.43\left(Q_W + Q_R + Q_p\right) \quad \text{…………………………………………..… (4.25)}$$

The cooling load will varies throughout the year and day due to monthly and hourly variation of ambient solar irradiance respectively. Therefore, by considering the hourly and monthly distribution of ambient temperature, the hourly and monthly variation of the cooling load were shown on Figure 4.4 and Figure 4.5 respectively. The maximum monthly load 621KWh/day on March and the maximum daily load 910KWh/day recorded at 13:15 hour.

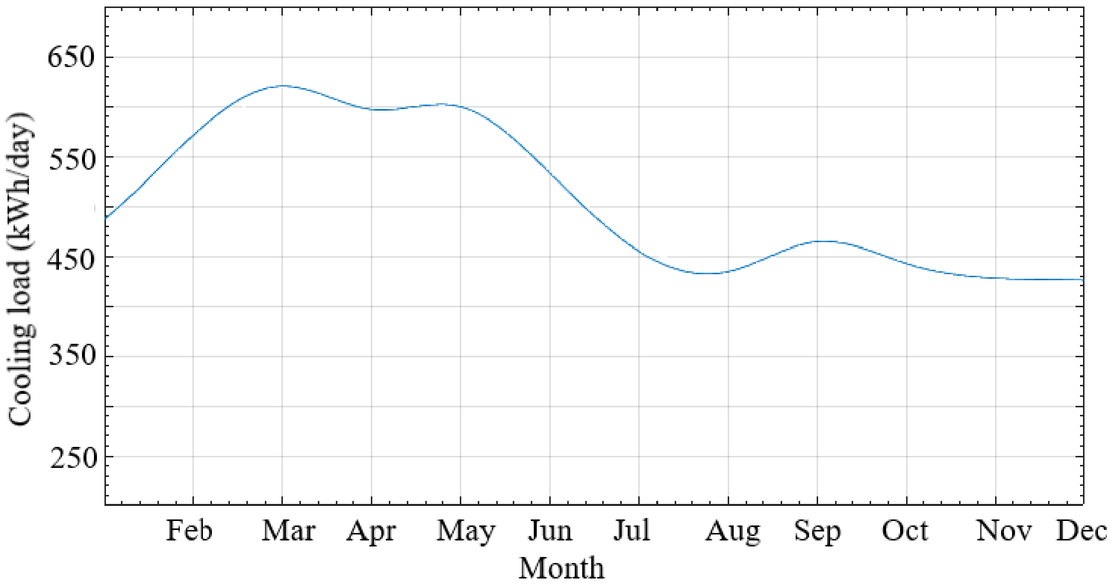

Figure 4.4 Monthly cooling load of storage room

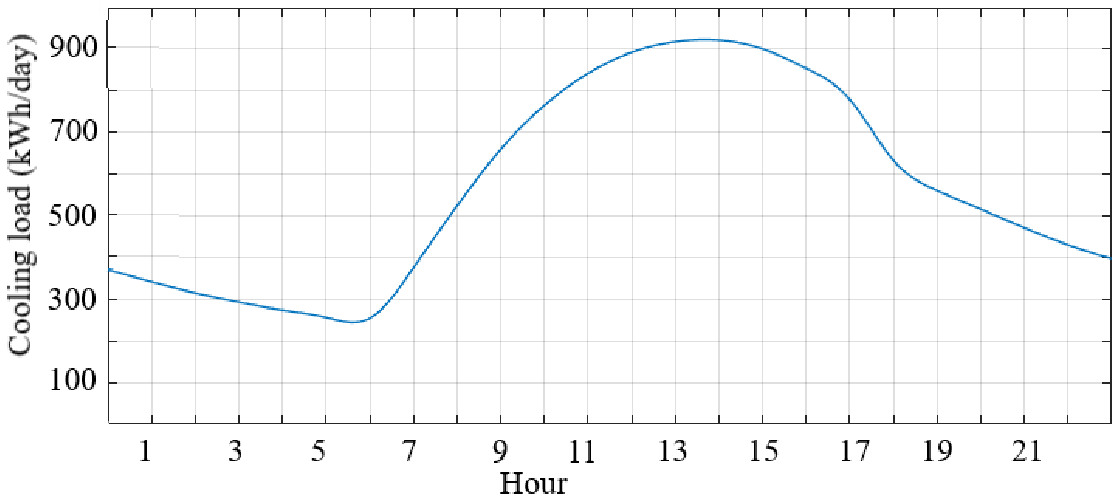

Figure 4.5 Hourly cooling load distribution of storage room on representative day of March

CHAPTER FIVE

MODELING OF ENHANCED EVAPORATIVE COOLING SYSTEM

5.1 Modeling of Storage Room

In this study, the cold-storage room shown on Figure 5.1 were used and in this cooling room, the produces are packed in the wooden boxes. The cold air introduced to the room by fans were distributed to the room uniformly and cool the produce to the required level temperature. The detail layout and design of the room were presented in ANNEX-D.

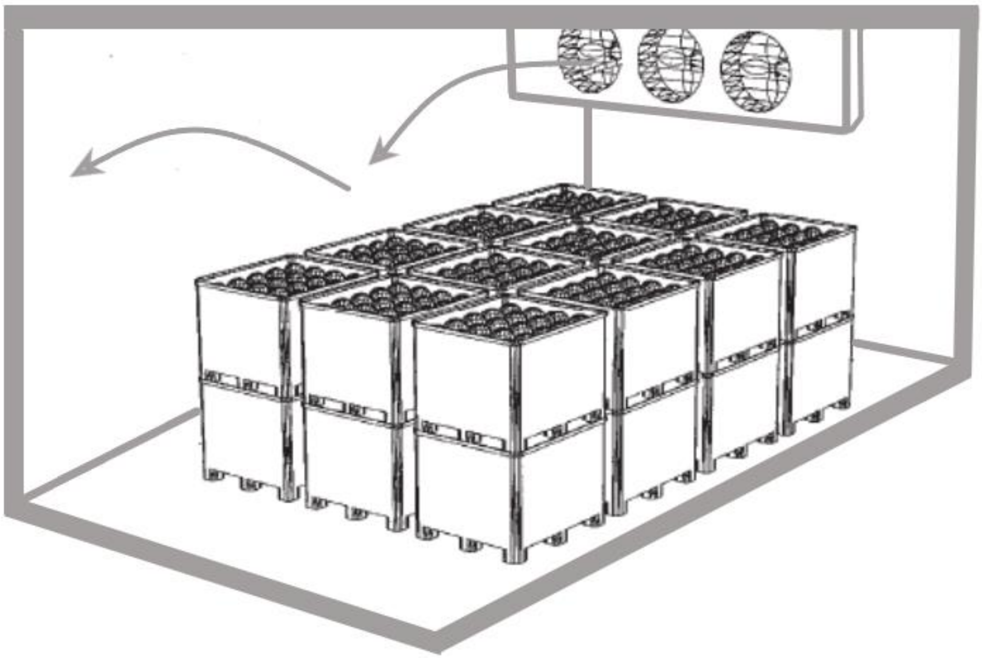

Figure 5.1 Cold-room storage

5.1.1 Warehouse sizing

From (Table 3.1), an average production area per farmer and the maximum yield per one cycle per hectare is 2.1ha and 28800kg respectively. As a result the warehouse should have a total storage capacity of 60480kg. A single crate that the produce harvested and transported can hold an average of 60kg of the produce and had a $0.1125m^3$ of volume. That means 1008 crates required in order to hold 60480kg of produce. Due to this, the production volume of the produce to be stored in the warehouse is $113.4m^3$. To provide volume for spacing of air movement and handling equipment, this volume should be 40% of the total warehouse volume. Therefore, the total volume of the storage/warehouse should be $284m^3$. In order to reduce the surface area to volume ratio to decrease heat dissipation through the surface area, cubic geometry of the storage is selected. As a result, 7m X 7m X 7m size of the storage warehouse is required. The computational model of storage room were given in ANNEX-D.

5.1.2 Governing equation

In order to predict the behavior of the system and know the distribution of temperature and velocity field of supply air inside storage room, the equation that needed to govern the flow and heat transfer process of supply air were developed. The well-known complete Naviers-stoke equation were used as a governing equation. The following assumptions were used to simplify the complexity of Naviers-stoke equation (Versteeg & Malalasekera, 2007).

- Since the supply air is flowing at lower speed, and effects of air viscosity is negligible the flow should considered as incompressible, inviscid, and laminar flow.
- The fan supply an air at constant speed, as a result the flow is steady in velocities field and unsteady in temperature field.
- The effect of body force on the flow is negligible.
- The thermal properties of the air is constant throughout the flow domain and do not vary with time.
- The flow were considered as 2D flow

Based on the above listed assumptions, the simplified Naviers-stoke equation were given by equations (28) to (31) as a general governing equations of supply air flow in storage room.

I. Continuity equation

$$\frac{\partial(\rho u)}{\partial x} + \frac{\partial(\rho v)}{\partial y} = 0 \quad \text{(5.1)}$$

II. Momentum equation

$$u\rho\frac{\partial u}{\partial x} + v\rho\frac{\partial u}{\partial y} = -\frac{\partial P}{\partial x} \quad \text{(5.2)}$$

$$u\rho\frac{\partial v}{\partial x} + v\rho\frac{\partial v}{\partial y} = -\frac{\partial P}{\partial y} \quad \text{(5.3)}$$

III. Energy equation

$$\rho c_v\frac{\partial T}{\partial t} + u\rho c_v\frac{\partial T}{\partial x} + v\rho c_v\frac{\partial T}{\partial y} = \rho\dot{q} + k\left[\frac{\partial^2 T}{\partial x^2} + \frac{\partial^2 T}{\partial y^2}\right] \quad \text{(5.4)}$$

Boundary conditions: -the governing equation of the supply air flow inside storage room given above shows the flow variables depends both on location and time. As a result the boundary conditions and initial conditions of the flow inside flow domain were required in order to solve these equations. The flow domain and boundaries representation is shown on Figure 5-1.

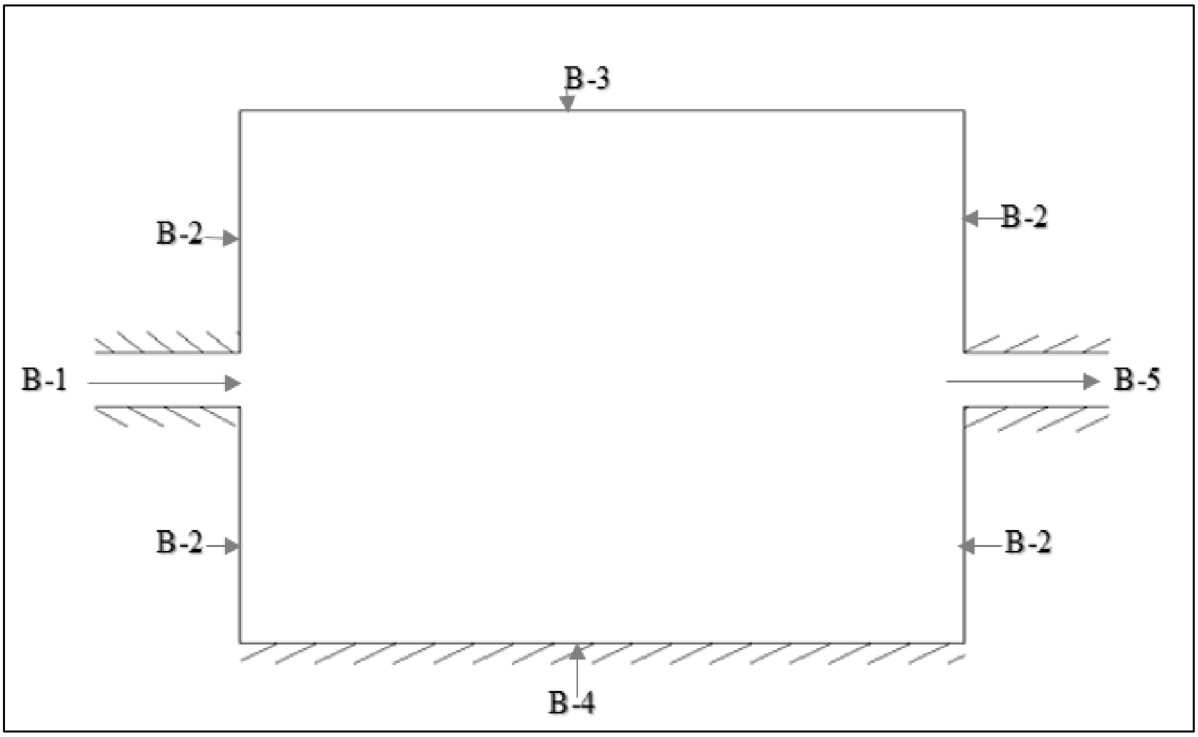

Figure 5.2 Flow domain and boundaries representation

The types and values of these boundary conditions were summarized on Table 5-2.

Table 5.1 Types and values of flow domain boundary conditions (Kanoğlu et al., 2020)

Boundary conditions	Types	Value/expressions
B-1	Drichlet boundary	$u_1, T_1,$ and ρ_1 known
B-2	Drichlet and Neumann boundary	$-k\dfrac{\partial T}{\partial x_2} = \acute{q}_2, v_2 \neq 0, u_2 = 0$
B-3	Drichlet and Neumann boundary	$-k\dfrac{\partial T}{\partial x_3} = \acute{q}_3, u_3 \neq 0, v_3 = 0$
B-4	Drichlet and Neumann boundary	$-k\dfrac{\partial T}{\partial x_4} = \acute{q}_4, u_4 \neq 0, v_4 = 0$
B-5	Neumann boundary	$\dfrac{\partial u}{\partial x} = 0 \rightarrow u_{1=}u_2$

Note: $\acute{q}_2, \acute{q}_3$ and $\acute{q}_4$ are the heat transfer load to the storage room through wall, ceiling and floor respectively. They directly computed from the room's transfer cooling load.

Grid generation: -The two-dimensional problem domain and its grid points were given below.

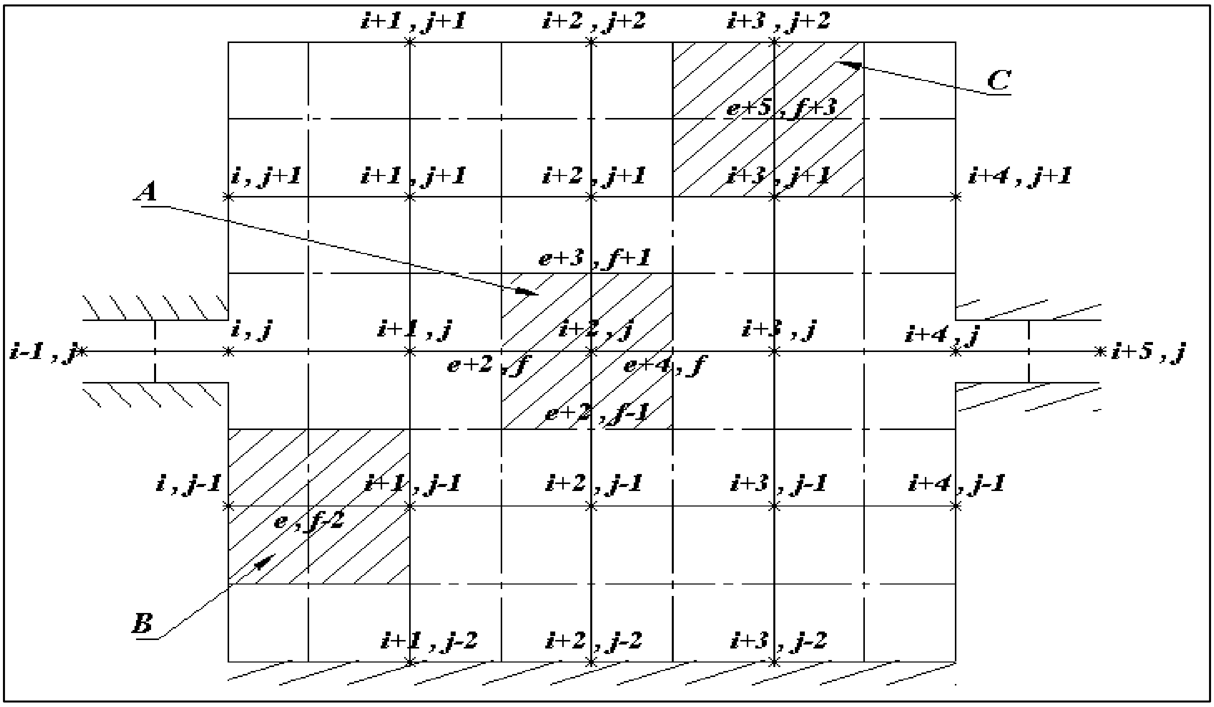

Figure 5.3 Two dimension control volume's main (A) and staggered (B and C) grid representation

Note: (i, j) or (e, f) and (I,J) are the face-point and control volume's grid-point index respectively.

5.1.3 Discretization of governing equation

In this computation, Finite volume discretization method were employed to discretize the general governing equation over each control volumes of the flow domain. Power-law scheme were used to interpolate the dependent variables at the control-volume's face-point. There are several assumptions made in the ways of discretizing the general governing equations. These are: -

- The dependent variable between adjacent grid-point has a piece-wise linear profile function variation.
- The new value of transient dependent variables were prevails over the entire time step.

- The heat generation inside the room is independent of transient temperature variation inside room.
- The mass flow rate through a control volume face-point is prevails over the whole interface.
- The velocity field were calculated at the control volume's face-point and all other dependent variables evaluated at the main grid-point.

The linear algebraic equation were obtained by integrating each of the governing equation over each control volume in finite-volume discretization.

a. Discretized continuity equation

$$(\rho u)_{i+1,j} - (\rho u)_{i,j} + (\rho v)_{i+1,j} - (\rho u)_{i+1,j} = 0 \quad \ldots\ldots\ldots\ldots \text{(5.5)}$$

b. Discretized momentum equation

$$a_{i,j}u_{i,j} = \sum a_{nb}u_{nb} + b_{i,j} + A_{xi,j}\left(P_{I-1,J} - P_{I+1,J}\right) \quad \ldots\ldots\ldots\ldots \text{(5.6)}$$

$$a_{i,j}v_{i,j} = \sum a_{nb}v_{nb} + b_{i,j} + A_{yi,j}\left(P_{I,J-1} - P_{I,J+1}\right) \quad \ldots\ldots\ldots\ldots \text{(5.7)}$$

The momentum equation can be solved only when the pressure field is given or estimated.

$$u'_{i,j} = d_{i,j}(P'_{I-1,J} - P'_{I+1,J}) \quad \ldots\ldots\ldots\ldots \text{(5.8)}$$

$$v'_{i,j} = d_{i,j}(P'_{I,J-1} - P'_{I,J+1})$$

$$a_{i,j}\acute{P}_{I,J} = a_{i+1,j}\acute{P}_{I+1,J} + a_{i-1,j}\acute{P}_{I-1,J} + a_{i,j+1}\acute{P}_{I,J+1} + a_{i,j-1}\acute{P}_{I,J-1} + b_{I,J} \quad \ldots\ldots\ldots \text{(5.9)}$$

c. Discretized Energy equation

$$a_{i,j}T_{I,J} = a_{i+1,j}T_{I+1,J} + a_{i-1,j}T_{I-1,J} + a_{i,j+1}T_{I,J+1} + a_{i,j-1}T_{I,J-1} + b_{I,J} \quad \ldots\ldots\ldots \text{(5.10)}$$

5.1.4 SIMPLE Algorithm for storage room

The SIMPLE-algorithm were developed to solve the unknown pressure and velocity field iteratively. This algorithm were given on Figure 5.4 to solve the velocity and pressure corrected equation that given in equation (4.33) and (4.34) respectively.

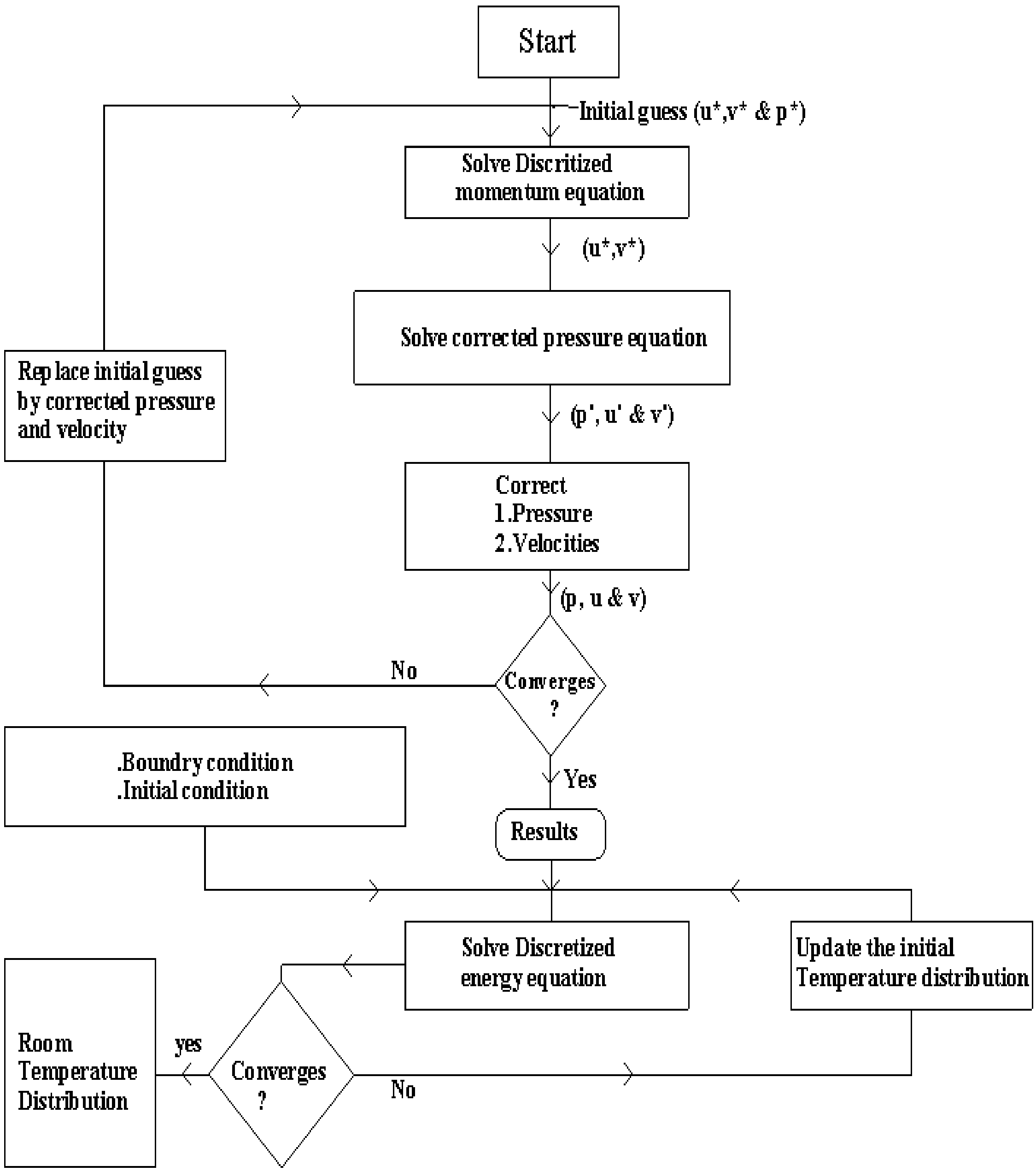

Figure 5.4 Simple algorithm of storage room's temperature and velocity distribution computation

5.2 Modeling of Heat Pipe Evacuated Tube Solar Collector

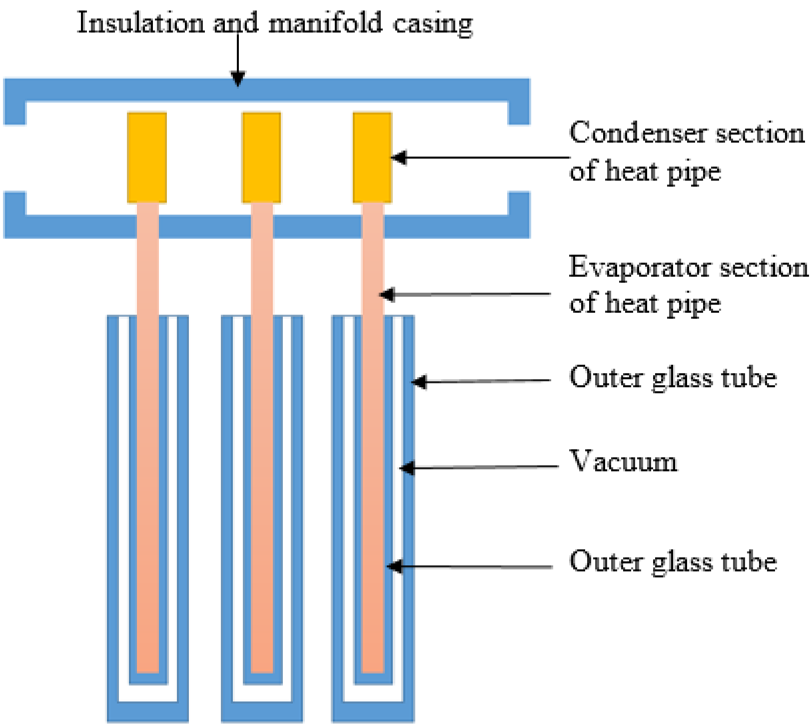

Figure 5.5 Schematic of heat pipe evacuated tube solar collector

Selection and sizing of HPETSC: - for this study heat pipe evacuated tube collector were used. This collector type preferred over others due to the presence of vacuum in annular space between two concentric glass tubes, this eliminates sun tracking by its tubular design. From the commercial available models ThermoPower-VHP30 heat pipe evacuated tube collector which manufactured by SunMaxx solar were selected. These collectors are cost-effective and extremely efficient even in low light condition. The manufacturer specification of this heat pipe evacuated tube collector is given in ANNEX-B, Table-B1.

Assumptions:- in order to develop a mathematical model for the selected heat pipe evacuated tube solar collector, the following assumptions were used.

- The temperature gradient along the longitudinal direction of absorber is negligible.
- Temperature variation is to be assumed in the radial direction only.
- Heat lost into the surrounding from the manifold is neglected.
- Heat loss coefficient between collector and ambient is constant.
- The inlet temperature of the working fluid is similar with an ambient temperature.

The solar energy is the source of heat in the solar collectors. These heat transfer can occur through conduction, convection and radiation process. The evacuated tube is comprising the heat pipe (comprising evaporator and condenser section), absorber, and outer glass cover. From the energy balance of these collector's part, the following conservation energy equation would drived.

i. Outer glass-cover

$$\frac{\rho_g V_g (C_p)_g \partial T_g}{\partial t} = A_g (1-\tau)_g I + A_g U_{ab,g}(T_{ab} - T_g) - A_g U_{g,amb}(T_g - T_{amb}) \quad (5.11)$$

ii. Absorber

$$\frac{\rho_{ab} V_{ab} (C_p)_{ab} \partial T_{ab}}{\partial t} = A_p\left[(\tau\alpha)_{ab} I - U_{ab,g}(T_{ab} - T_g) - U_{ab,ev}(T_{ab} - T_{ev})\right] \quad (5.12)$$

iii. Evaporator section

$$\frac{\rho_{ev} V_{ev} (C_p)_{ev} \partial T_{ev}}{\partial t} = A_{ab} U_{ab,g}(T_{ab} - T_{ev}) - A_{ev} U_{ev,con}(T_{ev} - T_{con}) \quad (5.13)$$

iv. Condenser section

$$\frac{\rho_{con} V_{con} (C_p)_{con} \partial T_{con}}{\partial t} = A_{ev} U_{ev,con}(T_{ev} - T_{con}) - A_{con} U_{con,w}(T_{con} - T_w) \quad (5.14)$$

v. Working fluid

$$\dot{m}_w C_{p,w} \frac{\partial T_w}{\partial t} = A_{con} U_{con,w}(T_{con} - T_w) - \dot{m}_w C_{p,w} \frac{\partial T_w}{\partial x} \quad (5.15)$$

The overall heat transfer coifficient between heat pipe, absorber, outer glass, ambient air and working fluid (water) are given by equation (5.16) to (5.20).

$$U_{ab,g} = \sigma(T_{ab}^2 + T_g^2)(T_{ab} + T_g) / \left(1/\varepsilon_{ab} + 1/\varepsilon_g - 1 \right) \quad (5.16)$$

$$U_{g,amb} = \varepsilon_g \sigma (T_{amb}^2 + T_g^2)(T_{amb} + T_g) + (5.7 + 3.8 v_w) \quad (5.17)$$

$$U_{ev,con} = (0.997 - 0.334 (cos\beta)^{0.108}) \left(\frac{k_l^2 \rho_w^2 g h_{fg}}{\mu L_{con}(T_{ev} - T_{con})} \right)^{0.25} \left(\frac{L_{con}}{D_{man,in}} \right)^{(0.254(cos\beta))^{0.38}} \quad (5.18)$$

$$U_{ab,ev} = 0.555 \left[g\rho_1(\rho_l - \rho_v) k_l^3 h_{fg} \Big/ \mu_1 (T_{ab} - T_{ev}) D_{ev} \right]^{\frac{1}{4}} \quad (5.19)$$

$$U_{con,w} = 0.555 \left[g\rho_1(\rho_l - \rho_v) k_l^3 h_{fg} \Big/ \mu_1 (T_{ab} - T_{ev}) D_{con} \right]^{\frac{1}{4}} \quad (5.20)$$

From the energy balance for the working fluid, the usefull energy gained by the wolking fluid is given by:

$$Q_u = \dot{m}c_p\left(T_{fo} - T_{fi}\right) \qquad (5.21)$$

The above listed differential equation were solved using finite difference method, in which the partial differentials replaced by difference equation.

$$T_{g,i}^{n} = T_{g,i}^{n-1} + \frac{\Delta t}{\rho_g V_g (C_p)_g}\Big(A_g(1-\tau)_g I + A_g U_{ab,g}\left(T_{ab} - T_g\right) - A_g U_{g,amb}\left(T_g - T_{amb}\right)\Big)_i^{n-1} \qquad (5.22)$$

$$T_{ab,i}^{n} = T_{ab,i}^{n-1} + \frac{\Delta t}{\rho_{ab} V_{ab} (C_p)_{ab}}\big(A_p\big[(\tau\alpha)_{ab} I - U_{ab,g}\left(T_{ab} - T_g\right) - U_{ab,ev}(T_{ab} - T_{ev})\big]\big)_i^{n-1} \qquad (5.23)$$

$$T_{ev,i}^{n} = T_{ev,i}^{n-1} + \frac{\Delta t}{\rho_{ev} V_{ev} (C_p)_{ev}}\Big(A_{ab} U_{ab,g}(T_{ab} - T_{ev}) - A_{ev} U_{ev,con}(T_{ev} - T_{con})\Big)_i^{n-1} \qquad (5.24)$$

$$T_{con,i}^{n} = T_{con,i}^{n-1} + \frac{\Delta t}{\rho_{con} V_{con} (C_p)_{con}}\Big(A_{ev} U_{ev,con}(T_{ev} - T_{con}) - A_{con} U_{con,w}(T_{con} - T_w)\Big)_i^{n-1} \qquad (5.25)$$

$$T_{w,i}^{n} = \frac{(\Delta x - 1)}{\Delta x} T_{w,i}^{n-1} + \frac{\Delta t}{m_w C_{p,w}}\Big(A_{con} U_{con,w}(T_{con} - T_w)\Big)_i^{n-1} + \frac{1}{\Delta x} T_{w,i-1}^{n-1} \qquad (5.26)$$

The reseonable initial guess for mean absorber plate of liquid heating collectors given by,

$T_{ab}{}^{0} = T_{amb}{}^{0} + 5°C$

$T_g{}^{0} = T_{amb}{}^{0} + 4°C$

$T_{ev}{}^{0} = T_{amb}{}^{0} + 4.5°C$

$T_{con}{}^{0} = T_{amb}{}^{0} + 3°C$

$T_{w_i}^{0} = T_{amb}{}^{0} + 2°C$

$T_{w_{i-1}}^{0} = T_{amb}{}^{0} + 1°C$

Where, n=1,2,3….,n And i= 1,2,3…,i

Sizing: - The total number of collectors required is calculated from the total load and gained usefull energy by collector as follow,

$$N = \frac{Q_L}{Q_u} * 3600 * 24 \qquad (5.27)$$

5.3 Packed Bed Thermal Energy Storage Modeling

From the available latent thermal energy storage, packed bed latent heat storage systems has high heat transfer area between and the heat transfer fluid and as a result it have been selected for this investigation. In packed bed latent heat storage systems spheres of phase change material serves as the storage medium.

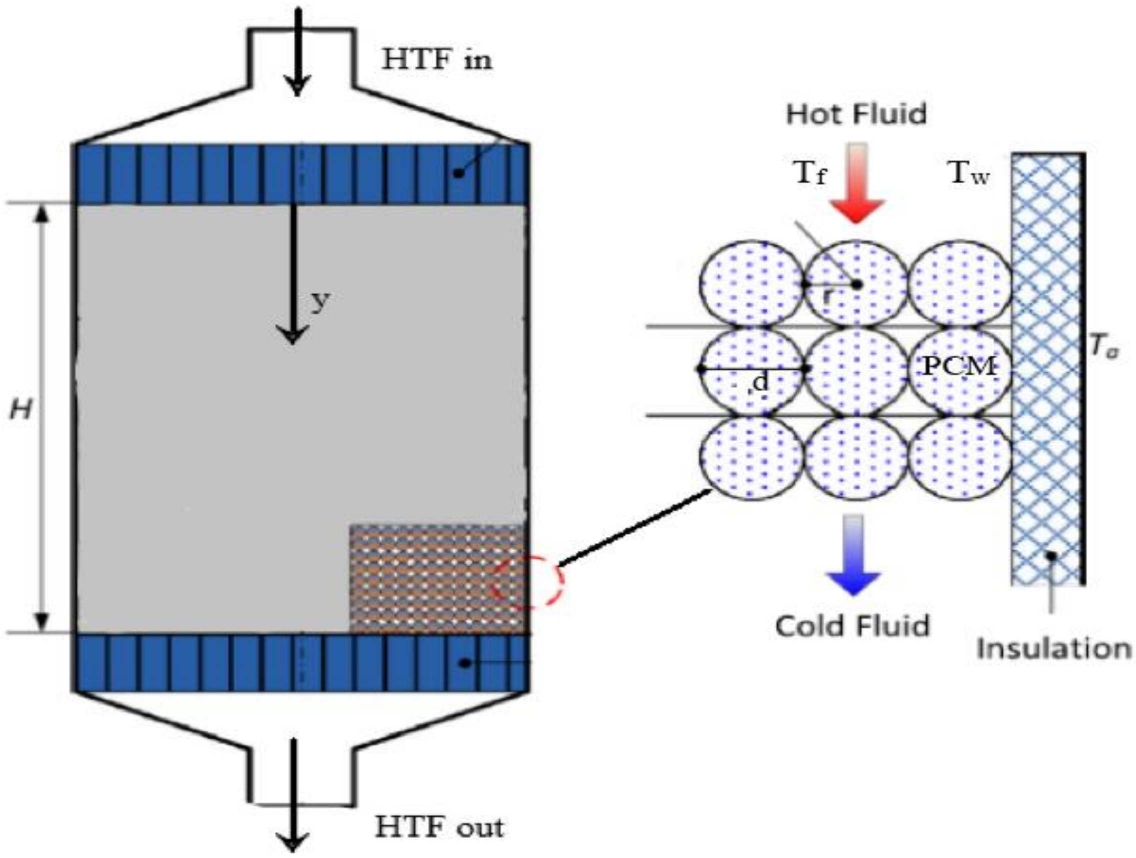

Figure 5.6 Schematics of PBTES model

Erytritol were selected as a phase change material in this study and it has a melting temperature of 117ºC.

Table 5.2 The thermos physical properties of Erytritol (Elias & Stathopoulos, 2019)

State	Melting temperature (ºC)	Thermal conductivity $(\frac{W}{m.K})$	Density $(\frac{kg}{m^3})$	Specific heat capacity $(\frac{kJ}{kg.K})$	Viscosity $(\frac{kg}{m.s})$	Melting enthalpy $(\frac{kJ}{kg})$
Solid	117	0.3261	1482	1.392	0.029	340
liquid	-	0.7332	1300	2.761	0.016	-

The Schumann's model, is one of the three's two phase models used for modeling the PCM packed bed system numerically. In this model the one-dimensional heat transfer were assumed and heat conduction is not considered neither for the axial nor the radial direction. The equation of energy conservation for heat transfer fluid and solid particle (bed) were given by equation (5.28) and (5.29) respectively.

The following assumptions were used to develop this model.

- Thermal and physical properties of both solid and fluid are uniform and constant.
- Heat transfer coefficient does not vary with time.
- No mass transfer heat loss occurs.
- The inlet temperatures of hot and cold fluids are constant.

$$\varepsilon\left(C_p\rho\right)_f\left(\frac{\partial T_f}{\partial t}+u\frac{\partial T_f}{\partial y}\right)=h_{pcm-htf}\left(T_{pcm}-T_f\right)-U_L\left(T_f-T_{amb}\right) \quad (5.28)$$

$$(1-\varepsilon)\rho_{pcm}\frac{\partial H}{\partial t}=h_{pcm-htf}\left(T_f-T_{pcm}\right) \quad (5.29)$$

The Nusselt number were required inorder to determine the heat transfer coefficient between the working fluid and PCM.

Sizing: - The size of thermal energy storage was determined based on the energy demands of the system. By assuming the total thermal heat stored in the storage is the total useful heat recovered from HPETSC, the mass of PCM required were given on equation (5.30).

$$m_{PCM}=\frac{Q_u}{C_p(\Delta T+\Delta h_m)} \quad (5.30)$$

5.4 Desiccant-Coated Heat and Mass Exchanger Modeling

In desiccant coated heat exchanger the fins of the tubes coated with a desiccant materials on its surface. The cooling water (to remove the sorption heat) and heating water (to regenerate the desiccant) can flows through the tubes during the dehumidification or regeneration of the exchanger respectively. For this study, silica gell were selected as the

In order to develop the mathematical model for desiccant coated heat exchanger and simplify the problem, the following assumptions are made:

- The desiccant material is uniformly coated on the surface of the heat exchanger.
- The heat and mass transfer coefficient are constant over the entire heat exchanger.
- During the dehumidification process, the sorption heat is released immediately and it occur at the interface.

By applying the conservation of mass on air and desiccant domain, the governing continuity equation of water-vapor in air and adsorbed water in desiccant given in equation (5.31) and (5.32) respectively.

$$\frac{\partial M_a}{\partial t} + U_a \frac{\partial M_a}{\partial x} = A_1\left(M_{d,s} - M_a\right) \quad (5.31)$$

$$\frac{\partial M_d}{\partial t} = D_{d,a}\left(\frac{\partial^2 M_d}{\partial x^2} + \frac{\partial^2 M_d}{\partial z^2}\right) + A_2 \quad (5.32)$$

The governing energy equation of air stream given in equation (5.33) were obtained by applying the conservation of energy on air and similarly, the governing energy equation of desiccant, fin and tubes carrying cooling or heating water given in equation (5.34).

$$\frac{\partial T_a}{\partial t} + U_a \frac{\partial T_a}{\partial x} = A_3(T_d - T_a) \quad (5.33)$$

$$A_4 \frac{\partial T_d}{\partial t} + A_5 \frac{\partial T_a}{\partial t} = A_6 T_d + A_7 T_a + A_8 \quad (5.34)$$

Where, M_a and M_d are the air and desiccant material humidity ratio respectively. T_a and T_d are the temperature in the air and desiccant domain respectively. $\eta_{f,app}$ and A_n (which given in ANNEX-C Table-C2) are the apparent fin efficiency and coefficients respectively (n is from 1 to 9).

Equations (5.35) to (5.38) can be solved numerically using finite difference method. The difference equation of these equations were given by,

$$M_{a,i}^{n} = M_{a,i}^{n-1} + \frac{\Delta t U_a}{\Delta x}\left(M_{a,i-1}^{n-1} - M_{a,i}^{n}\right) + \Delta t A_1\left(M_{d,s} - M_a\right)_i^{n-1} \quad (5.35)$$

$$M_{d,i}^{n} = M_{a,i}^{n-1} + \Delta t D_{d,a}\left(\frac{M_{a,i}^{n-1} - 2M_{a,i-1}^{n-1} - M_{a,i}^{n-1}}{\Delta x^2}\right) + \Delta t A_2 \quad (5.36)$$

$$T_{a,i}^{n} = T_{a,i}^{n-1} + \frac{\Delta t U_a}{\Delta x}\left(T_{a,i-1}^{n-1} - t_{a,i}^{n}\right) + \Delta t A_3(T_d - T_a)_i^{n-1} \quad (5.37)$$

$$T_{d,i}^{n} = T_{d,i}^{n-1} + \frac{A_5}{A_4}\left(T_{a,i}^{n-1} - T_{a,i}^{n}\right) + \frac{A_6}{A_4} T_{d,i}^{n-1} + \frac{A_7}{A_4} T_{a,i}^{n-1} + \frac{A_8}{A_4} \quad (5.38)$$

Initial conditions:-The initial conditions for air and desiccant is assumed to be their inlet condition at the start of the process and it is uniform.

$$T_{a,i}^{(n=0)} = T_{a,in}$$

$$T_{d,i}^{(n=0)} = T_{d,in}$$

$$M_{a,i}^{(n=0)} = M_{a,in}$$

$$M_{d,i}^{(n=0)} = M_{d,in}$$

Boundary conditions: - similarly the inlet boundary conditions for the air stream will be the inlet condition of the air.

$$T_{a,(i=0)}^{n} = T_{a,in}$$

$$M_{a,(i=0)}^{n} = M_{a,in}$$

5.5 M-cycle Indirect- Evaporative Cooling Heat and Mass Exchanger Modeling

The common methods that used for evaluating the thermal performance of a sensible heat exchanger is a log mean temperature difference (LMTD). However, directly it does not applied for a heat exchanger where the latent heat is associated. Here the mathematical model were developed and it is useful in evaluating the performances of regenerative indirect evaporative cooling heat and mass exchangers.

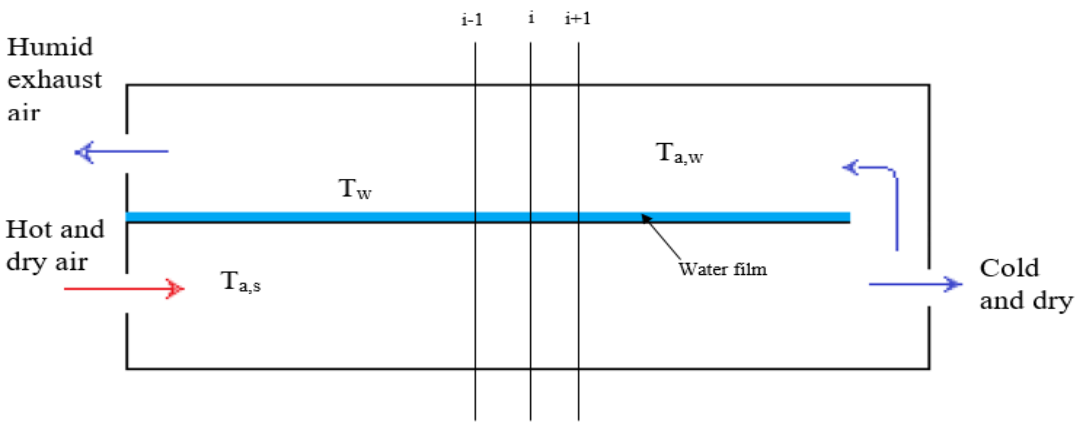

Figure 5.7 Schematics of M-cycle model

The following assumptions were made to develop mathematical model:

- The water film is evenly distributed on wet surfaces
- The heat and mass transfer occurs in the direction normal to the air flow
- The air flow is fully developed and laminar
- No heat transfer occurs to the surrounding

The governing energy equation of air stream given in equation (5.39) and (5.40) were obtained by applying the conservation of energy on dry wet channel air stream respectively.

$$\frac{dT_{a,s}}{dx} = C_1(T_w - T_{a,s}) \quad \text{(5.39)}$$

$$\frac{dT_{a,w}}{dx} = C_2\left(T_w - T_{a,w}\right) + \frac{dM_{a,w}}{dx}(T_w - T_{a,w}) \quad \text{(5.40)}$$

Similarly, from the mass balance of wet channel, the differential equation for humidity ration were given by equation (5.41)

$$\frac{dM_{a,w}}{dx} = C_3(M_w - M_{a,w}) \quad \text{(5.41)}$$

CHAPTER SIX

THERMAL PERFORMANCE ANALYSIS

6.1 Performances of Heat-Pipe Evacuated-Tube Solar Collector

The instantaneous efficiency of collector and the useful heat gained by collector are the main performance's measurements of HPETSC. Instantaneous efficiency of the collector is the ratio of useful heat gained by a collector to the absorbed solar radiation by a collector. The useful heat gained and instantaneous efficiency of the collector were given by equation (6.1) and (6.2) respectively.

$$Q_u = \dot{m}C_p\left(T_{fo} - T_{fi}\right) \qquad (6.1)$$

$$\eta = \frac{Q_u}{I_T A_{ab}} \qquad (6.2)$$

Where, usefull heat gain is the same as the net heat transferred to the working fluid.

6.2 Performances of Packed-bed Thermal Energy Storage

The key performances indicator of many thermal energy storage are an energy storage efficiency and the charging or discharging time. The storage efficiency measures the amount thermal energy extracted during discharging in reference to the energy stored during the charging process. It is given by the ratio of extracted energy to stored energy as shown on equation (6.3).

$$\eta_{st} = \frac{Q_{ext}}{Q_{st}} \qquad (6.3)$$

Similarly, the charging or discharging time show the total time required to fully charge the storage or to fully discharge the storage. It given by equation (6.4).

$$t_{charge} = \frac{m_{HTF}}{\dot{m}_{HTF}} \qquad (6.4)$$

6.3 Performances of Desiccant Coated Heat Exchanger

The cooling capacity and dehumidification capacity are the two indicators that used to evaluate the performances of the desiccant coated heat exchanger. The cooling capacity which given by equation (5.5) indicates how much the air passes through the heat exchanger will decreases in temperature as it loose its humidity to the desiccant material.

$$CC = m_a\left(H_{a,in} - H_{a,out}\right) \qquad (6.5)$$

Where, m_a is mass of dehumidified air and H_a is enthalpy of dehumidifying air.

Similarly, the dehumidification capacity, which is given by equation (6.6) indicates how much of the moisture removed from an incoming ambient air to the desiccant materials.

$$DC = m_a(w_{a,in} - w_{a,out}) \qquad (6.6)$$

Where, m_a is mass of dehumidified air and w_a is humidity ratio of dehumidifying air.

6.4 Performances of M-cycle Indirect Evaporative Cooler

The performances of M-cycle indirect evaporative cooler were measured primarily by the wet-bulb and dew-point effectiveness. Wet-bulb effectiveness measures the ability of wet-channel of the cooler to achieve the wet-bulb temperature of the dry channel air. Similarly, dew-point effectiveness measures the ability of dry-channel of the cooler to achieve the dew-point temperature of the inlet ambient air. The mathematical expressions for wet-bulb and dew-point effectiveness were given by equation (6.7) and (6.8) respectively.

$$\varepsilon_{wb} = {T_{db,in} - T_{db,out}}\Big/{T_{db,in} - T_{wb,in}} \qquad (6.7)$$

$$\varepsilon_{dp} = {T_{db,in} - T_{db,out}}\Big/{T_{db,in} - T_{dp,in}} \qquad (6.8)$$

6.5 Performances of Storage-room

Cooling coefficient and half-cooling time are the two performances indicators of cold storage. Cooling coefficient measures the cooling ability of the produce during the cooling process. It is given by equation (6.9).

$$CC = \frac{hA}{mc_p} \qquad (6.9)$$

The other parameters that used to evaluate the performances the cold storage is the half-cooling time. It indicates the length of time a produce can take to achieve an acceptable level of cooling. It given by equation (6.10).

$$HCT = \frac{\ln(0.5)}{CC} \qquad (6.10)$$

CHAPTER SEVEN

RESULTS AND DISCUSSIONS

7.1 Heat-pipe Evacuated Tube Solar Collector

7.1.1 Useful gained-heat

The hourly useful heat gained by HTF is shown on Figure 7-1 for the representative day of March. The highest hourly useful heat gained were 2.12MW at 0.012kg/s mass flow rate of HTF.

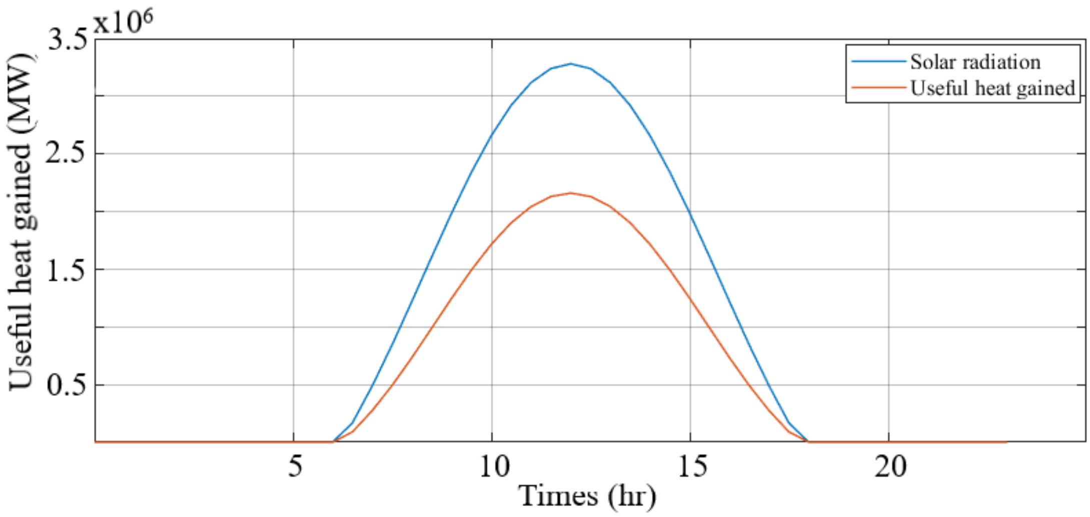

Figure 7.1 Variation of useful heat gained with time

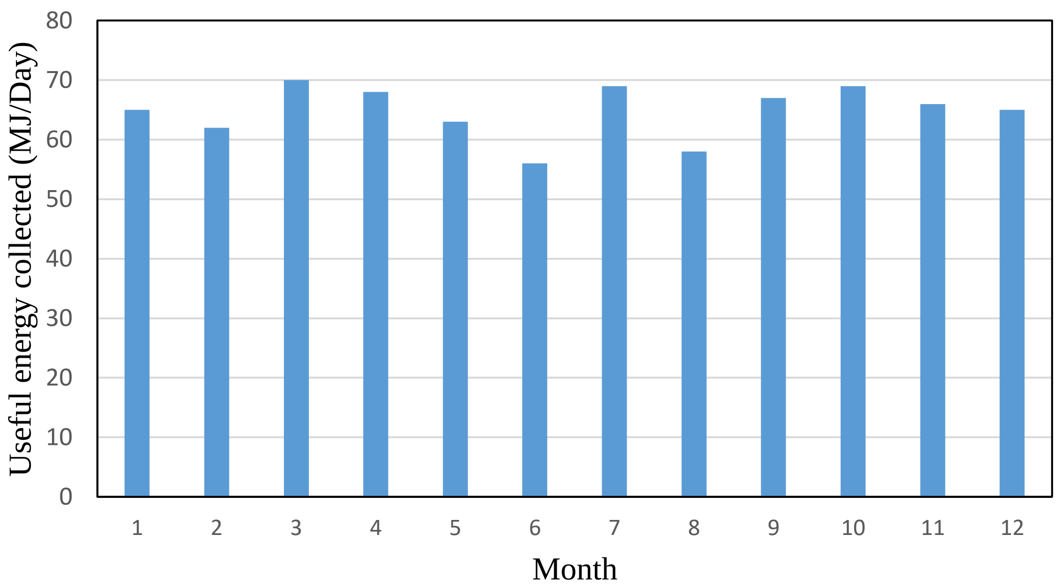

Figure 7.2 Useful energy collected from a single HPETSC for the representative day

7.1.2 Transient outlet temperature of HTF from collector's manifold

The outlet temperature of the HTF or glycol is highly depends on the solar irradiance on the surface of collector. Figure 7-3 shows the outlet temperature variation of the representative day of March. The maximum 139ºC were recorded at 12:40 hour during day. During night since there is no sufficient solar irradiance, the outlet temperature of the HTF almost similar with an ambient temperature. In addition to the solar irradiance, the mass flow rate of HTF greatly affect the outlet temperature. As depicted on Figure 7-4, the outlet temperature decreases as the mass flow rate increases and the maximum outlet temperature 139ºC obtained at 0.012kg/s.

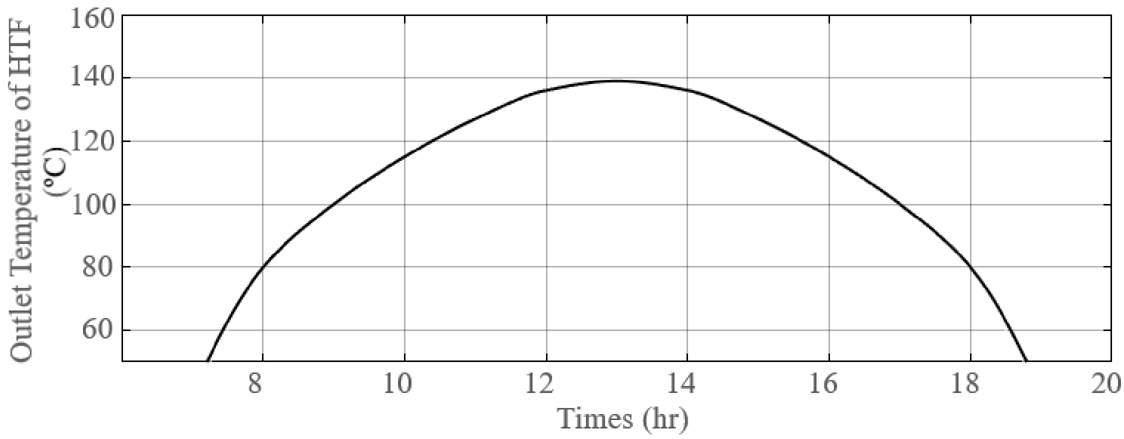

Figure 7.3 Variation of working fluid (glycol) outlet temperature with time

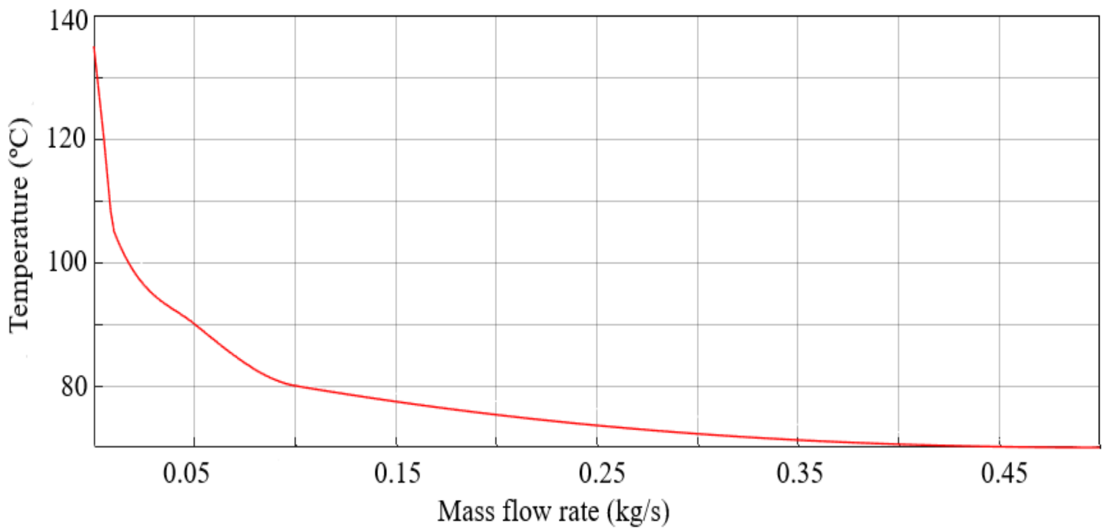

Figure 7.4 Variation of outlet temperature of HTF with mass flow rate

7.1.3 Instantaneous efficiency of HPETSC

The instantaneous efficiency of HPETSC for representative day of March were shown on Figure 7.5. Similar to the outlet temperature of the manifold, instantaneous efficiency affected by the solar radiation reaching the surface of the collector. An instantaneous efficiency inversely related with the solar radiation. This is due to an increase of heat loss to an ambient as the solar irradiance reaching the collector surface increase. The maximum 93.7% efficiency occurred on 16:40 hour and the minimum 85.21% efficiency occurred on 11:20 hour.

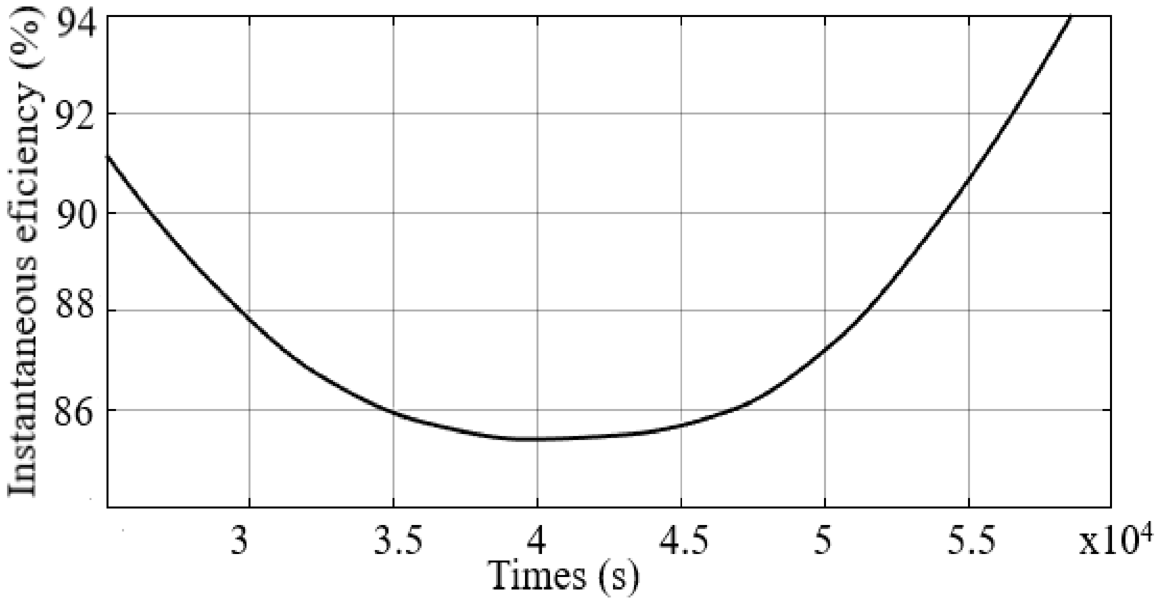

Figure 7.5 Variation of instantaneous efficiency of evacuated tube with time

7.2 Packed-bed Thermal Energy Storage

7.2.1 Charging and discharging temperature

The temperature PCM during charging mode are presented in Figure 7-6. Glycol with flow rate of 0.012kg/s were used as the HTF. From result, the HTF reach the maximum temperature of 117ºC after 5 hours of charging and remain constant at this temperature for the next 5 hour. This imply that the Erytritol starts to melt store the thermal energy at its melting temperature of 18ºC after 4 hour of charging. However, the minimum regeneration temperature required were attained less than 30 minute after charging process started.

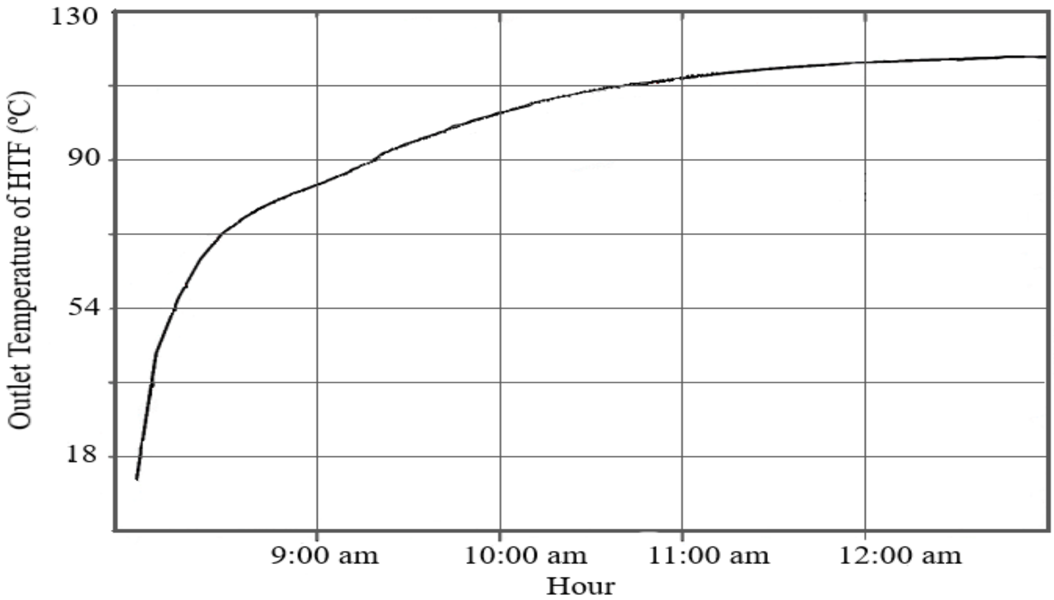

Figure 7.6 Variation of charging temperature with charging time

Figure 7-7 shows the temperature of HTF during the discharging time. From the figure, the glycol draw the thermal energy from the storage thank as a HTF and reach the minimum required temperature for regeneration of 50ºC after 6 hour of discharging process. This shows that the storage tank has a capability of storing thermal energy 6 hour after charging process were halted.

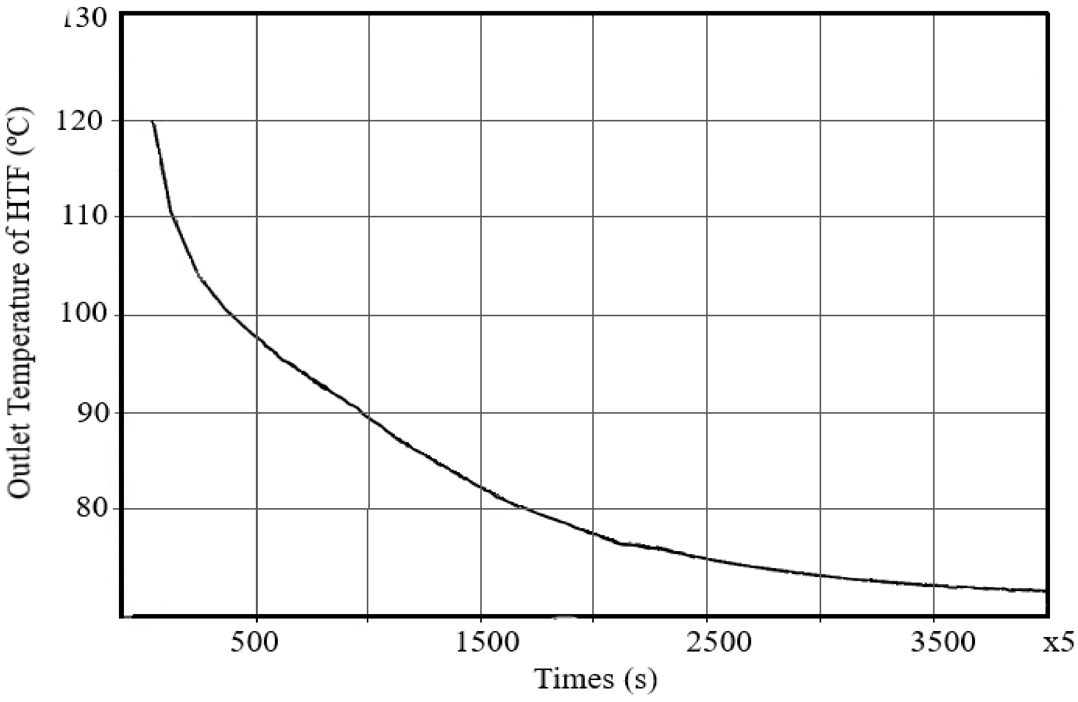

Figure 7.7 Variation of discharging temperature with discharging time

7.2.2 Storage efficiency of PBTES

Figure 7-8 shows that the storage efficiency variation along the length of the storage tank. The result reveals that the efficiency of the storage decreases from 100 to 72% with the tanks length or height increase from 0 to 2m. This is due to, a significant increase of the stored energy along the length while the extracted energy insignificantly increases.

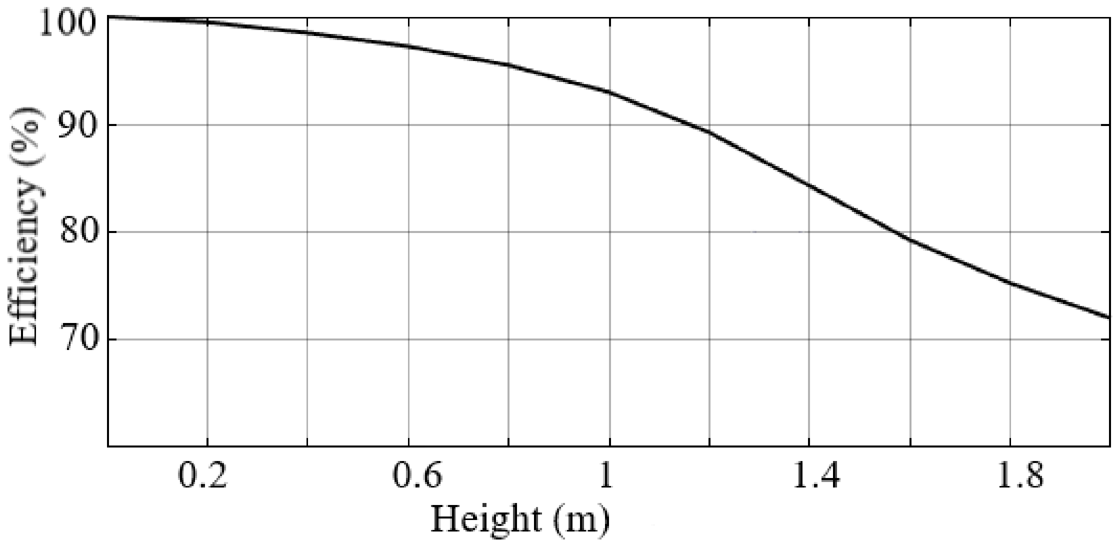

Figure 7.8 Variation of storage efficiency of PBTES with height of the tank

The storage efficiency also affected by the time changes as shown on Figure 7-9. In all points along the length of the tank, the storage efficiency increases with time. The maximum 92.3% storage efficiencies recorded after of charging 50 min. This is due to the decrease of HTF and PCM temperature difference as the charging time increases.

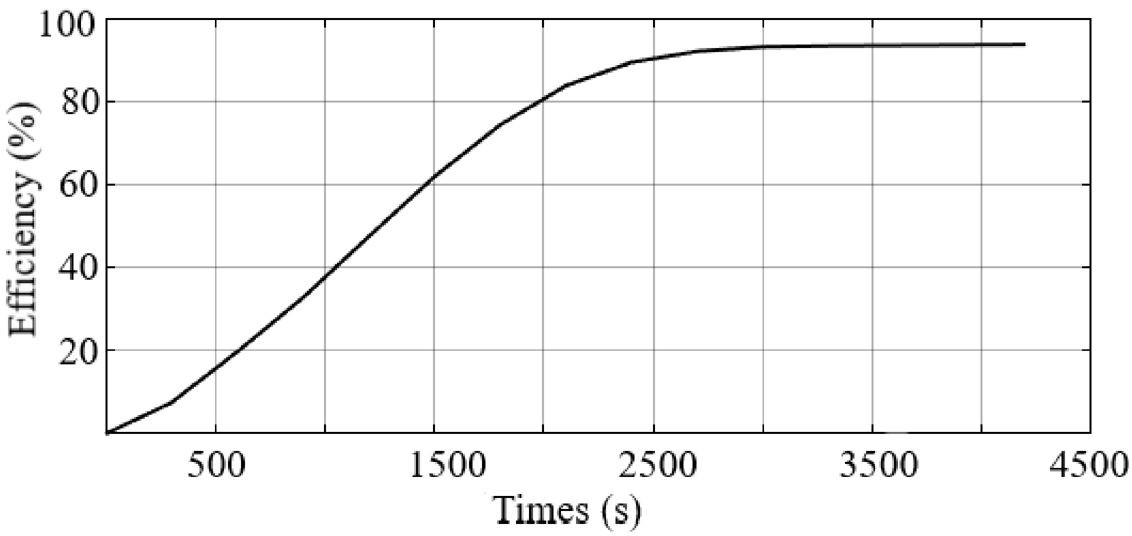

Figure 7.9 Variation of storage efficiency of PBTES with charging time

7.3 Desiccant-coated Heat and Mass Exchanger

7.3.1 Desiccant and process air temperature and humidity ratio

On Figure 7-10 the transient state of desiccant material (silica ge1) temperature and humidity ratio were represented. It can be found that in the dehumidification cycle (between 0 and 520s), the temperature of desiccant insignificantly decreases toward the cooling water temperature and attain its minimum 28ºC. During this cycle, due to the transfer of mass occurred from process air to desiccant material, the humidity ratio of the desiccant significantly increases and attain its maximum 0.024 kg/kg saturation humidity ratio, at the end of the cycle. The maximum moisture removed from the process air is 0.008kg/kg.

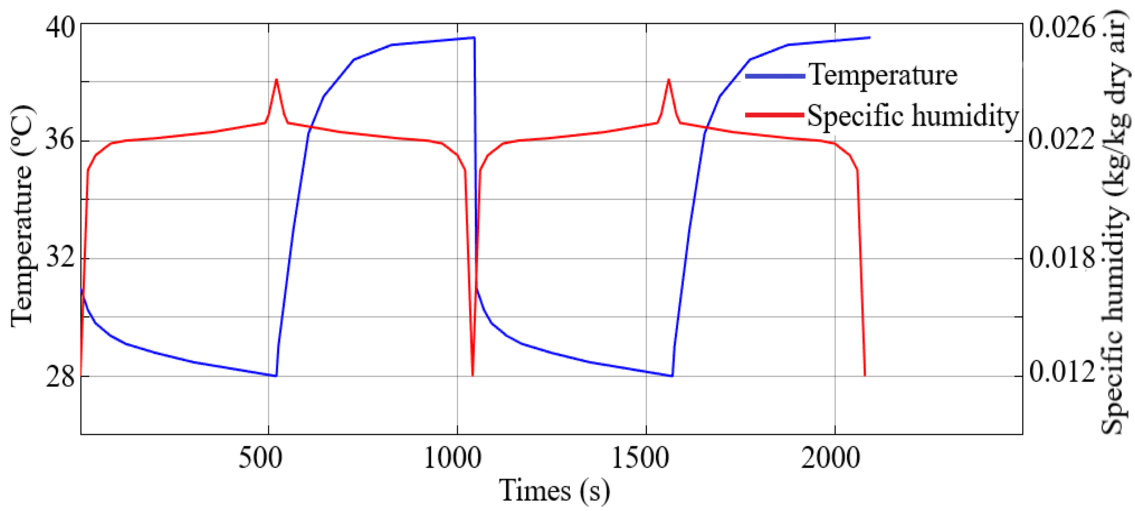

Figure 7.10 Variation of desiccant temperature and humidity ratio with time

In the regeneration cycle (between 520 and 1040s), opposite to the dehumidification cycle, the temperature of desiccant significantly increases toward the heating water temperature and attain its maximum 39.5ºC. In this regeneration cycle, the humidity ratio of the desiccant significantly decreases due to removal of moisture from the desiccant occurred by desorption process. The result reveals that the operation time of one cycle of both dehumidification and regeneration cycle is 520s.

Figure 7-11 shows the transient variation of process air's outlet temperature and humidity ration for dehumidification process only. It can be found that the temperature of process air (inlet ambient air) decreases to the minimum values of 28ºC. However, during the cycles switch on, suddenly the temperature increases to the 31ºC. But this increases in temperature were temporal and again the temperature would decreases due to re-stablish dehumidification process of other DCHE's.

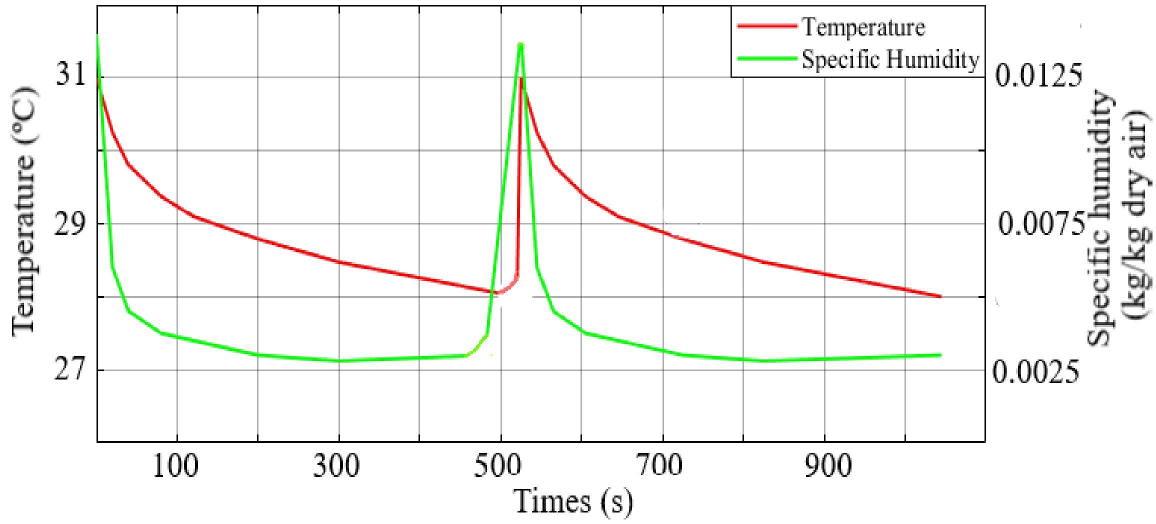

Figure 7.11 Variation of process air temperature and humidity ratio with time

7.3.2 Dehumidification and cooling capacity of DCHE

The dehumidification and cooling capacity are the crucial parameter in measuring the performances of DCHE. These parameter highly influenced by the temperature of heating and cooling water and air flow velocity or mass flow rate of an air.

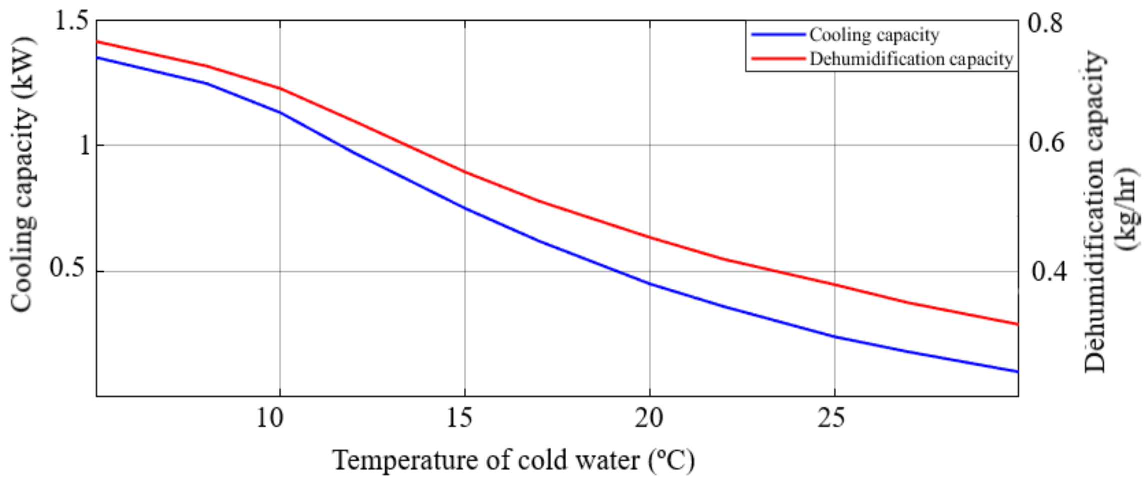

Figure 7.12 Variation of desiccant cooling and dehumidification capacity with cooling water temperature

Figure 7-12 presents the variation of dehumidification and cooling capacity of DCHE with the temperature of cooling water. Both dehumidification and cooling capacity decreases rapidly while the temperature of cooling water increases from 5 to 30°C. Because, as the lower cooling water temperature circulate around the desiccant, the adsorption heat generated during dehumidification removed effectively; and the capability of desiccant removing the moisture would increase greatly. As a result the higher dehumidification achieved with lower cooling temperature. As the lower the cooling water temperature circulate, the higher the heat removed from process air and higher cooling capacity resulted.

Similarly, the heating water temperature influence on both dehumidification and cooling capacity presented on Figure 7-13. From the figure, the dehumidification capacity increases with heating water temperature while the cooling capacity decreases. Higher regeneration temperature favors the desorption process in the desiccant and increases the rate of moisture removal from desiccant to the regeneration air. However, the increase in the heating temperature negatively affect the cooling capacity of DCHE. This is due to the increase of desiccant when the dehumidification cycle starts and it increases the cooling load on the cooling water that could decreases the cooling capacity of the exchangers. An appropriate hot water temperature to get a required level of outlet process air humidity ratio and dry bulb temperature is 54ºC.

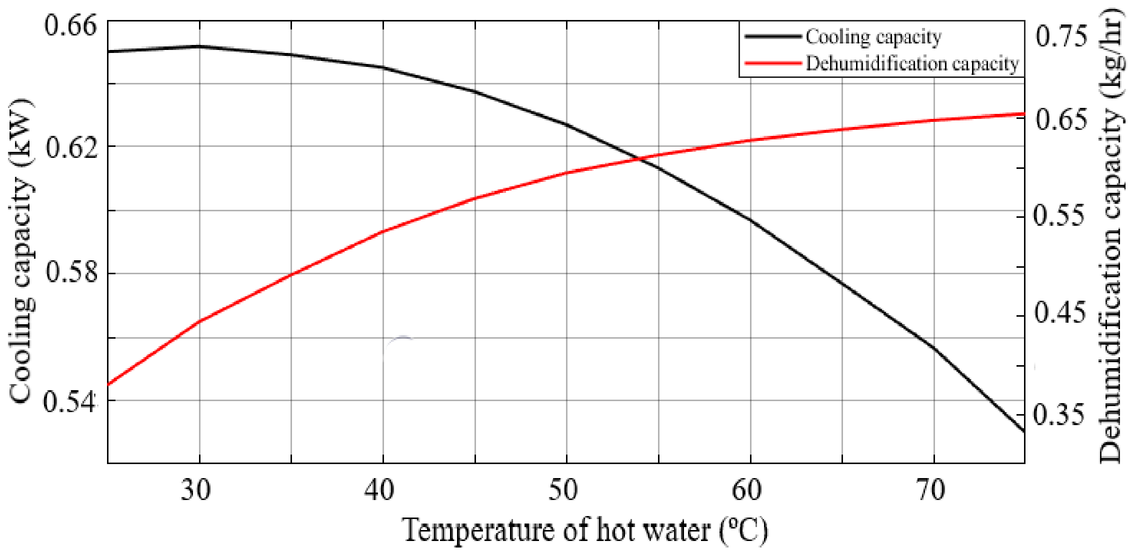

Figure 7.13 Variation of desiccant cooling and dehumidification capacity with hot regeneration water temperature

Figure 7-14 presents the variation of dehumidification and cooling capacity with process air flow velocity. The result reveals that the cooling capacity increases as the air velocity increases. This is due to the higher flow velocity facilitate higher convective heat transfer coefficient that increases the rate of heat transfer. However, the dehumidification capacity increases only up to 1.1m/s and then it start to decreases slightly.

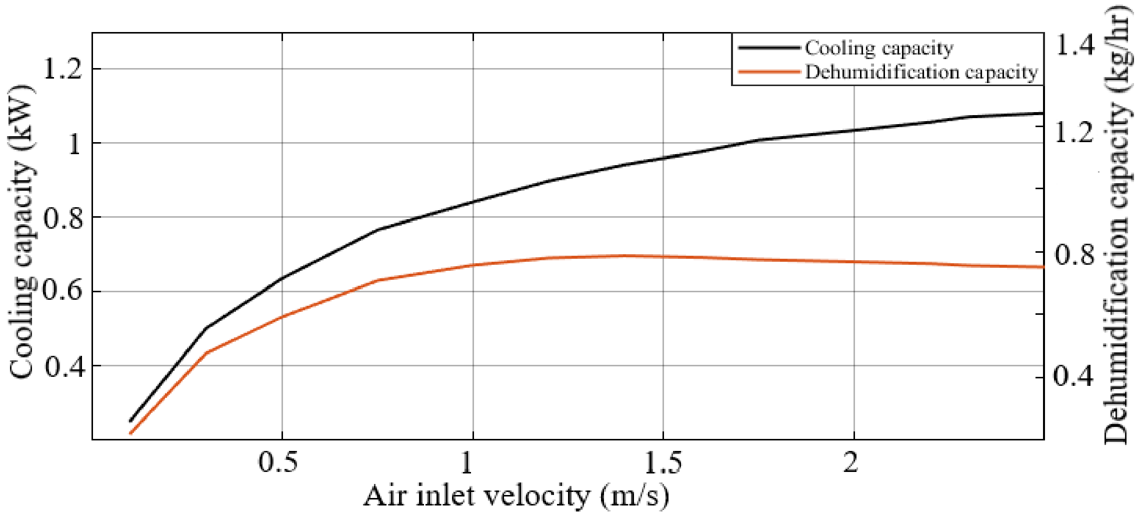

Figure 7.14 Variation of desiccant cooling and dehumidification capacity with inlet air velocity

7.4 M-cycle Indirect Evaporative Cooler

7.4.1 Outlet temperature and humidity ratio

Figure 7-15 presents the temperature variation in dry and wet channel along the length of the channel. The temperature of process air enter the dry channel at 28ºC and decreases to the minimum 7.5ºC at the end of channel length(3m). A fraction of this air diverted to the wet channel and leave the wet channel at a temperature of 20ºC.

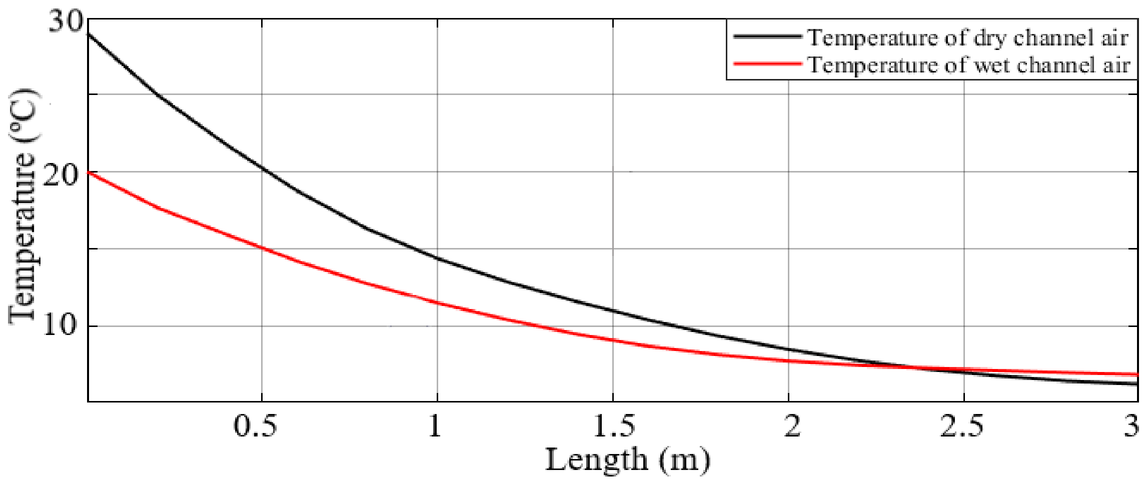

Figure 7.15 Variation of dry and wet channel air temperature with channel length

As shown on Figure 7-16, the humidity ratio of process air in dry channel is constant throughout the channel due to there is no mass transfer occur inside this channel. However, in the wet channel the humidity ration of the working air increases as it gets a moisture from the wicking paper in this channel. The working air leave the wet channel by 14.2g/kg of humidity ratio.

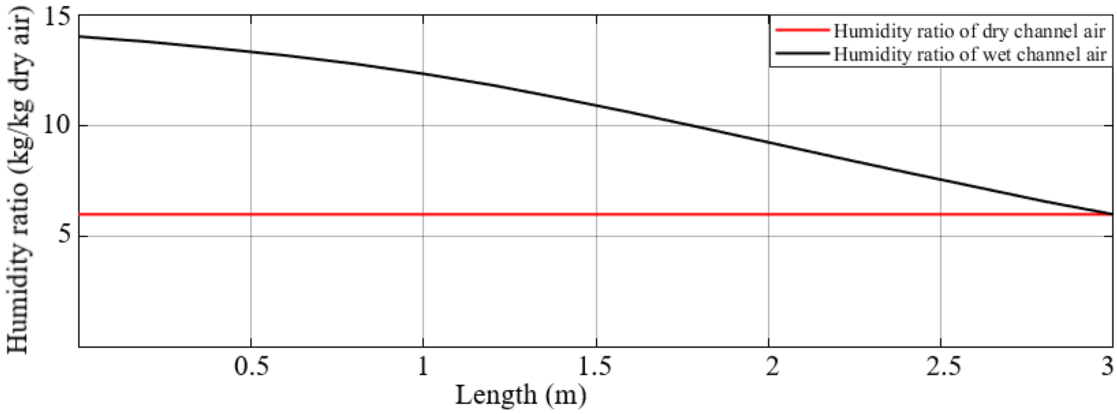

Figure 7.16 Variation of dry and wet channel air humidity ratio with channel length

7.4.2 Wet-bulb and dew-point effectiveness

Wet-bulb and dew-point effectiveness are the key performances measurement of M-cycle indirect evaporative cooler. These effectiveness were influence greatly by the ratio of product air to working air. Figure 7-17 presents the variation of these effectiveness with the product to working air ratio. The result reveals that both decreases as the air ratio increased. This is because since the total cooling effect were produced by the wet channel air, the decrease of this air volume results the decrease of both effectiveness. An optimum air to achieve the required supply air temperature level are 0.55.

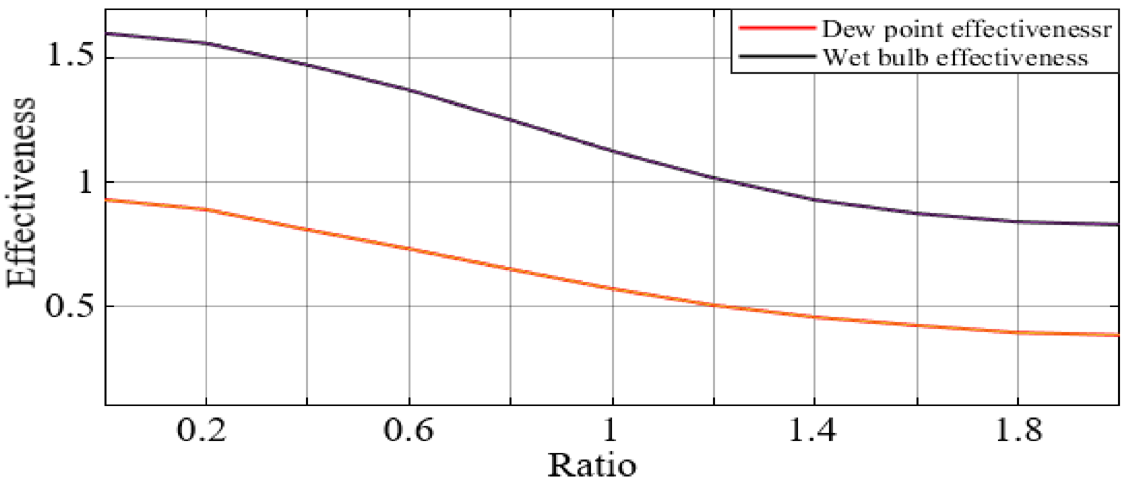

Figure 7.17 Variation of wet-bulb and dew-point effectiveness with product to working air ratio

7.5 Storage Room

7.5.1 Transient variation of storage room temperature

Figure 7-18 presents the 2D storage room temperature distribution as the time increases. The result reveals that the product air were supplied with constant 8ºC to the storage room. The room temperature which represents the produce temperature decreases as the operation time increases. As shown on the figure, due to concentration of heat around the produce by field and respiration heat, the distribution of temperature is not uniform and the points far from the produce concentration cool quickly. After 2 hours of operation, the minimum 20ºC required storage temperature were achieved. The maximum (12.5ºC) and minimum (9ºC) possible room temperature achieved were obtained after 5 hours of operation.

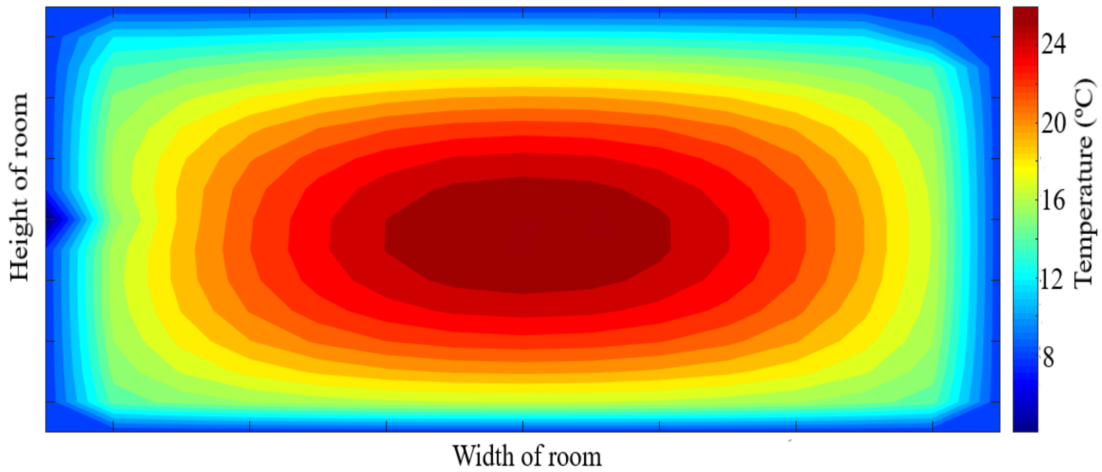

Figure 7.18 Temperature distribution of storage room after one hour of cooling

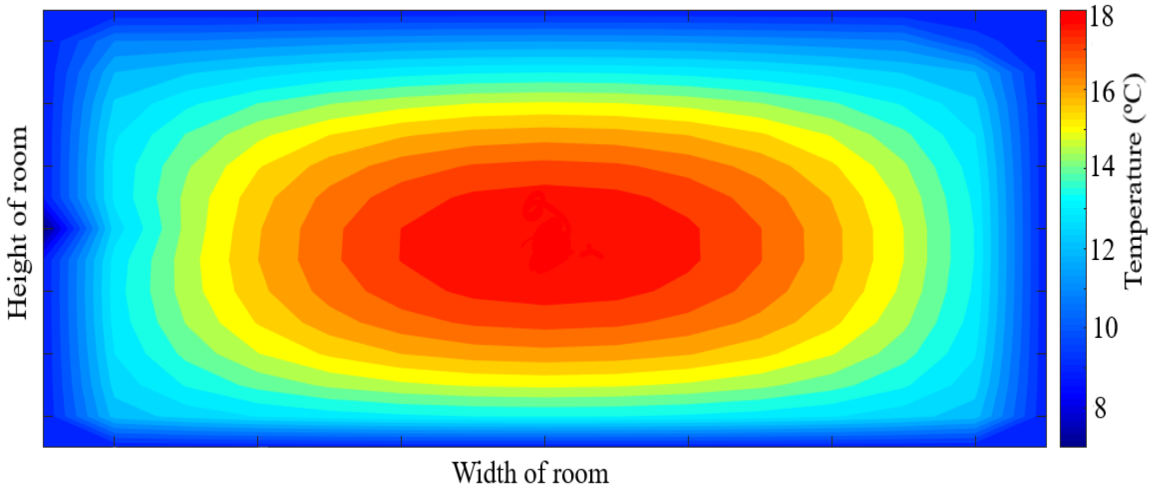

Figure 7.19 Temperature distribution of storage room after three hour of cooling

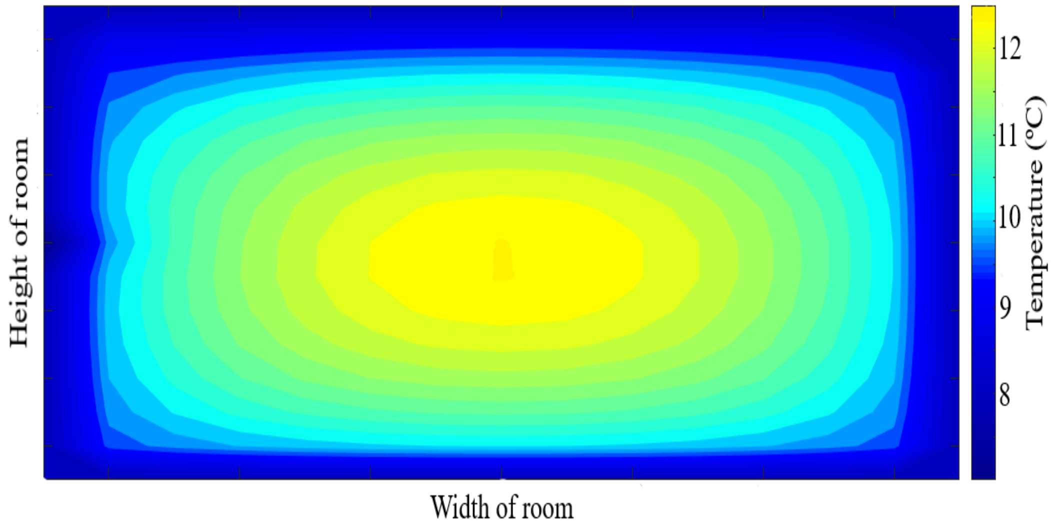

Figure 7.20 Temperature distribution of storage room after five hour of cooling

Where, on Figure 6.18 to 6.20 vertical is representing Y-axis and horizontal is representing X-axis of computational model (given in ANNEX-D).

7.5.2 Cooling time

The cooling time indicating the length of time a produce can take to achieve the required level of cooling temperature. Figure 7-19 presents the half-cooling time for 25ºC initial inlet temperature of the produce. The result shows that the half cooling time were 3-hour. This implies after 3 hour of cooling process the difference between the produce and surrounding air is half of the initial difference.

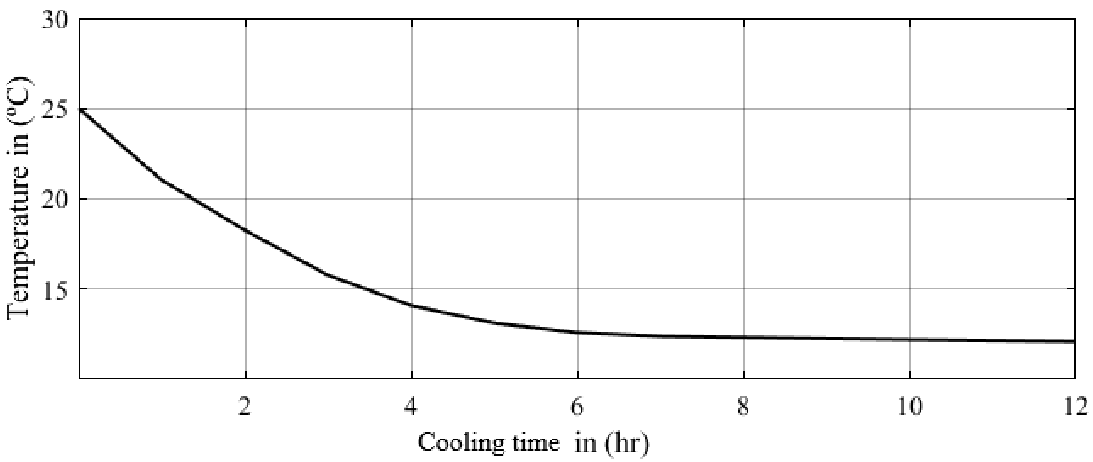

Figure 7.21 Variation of produce temperature with half-cooling time

7.6 Model Validation

To validate the reliability of the mentioned numerical models, the results from the solved models using MATLAB program, are related against an experimental work done by different scholars.

7.6.1 Variation of PCM temperature

The developed numerical method for PBTES that has been solved using MATLAB code is validated against an experimental work done by Rachek et al., (2018). The authors studied the charging and discharging performance of spherically encapsulated phase change material. In their study, the compact finned-tube-in-tank was built and the tank has the following dimensions 310mm×280mm×70mm and its walls are considered adiabatic. During the charging/discharging stage, hot/cold water is introduced to the tube domain to exchange heat by forced convection with the inner tube wall which, in turn, transfers heat to the PCM. The HTF flow rates that were applied during charging and discharging are 0.8 and 0.62 l/min respectively. Fig 7.22 and Figure 7.23 shows the water outlet temperature variation over time for numerical and experimental results during charging and discharging processes respectively.

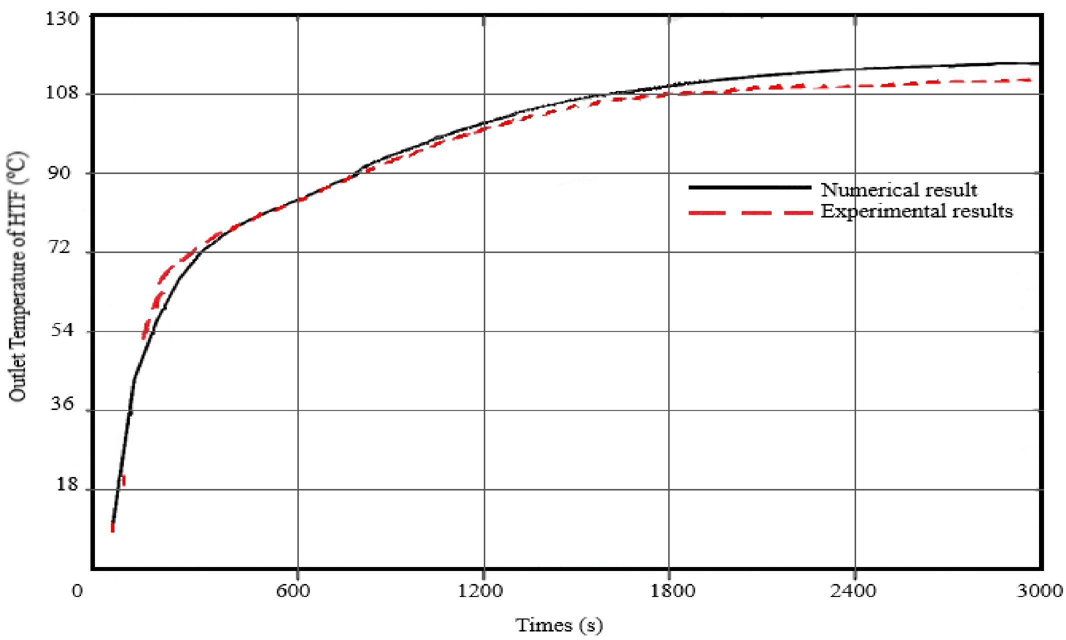

Figure 7.22 Validation of PCM temperature variation in charging mode

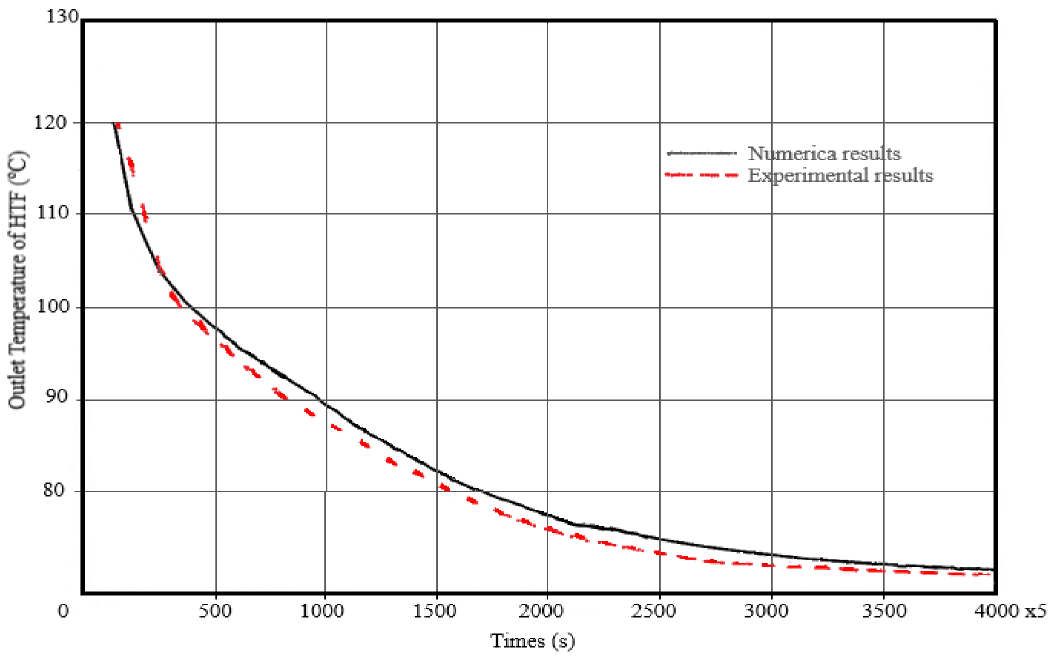

Figure 7.23 Validation of PCM temperature variation in discharging mode

Comparing the numerical and the experimental result curves, there is a little variation on the charging and discharging time of PCM. This is due to the geometric size of latent heat storage system considered for the numerical model and neglecting the effect of heat loss to the atmosphere.

7.6.2 Variation of DCHE air temperature and humidity ratio

In order to validate the numerical result of DCHE under assumed condition, the experimental results from zhao et al., (2018) investigation were considered. In their investigation they used DCHE coated with silica gel. The experiments were carried out under the operating conditions of 0.22m/s, 0.0117l/s, 20ºC, 50ºC and 13g/kg of an average inlet air velocity, water flow rate, cooling water temperature, heating water temperature and ambient humidity ratio respectively. On Figure 7.24 and Figure 7.24 the experimental results and numerical results of the outlet humidity ratio and outlet temperature of the outlet air were plotted respectively. From comparison, there is a little variation between the experimental results and numerical results and it is less than 5%. This variation were resulted due to some assumptions used to simplify the governing equation.

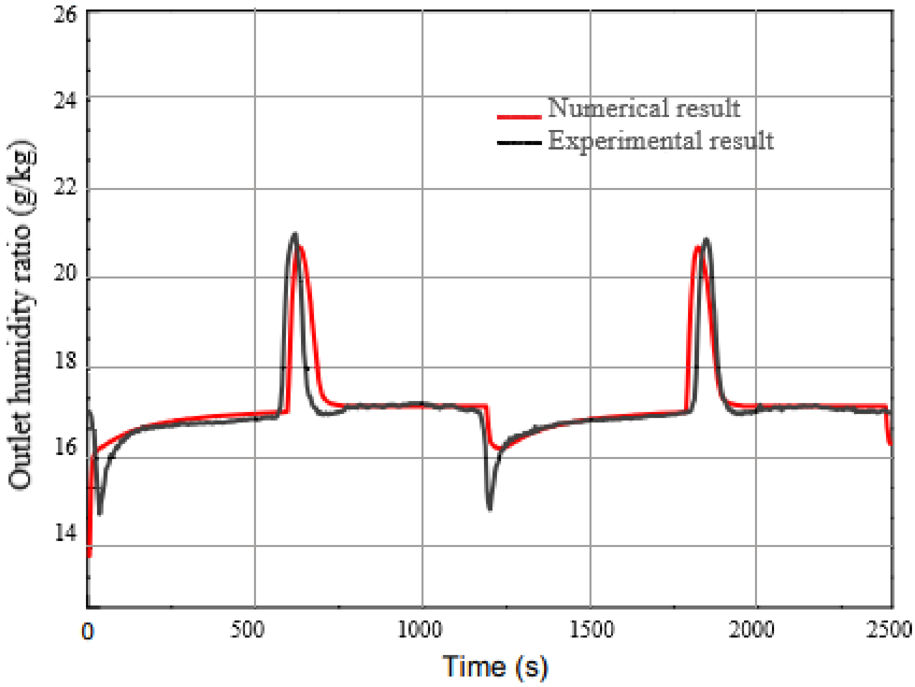

Figure 7.24 Validation of DCHE air humidity ratio

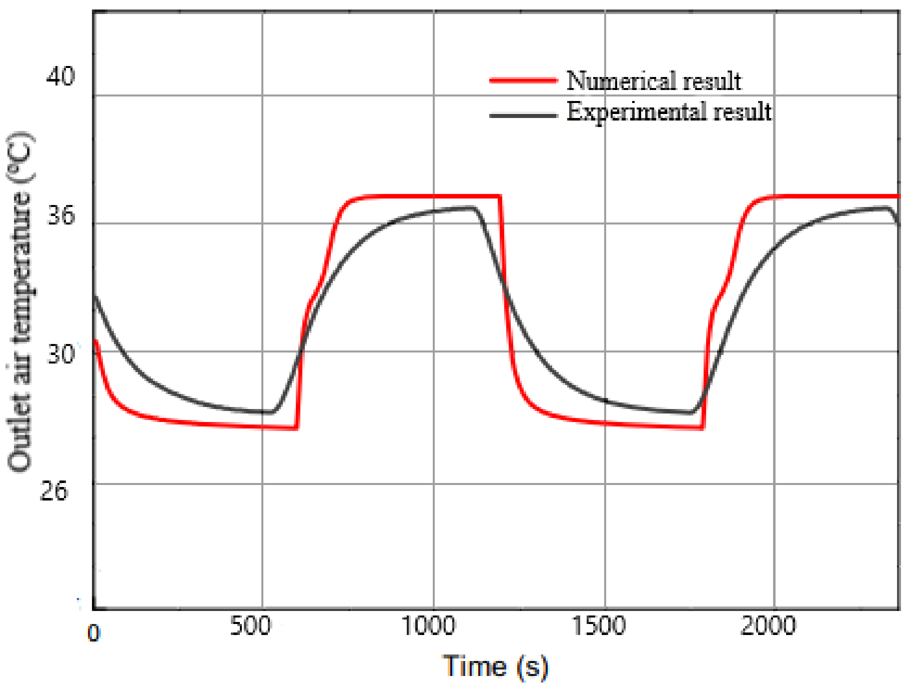

Figure 7.25 Validation of DCHE air temperature

CONCLUSIONS

In this study, the performance of enhanced evaporative cooling system to store tomatoes harvested from the field at Meki area is investigated. Meki is an areas were tomatoes produced widely and the storage facilities are not available. Solar energy were used as an energy sources for the investigated system and the based on the regeneration temperature requirement of the system, the heat pipe evacuated solar collector and packed bed thermal energy storage are selected and sized.

The simulation performance analysis of the storage room has done. A mathematical model has been developed for each unit of the system, based on the conservation of mass and energy. The SIMPLE algorithm were used in order to solve the developed mathematical model of storage room and an algorithm were solved using the developed MATLAB codes.

Based on the cooling load of the storage room and regeneration temperature of DCHE, the ThermoPower-VHP30 heat pipe evacuated tube solar collector were selected. The result reveals that an ideally modeled system would achieve adequate supply temperature and relative humidity for storage room air conditioning in selected study area. The wet bulb and dew point effectiveness of the M-cycle attained 1.43 and 0.76 respectively. The storage room reaches 12ºC and 87% room temperature and relative humidity respectively after 5 hours of operation. The half cooling time of 3 hour were achieved by the modeled system. Therefore, the modeled system had a capability of reducing postharvest losses and also generate more income for farmers.

RECOMMENDATIONS

The following recommendations are given based on the results from investigation:

- If the enhanced evaporative cooling system based tomatoes storage warehouse is built and used at the farm, the post-harvest losses resulted from poor storage is reduced highly.
- This investigation is purely numerical analysis. Therefore, an experimental validation is needed in order to prove the applicability of the system.
- The investigated system can store others produces other than tomatoes; which has the same storage condition with tomatoes such as papaya and peppers.
- Storing more than one produces together is not recommended, due to the respiration from one produce can cause a deterioration to another one.
- The working fluid's outlet temperature from the collector highly affect the discharging time of the PBTES. Hence, selecting and designing high temperature collector other than HPETSC were recommended.

REFERENCES

Abera, G., Ibrahim, A. M., Forsido, S. F., and Kuyu, C. G. (2020). Assessment on post-harvest losses of tomato (Lycopersicon esculentem Mill.) in selected districts of East Shewa Zone of Ethiopia using a commodity system analysis methodology. Heliyon, 6(4), e03749.

Abd Manaf, I., Durrani, F., and Eftekhari, M. (2021). A review of desiccant evaporative cooling systems in hot and humid climates. Advances in Building Energy Research, 15(1), 1-42.

Adam, A., Han, D., He, W., and Amidpour, M. (2021). Analysis of indirect evaporative cooler performance under various heat and mass exchanger dimensions and flow parameters. International Journal of Heat and Mass Transfer, 176, 121299.

Alahmer, Salman, and Ajib. (2018). Solar Cooling Technologies, Energy Conversion - Current Technologies and Future Trends. Intech Open,111,64-81.

Almasri, R. A., Abu-Hamdeh, N. H., Esmaeil, K. K., and Suyambazhahan, S. (2022). Thermal solar sorption cooling systems-A review of principle, technology, and applications. Alexandria Engineering Journal, 61(1), 367-402.

Alazazmeh, A. J., and Mokheimer, E. M. (2015). Review of solar cooling technologies. J. Appl. Mech. Eng, 4(5), 180.

Amarnath, G., Malik, R. P. S., and Taron, A. (2021). Scaling up Index-based Flood Insurance (IBFI) for agricultural resilience and flood-proofing livelihoods in developing countries (Vol. 180). International Water Management Institute (IWMI).

Amer, A. E. A., and Lebedev, V. (2018). Thermal Energy Storage by Using Latent Heat Storage Materials International. Journal of Scientific& Engineering Research, 9(5), 1442-1447.

Amer, O., Boukhanouf, R., and Ibrahim, H. G. (2015). A review of evaporative cooling technologies. International journal of environmental science and development, 6(2), 111.

Anisimov, S., and Pandelidis, D. (2011). Heat-and mass-transfer procesess in indirect evaporative air conditioners through the Maisotsenko cycle. International Journal of Energy for a Clean Environment, 12(2-4).

Ayandiji, A., Adeniyi, O. D., and Omidiji, D. (2011). Determinant post-harvest losses among tomato farmers in Imeko-Afon local government area of Ogun State, Nigeria. Global Journal of Science Frontier Research, 11(5), 23-27.

Babaremu, K. O., Adekanye, T. A., Okokpujie, I. P., Fayomi, J., and Atiba, O. E. (2019). The significance of active evaporative cooling system in the shelf life enhancement of vegetables (red and green tomatoes) for minimizing post-harvest losses. Procedia Manufacturing, 35, 1256-1261.

Bhagat K, and Saha K. (2016). Numerical analysis of latent heat thermal energy storage using encapsulated phase change material for solar thermal power plant. Renewable Energy. 323 336.

Bongs, C., Morgenstern, A., Lukito, Y., and Henning, H. M. (2014). Advanced performance of an open desiccant cycle with internal evaporative cooling. Solar Energy, 104, 103-114.

Chaudhary, G. Q., Ali, M., Sheikh, N. A., and Khushnood, S. (2018). Integration of solar assisted solid desiccant cooling system with efficient evaporative cooling technique for separate load handling. Applied Thermal Engineering, 140, 696-706.

Chien, L. H., Chen, D. C., Liu, Y. J., Yan, W. M., and Ghalambaz, M. (2021). Heat and mass transfer of evaporative cooler with elliptic tube heat exchangers-an experimental study. International Communications in Heat and Mass Transfer, 127, 105502.

Cochrane, L., and Bekele, Y. W. (2018). Average crop yield (2001–2017) in Ethiopia: Trends at national, regional and zonal levels. Data in brief, 16, 1025-1033.

Cui, X., Chua, K. J., Islam, M. R., and Yang, W. M. (2014). Fundamental formulation of a modified LMTD method to study indirect evaporative heat exchangers. Energy conversion and management, 88, 372-381.

Daou, K., Wang, R. Z., and Xia, Z. Z. (2006). Desiccant cooling air conditioning: a review. Renewable and Sustainable Energy Reviews, 10(2), 55-77.

Da Cunha, J. P., and Eames, P. (2016). Thermal energy storage for low and medium temperature applications using phase change materials–a review. Applied energy, 177, 227-238.

Desalegn, R., Wakene, T., and Addis, S. (2016). Tomato (Lycopersicon esculentum Mill.) varieties evaluation in Borana zone, Yabello district, southern Ethiopia. Journal of Plant Breeding and Crop Science, 8(10), 206-210.

Dezfouli, M. M. S., Mat, S., Pirasteh, G., Sahari, K. S. M., Sopian, K., and Ruslan, M. H. (2014). Simulation analysis of the four configurations of solar desiccant cooling system using evaporative cooling in tropical weather in Malaysia. International Journal of Photoenergy, 2014.

Deoraj, S., Ekwue, E. I., and Birch, R. (2015). An Evaporative Cooler for the Storage of Fresh Fruits and Vegetables. West Indian Journal of Engineering, 38(1).

Dizaji, H. S., Hu, E. J., Chen, L., and Pourhedayat, S. (2020). Analytical/experimental sensitivity study of key design and operational parameters of perforated Maisotsenko cooler based on novel wet-surface theory. Applied Energy, 262, 114557.

Doğramacı, P. A., Riffat, S., Gan, G., and Aydın, D. (2019). Experimental study of the potential of eucalyptus fibres for evaporative cooling. Renewable Energy, 131, 250-260.

Duffie, J.A, Beckman, W.A. (2013). Solar Engineering of Thermal Processes. Hoboken, New Jersey: John Wiley & Sons, Inc.

Eduardo, C., and Nóbrega, L. (2014). Desiccant-Assisted Cooling Fundamentals and Applications.

El-Dessouky, H. T., Ettouney, H. M., and Bouhamra, W. (2000). A novel air conditioning system: membrane air drying and evaporative cooling. Chemical Engineering Research and Design, 78(7), 999-1009.

Elias, C. N., and Stathopoulos, V. N. (2019). A comprehensive review of recent advances in materials aspects of phase change materials in thermal energy storage. Energy Procedia, 161, 385-394.

Evangelisti, L., Vollaro, R. D. L., and Asdrubali, F. (2019). Latest advances on solar thermal collectors: A comprehensive review. Renewable and Sustainable Energy Reviews, 114, 109318.

Faizur Rahman, Al-zakri, A.S, and M.A Rahman. (2014). Two-dimensional mathematical model of evacuated tube solar collector. Journal of solar energy engineering. 231-248.

Fong, K. F., and Lee, C. K. (2020). Solar desiccant cooling system for hot and humid region–A new perspective and investigation. Solar Energy, 195, 677-684.

Gagliano, A., Patania, F., Nocera, F., and Galesi, A. (2014). Performance assessment of a solar assisted desiccant cooling system. Thermal Science, 18(2), 563-576.

Goldsworthy, M., and White, S. (2011). Optimisation of a desiccant cooling system design with indirect evaporative cooler. International Journal of refrigeration, 34(1), 148-158.

Gross, K. C., Wang, C. Y., and Saltveit, M. E. (Eds.). (2016). The commercial storage of fruits, vegetables, and florist and nursery stocks (p. 66). Washington, DC, USA: United States Department of Agriculture, Agricultural Research Service.

Haile, A. T., Alemayehu, M., Rientjes, T., and Nakawuka, P. (2020). Evaluating irrigation scheduling and application efficiency: baseline to revitalize Meki-Ziway irrigation scheme, Ethiopia. SN Applied Sciences, 2(10), 1-12.

Haileslassie, A., Agide, Z., Erkossa, T., Hoekstra, D., Schmitter, P. S., and Langan, S. J. (2016). On-farm smallholder irrigation performance in Ethiopia: From water use efficiency to equity and sustainability. International Livestock Research Institute.

Ismanizam Abd Manaf, Faisal Durrani and Mahroo Eftekhari. (2018). A review of desiccant evaporative cooling systems in hot and humid climates. Advances in Building Energy Research.78(2), 112-125.

Haile, D., Tesfaye, B., and Assefa, F. (2022). Assessment of Smallholders Tomato Production Trends in Koka, Meki and Ziway Zuria, Ethiopia. Meki and Ziway Zuria, Ethiopia.

Jain, J. K., and Hindoliya, D. A. (2011). Experimental performance of new evaporative cooling pad materials. Sustainable Cities and Society, 1(4), 252-256.

Kalogirou S. (2004). Solar thermal collectors and applications. Progress in Energy and Combustion Science.231–295.

Kanoğlu, M., Çengel, Y. A., and Cimbala, J. M. (2020). Fundamentals and applications of renewable energy. McGraw-Hill Education.

Karellas, S., Roumpedakis, T. C., Tzouganatos, N., and Braimakis, K. (2018). Solar cooling technologies. CRC Press.

Khalid, A., Mahmood, M., Asif, M., and Muneer, T. (2009). Solar assisted, pre-cooled hybrid desiccant cooling system for Pakistan. Renewable Energy, 34(1), 151-157.

Khosravi, N., Aydin, D., Nejhad, M. K., and Dogramaci, P. A. (2020). Comparative performance analysis of direct and desiccant assisted evaporative cooling systems using novel candidate materials. Energy Conversion and Management, 221, 113167.

Kiaya, V. (2014). Post-harvest losses and strategies to reduce them. Technical Paper on Postharvest Losses, Action Contre la Faim (ACF), 25, 1-25.

Krishnakumar, T. (2017). Design of cold storage for fruits and vegetables. Trivandrum: Researchgate

Kumar, A., Tiwari, A. K.,and Said, Z. (2021). A comprehensive review analysis on advances of evacuated tube solar collector using nanofluids and PCM. Sustainable Energy Technologies and Assessments, 47, 101417.

Lai, L., Wang, X., Kefayati, G., and Hu, E. (2021). Evaporative cooling integrated with solid desiccant systems: a review. Energies, 14(18), 5982.

Libertya J.T, Ugwuishiwua B.O, Pukumab S.A, and Odo C.E. (2013). Principles and Application of Evaporative Cooling Systems for Fruits and Vegetables Preservation. International Journal of Current Engineering and Technology, 2277-2284.

Limeneh, D. F. (2021). Review on Production Status of Onion Seed Yield, Nutrient Uptake and Use Efficiency of Nitrogen and Phosphorus Fertilizations in Ethiopia.

Lin, J., Wang, R. Z., Kumja, M., Bui, T. D., and Chua, K. J. (2017). Modelling and experimental investigation of the cross-flow dew point evaporative cooler with and without dehumidification. Applied Thermal Engineering, 121, 1-13.

Li, S. F., Liu, Z. H., and Wang, X. J. (2019). A comprehensive review on positive cold energy storage technologies and applications in air conditioning with phase change materials. Applied Energy, 255, 113667.

Mahmood, M. H., Sultan, M., Miyazaki, T., Koyama, S., and Maisotsenko, V. S. (2016). Overview of the Maisotsenko cycle–A way towards dew point evaporative cooling. Renewable and sustainable energy reviews, 66, 537-555.

Malik, M. S., Iftikhar, N., Wadood, A., Khan, M. O., Asghar, M. U., Khan, S.,and Rizvi, S. T. U. I. (2020). Design and fabrication of solar thermal energy storage system using potash alum as a pcm. Energies, 13(23), 6169.

Misha, S., Mat, S., Ruslan, M. H., and Sopian, K. (2012). Review of solid/liquid desiccant in the drying applications and its regeneration methods. Renewable and Sustainable Energy Reviews, 16(7), 4686-4707.

Mohamed, S. A., Al-Sulaiman, F. A., Ibrahim, N. I., Zahir, M. H., Al-Ahmed, A., Saidur, R., and Sahin, A. Z. (2017). A review on current status and challenges of inorganic phase change materials for thermal energy storage systems. Renewable and Sustainable Energy Reviews, 70, 1072-1089.

Moshari, S., Heidarinejad, G., and Fathipour, A. (2016). Numerical investigation of wet-bulb effectiveness and water consumption in one-and two-stage indirect evaporative coolers. Energy conversion and management, 108, 309-321.

Mrinal Jagirdara and Poh Seng Lee. (2018). Mathematical modeling and performance evaluation of a desiccant coated fin-tube heat exchanger. Applied Thermal Engineering, 73(1), 401-415.

Nakabayashi, S., Nagano, K., Nakamura, M., Togawa, J., and Kurokawa, A. (2011). Improvement of water vapor adsorption ability of natural mesoporous material by impregnating with chloride salts for development of a new desiccant filter. Adsorption, 17(4), 675-686.

Nakaso, K., Teshima, H., Yoshimura, A., Nogami, S., Hamada, Y., and Fukai, J. (2008). Extension of heat transfer area using carbon fiber cloths in latent heat thermal energy storage tanks. Chemical Engineering and Processing: Process Intensification, 47(5), 879-885.

Narayanan, R., Saman, W. Y., White, S. D., and Goldsworthy, M. (2011). Comparative study of different desiccant wheel designs. Applied Thermal Engineering, 31(10), 1613-1620.

Nkolisa, N. S. (2017). Evaluation of a low-cost energy-free evaporative cooling system for postharvest storage of perishable horticultural products produced by smallholder farmers of Umsinga in KwaZulu-Natal (Doctoral dissertation).

Olfian, H., Ajarostaghi, S. S. M., and Ebrahimnataj, M. (2020). Development on evacuated tube solar collectors: A review of the last decade results of using nanofluids. Solar Energy, 211, 265-282.

Olunloyo, O. O., Olunloyo, A. A., and Ibiyeye, D. E. (2019). Development and assessment of a direct evaporative cooling facility for storing fruit and vegetables. Development.

Parmar, H., and Hindoliya, D. (2012). Performance of solid desiccant-based evaporative cooling system under the climatic zones of India. Parmar, H.; Hindoliya, D.A. Performance of solid desiInternational journal of Low-Carbon Technology, 52–57.

Refrigerating. (2006). ASHRAE Handbook: Refrigeration systems and applications. American Society of Heating, Refrigerating and Air Conditioning Engineers.

Sabiha, M. A., Saidur, R., Mekhilef, S., and Mahian, O. (2015). Progress and latest developments of evacuated tube solar collectors. Renewable and Sustainable Energy Reviews, 51, 1038-1054.

Sajjad, U., Abbas, N., Hamid, K., Abbas, S., Hussain, I., Ammar, S. M., and Wang, C. C. (2021). A review of recent advances in indirect evaporative cooling technology. International Communications in Heat and Mass Transfer, 122, 105140.

Samuel, D. V. K., and Beera, V. (2013). Evaporative cooling system for storage of fruits and vegetables-a review. Journal of food science and technology, 50(3), 429-442.

Shahzad, M. K., Chaudhary, G. Q., Ali, M., Sheikh, N. A., Khalil, M. S., and Rashid, T. U. (2018). Experimental evaluation of a solid desiccant system integrated with cross flow Maisotsenko cycle evaporative cooler. Applied Thermal Engineering, 128, 1476-1487.

Sipho, S., and Tilahun, S. W. (2020). Potential causes of postharvest losses, low-cost cooling technology for fresh produce farmers in Sub-Sahara Africa. African Journal of Agricultural Research, 16(5), 553-566.

Sun, X. Y., Dai, Y. J., Ge, T. S., Zhao, Y., and Wang, R. Z. (2018). Experimental and comparison study on heat and moisture transfer characteristics of desiccant coated *heat exchanger with variable structure sizes. Applied Thermal Engineering, 137, 32-46.*

Tariq, R., Zhan, C., Zhao, X., and Sheikh, N. A. (2018). Numerical study of a regenerative counter flow evaporative cooler using alumina nanoparticles in wet channel. Energy and Buildings, 169, 430-443.

Taye, S. M., and Olorunisola, P. F. (2011). Development of an evaporative cooling system for the preservation of fresh vegetables. African Journal of Food Science, 5(4), 255-266.

Zhao, L. H., Wang, R. Z., and Ge, T. S. (2021). Desiccant coated heat exchanger and its applications. International Journal of Refrigeration, 130, 217-232.

Urge, M., Negeri, M., Selvaraj, T., and Gebresenbet, G. (2014). Assessment of post-harvest losses of ware potatoes (Solanum tuberosum l.) in Chelia and Jeldu districts of West Shewa, Ethiopia. Int J Res Sci, 1(1), 16-29.

Versteeg, H.K., and Malalasekera, W. (2007). An Introduction to Computational Fluid Dynamics. Edinburgh Gate England: Pearson Education Limited.

Velasco-Gómez, E., Tejero-González, A., Jorge-Rico, J., and Rey-Martínez, F. (2020). Experimental Investigation of the Potential of a New Fabric-Based Evaporative Cooling Pad. Sustainability, 12-25.

Venegas, T., Qu, M., Nawaz, K., and Wang, L. (2021). Critical review and future prospects for desiccant coated heat exchangers: Materials, design, and manufacturing. Renewable and Sustainable Energy Reviews, 151, 111531.

Venu, v. H. (2016). Development and perfromance evaluation of evaporative cooling storage systems for horticultural produce. An international journal of life science, 1793-1803.

Vivekh, P., Kumja, M., Bui, D. T., and Chua, K. J. (2018). Recent developments in solid desiccant coated heat exchangers–A review. Applied energy, 229, 778-803.

Wondim, D. (2021). Value chain analysis of vegetables (onion, tomato, potato) in Ethiopia: A review. International Journal of Agricultural Science and Food Technology, 7(1), 108-113.

Xuan, Y. M., Xiao, F., Niu, X. F., Huang, X., and Wang, S. W. (2012). Research and application of evaporative cooling in China: A review (I)–Research. Renewable and Sustainable Energy Reviews, 16(5), 3535-3546.

Xu, P., Ma, X., Zhao, X., and Fancey, K. (2017). Experimental investigation of a super performance dew point air cooler. Applied Energy, 203, 761-777.

Zalba, B., Marín, J. M., Cabeza, L. F., and Mehling, H. (2004). Free-cooling of buildings with phase change materials. International Journal of Refrigeration, 27(8), 839-849.

Zhao, D., and Tan, G. (2015). Numerical analysis of a shell-and-tube latent heat storage unit with fins for air-conditioning application. Applied energy, 138, 381-392.

Zhao, L. H., Wang, R. Z., and Ge, T. S. (2021). Desiccant coated heat exchanger and its applications. International Journal of Refrigeration, 130, 217-232.

Zhao, Y., Ge, T. S., Dai, Y. J., and Wang, R. Z. (2014). Experimental investigation on a desiccant dehumidification unit using fin-tube heat exchanger with silica gel coating. Applied Thermal Engineering, 63(1), 52-58.

APPENDICES

ANNEX A: Thermal and Thermo-physical properties

Table A 1: The thermal property models of food components (ASHRAE, 2006)

Thermal property	Food component	Thermal Property model
Thermal conductivity k, W/(m.k)	Water	$k = 5.7109\times10^{-1} + 1.7625\times10^{-3}t - 6.7036\times10^{-6}t^2$
	Protein	$k = 1.7881\times10^{-1} + 1.1958\times10^{-3}t - 2.7178\times10^{-6}t^2$
	Fat	$k = 1.8071\times10^{-1} - 2.7604\times10^{-4}t - 1.7749\times10^{-7}t^2$
	Carbohydrate	$k = 2.0141\times10^{-1} + 1.3874\times10^{-3}t - 4.3312\times10^{-6}t^2$
	Fiber	$k = 1.8331\times10^{-1} + 1.2497\times10^{-3}t - 3.1683\times10^{-6}t^2$
	Ash	$k = 3.2962\times10^{-1} + 1.4011\times10^{-3}t - 2.9069\times10^{-6}t^2$
Density, kg/m^3	Water	$\rho = 9.9718\times10^{2} + 3.1439\times10^{-3}T - 3.7574\times10^{-3}T^2$
	Protein	$\rho = 1.3299\times10^{3} - 5.184\times10^{-1}T$
	Fat	$\rho = 9.2559\times10^{2} - 4.1757\times10^{-1}T$
	Carbohydrate	$\rho = 1.5991\times10^{3} - 3.1046\times10^{-1}T$
	Fiber	$\rho = 1.3115\times10^{3} - 3.6589\times10^{-1}T$
	Ash	$\rho = 2.4238\times10^{3} - 2.8063\times10^{-1}T$
Specific heat, kJ/kg.k	Water	$c_p = 4.1289 - 9.0864\times10^{-5}T + 5.4731\times10^{-6}T^2$
	Protein	$c_p = 2.0082 + 1.2089\times10^{-3}T - 1.3129\times10^{-6}T^2$
	Fat	$c_p = 1.9842 + 1.4733\times10^{-3}T - 4.8008\times10^{-6}T^2$
	Carbohydrate	$c_p = 1.5488 + 1.9625\times10^{-3}T - 5.9399\times10^{-6}T^2$
	Fiber	$c_p = 1.8459 + 1.8306\times10^{-3}T - 4.6509\times10^{-6}T^2$
	Ash	$c_p = 1.0926 + 1.8896\times10^{-3}T - 3.6817\times10^{-6}T^2$

Table A 2: Mass fraction of food components of tomato (ASHRAE, 2006)

Food item	Moisture content (%)	Protein (%)	Fat (%)	Carbohydrate (%)	Fiber (%)	Ash (%)	Latent heat kJ/kg
Tomato (mature green)	93	1.2	0.2	5.1	1.1	0.5	31.1
Tomato (ripe)	9.76	0.85	0.33	4.64	1.1	0.42	31.3

Table A 3: Empirical equation of thermo-physical property (ASHRAE, 2006)

Thermo-physical property	Empirical equation	Discription of variables	Sources
Density	$\rho = \frac{(1-\varepsilon)}{\sum x_i / \rho_i}$	Where, x_i and ρ_i are the mass fraction and density of the food component respectively	
Specific heat	$c_u = \sum c_i x_i$	Where, c_i and x_i are the specific heat and the mass fraction of the individual food components respectively	
Enthalpy	$H = \sum H_i x_i$	Where, H_i and x_i are the enhalpy and the mass fraction of the individual food components respectively	
Thermal conductivity	$k = \sum x_i^v k_i$ (parallel) $k = \frac{1}{\sum \left(x_i^v / k_i \right)}$ (perpendicular)	Where $x^v{}_i$ and k_i are the volume fraction and thermal conductivity of constituent respectively. $x_i^v = \frac{x_i / \rho_i}{\sum \left(x_i / \rho_i \right)}$	
Thermal diffusivity	$\alpha = \frac{k}{\rho c}$		
Heat of respiration	$w = \frac{10.7 f}{3600} \left(\frac{9T}{5} + 32 \right)^g$ f= 2.0074×10^{-4} g=2.835	Where, f and g are the respiration coefficients. The respiration rate W is in W/kg as a function of temperature T in °C,	Becker et al., (1996)
Transpiration of vegetables	$\dot{m} = k_t \left(p_s - p_a \right)$ K_t=140 kg/(s.pa) for all variety of tomato	Where ṁ is the transpiration (moisture transpired per unit area of produce surface per unit time). Ps and pa are the vapour pressure of the produce surface and surrounding air respectively. K_t is the transpiration coefficient.	

A. Surface heat transfer coefficient

The surface heat transfer coefficient *h* of the produce mostly depends on the velocity of the surrounding fluid, product geometry and surface roughness.

Table A 4: The surface heat transfer coefficient h of the produce (ASHRAE, 2006)

Product	Shape, mm^3	Transfer medium	Temperature of medium,ºC	Velocity of medium, m/s	Surface heat transfer coefficient, h $W/(m^2.K)$	Nu-Re-Pr, correlation
Tomatoes	Spherical	Air	T=4	1	10.9	$Nu=1.56Re^{0.426}Pr^{0.333}$
				1.25	13.1	
				1.5	13.6	
				1.75	14.9	
				2	17.3	

Table A 5: Thermal properties of warehouse construction materials (ASHRAE, 2006)

Thermal properties	Materials	
	Bricks	Cement plaster
Density (Kg/m^3)	1970.3	2114.4
Specific heat (KJ/Kg.k)	08374	0.9211
Emissivity	0.93	0.91
Thermal conductivity (W/m.k)	0.6923	0.7442

Table A 6: Thermo-physical properties of selected organic compound (Elias & Stathopoulos, 2019)

Compound	T_m (ºC)	ΔH_m (kJ/kg)	C_{ps} (kJ/kgK)	C_{pl} (kJ/kgK)	k_s (W/mK)	k_l (W/mK)	ρ_s (kg/m^3)	$V_{expansion}$ ($/m^3/m^3$)	$E_{density}$ (kWh/m^3)
Formic acid	8	277	1	1.17	0.3	0.27	1227	12	96
Acetic acid	17	192	1.33	2.04	0.26	0.19	1214	13.5	71
Lauric acid	44	212	2.02	2.15	0.22	0.15	1007	13.6	66
Stearic acid	54	157	1.76	2.27	0.29	0.17	940	9.9	49
Palmitic acid	61	222	1.69	2.2	0.21	0.17	989	14.1	67
Paraffin wax	0-90	150-250	3	2	0.2	-	880-950	12-14	50-70
Acetamide	82	260	2	3	0.4	0.25	1160	13.9	93
Oxalic acid	105	356	1.62	2.73	-	-	1900	-	211

Table A 7: Thermo-physical properties of selected salt hydrate (Elias & Stathopoulos, 2019)

Compound	T_m (ºC)	ΔH_m (kJ/kg)	C_{ps} (kJ/kgK)	C_{pl} (kJ/kgK)	k_s (W/mK)	k_l (W/mK)	ρ_s (kg/m^3)	$V_{expansion}$ (/m^3/m^3)	$E_{density}$ (kWh/m^3)
Water	0	333	3.3	4.18	1.6	0.61	920	-8.7	109
Calcium chloride hexahydrate	30	125	1.42	2.2	1.09	0.53	1710	11	64
Sodium sulphate decahydrate	32	180	1.93	2.8	0.56	0.45	1485	4	82
Sodium thiosulphate pentahydrate	46	210	1.46	2.39	0.76	0.38	1666	6	103
Sodium acetate trihydrate	58	266	1.68	2.37	0.43	0.34	1450	3	113
Barium hydroxide octahydrate	78	280	1.34	2.44	1.26	0.66	2180	11	171
Magnesium nitrate hexahydrate	89	140	2.5	3.1	0.65	0.5	1640	5	74
Oxalic acid dihydrate	115	264	2.11	2.89	0.9	0.7	1653	0	133

Table A 8 Thermo-physical properties of selected eutectic compound (Elias & Stathopoulos, 2019)

Compound	Mass ratio	T_m (ºC)	ΔH_m (kJ/kg)	C_{ps} (kJ/kgK)	C_{pl} (kJ/kgK)	k_s (W/mK)	k_l (W/mK)	ρ_s (kg/m^3)	$E_{density}$ (kWh/m^3)
$C_aCl_2.(H_2o)_6$ $MgCl_2.(H_2o)_6$	67-33	25	127	1620	2270	930	550	1661	57
Urea $CH_3COON_a.(H_2o)_3$	60-40	30	200	1750	2210	630	480	1370	74
$Mg(NO_3)_2.(H_2o)_6$ NH_4 NO_3	61-39	52	125	2130	2670	590	500	1672	58
Urea acetamide	38-62	53	224	1920	2660	510	340	1216	73
Stearic acid palmitic acid	36-64	53	182	1720	2230	234	169	971	46
$Mg(NO_3)_2.(H_2o)_6$ - $MgCl_2.(H_2o)_6$	59-41	59	132	2290	2810	670	530	1610	58
Stearic acid-acetamide	83-17	65	213	1800	2400	300	180	972	56
$LiNO_3$ $MgNO_3.(H_2o)_6$	14-86	72	180	2380	2900	700	510	1713	84
Urea N_aNO_3	71-29	83	187	1600	2030	750	590	1502	76
Urea NH_4Cl	85-115	102	214	1770	2090	760	580	1348	77

ANNEX B: Specification of solar collector

Table B 1: - Detail specification of heat pipe evacuated tube solar collector

Variable	Values
Tube length (m)	1.78
Tube outer diameter (m)	0.056
Tube inner diameter (m)	0.0533
Dimension (m)	2.61x2.01
Gross area (m^2)	5.241
Net aperture area (m^2)	2.983
Absorber area (m^2)	2.563
Weight (kg)	114.3
Rated flow rate (Lpm)	3.18
Tilt angles (ºC)	15-75
Operating pressure (bar)	1.4-4.8
Stagnation temperature (ºC)	220
Thermal expansion (mm)	$84*10^{-6}$
Coat emissivity	<0.08
Coating absorbance	>0.92
Overall heat loss coefficient($W/m^2.K$)	≥0.7
Heat transfer fluid	Water/glycol
Material of glass	Borosilicate Glass Tube
Thermal conductivity (W/mK)	1.125
Solar transmittance (τ)	0.9
Solar absorptance (σ)	0.05
Solar reflectance (ρ)	0.05
Thermal emittance (ε)	0.85

ANNEX C: Detail of mathematical modeling

Table C 1: Equations of cooling loads (Krishnakumar, 2017).

Loads	Equation	Description
Transmission load	$Q_{Tr} = U * A * (T_o - T_i) * \left(\frac{24}{1000}\right)$	Q_{Tr} = transmission heat load($\frac{kWh}{day}$) U = overall heat transfer coefficient($\frac{W}{m^2.k}$) A = surface area in m^2 T_o = outside ambient air temperature T_i = inside room temperature
Product load	$Q_P = Q_F + Q_R$ $Q_F = m * c_p * (T_f - T_i) * \frac{1}{3600}$ $Q_R = m * H_R * \frac{1}{3600}$	Q = Load in kWh / day c_p = specific heat capacity ($\frac{kJ}{kg.^\circ C}$) m = mass of new product each day for Q_F (kg) = Total mass of product in storage for Q_R T_f = Field temperature of produce ($^\circ$C) H_R = Heat of respiration (kJ / kg)
Internal load	$Q_{Pe} = No.Person * t_P * H_p / 1000$ $Q_L = No.Lamps * t_L * W_L / 1000$ $H_P = 272 - 6T_i$	Q_{Pe} and Q_L = people and lamp load($\frac{kWh}{day}$) t_P = length of time they spend inside(h) t_L = length of time thy used per day(h) H_P = heat loss per person per hour (W) W_L = power rating of lamps(W)
Infiltration load	$Q_I = \Delta v * V * E_A * (T_o - T_i) * \frac{1}{3600}$	Q_I = inf iltration load(kWh / day Δv = number of volume change per day V = volume of the storage E_A = Energy of air per cubic meter per $^\circ$C T_O = outside ambient air T_i = inside room temperature

Table C 2: Coefficients of desiccant-coated heat and mass exchanger modeling

$A_1 =$	$\frac{2h_m}{H_a}$, $A_2 = \frac{-(1-\varepsilon_d)\rho_d f_d}{\varepsilon_d \rho_{a,dry}}\left(\frac{\partial W}{\partial t} - D_s\left(\frac{\partial^2 W}{\partial x^2} + \frac{\partial^2 W}{\partial z^2}\right)\right)$
$A_3 =$	$\frac{2h}{H_a \rho_a C_{p,a}} + \frac{2h_m C_{p,v}}{H_a \rho_a}\left(M_{d,s} - M_a\right) + \frac{1}{\beta \eta_{f,app}}\left(\frac{h}{\rho_a C_{p,a}} \frac{\pi r_{1,o}}{A_d}\right)$
$A_4 =$	$\left(\rho c_p\right)_{meq} A_d\left(\frac{H_f}{2} + H_d\right) + \frac{m_t c_{p,t}}{\beta \eta_{f,app}}$, $A_5 = \frac{m_t c_{p,t}}{\beta}\left(1 - \frac{1}{\eta_{f,app}}\right)$
$A_6 =$	$-\left(h_d A_d + \frac{h_d A_{t,a}}{\beta \eta_{f,app}} + \frac{h_w A_w}{\beta \eta_{f,app}}\right)$, $A_7 = \left(h_d A_d + \frac{h_d A_{t,a}}{\beta \eta_{f,app}} - \frac{h_w A_w}{\beta}\left(1 - \frac{1}{\eta_{f,app}}\right)\right)$
$A_8 =$	$q_{ads}(1 - \varepsilon_d)\rho_d f_d W_{eq} \int_{u,c}^{\cdot} \int W_{gen} \delta z \delta x + \frac{h_w A_w T_{w,s-avr}}{\beta}$
$A_9 =$	$\left(\frac{h_w A_{t,i,total}}{\dot{m}_w c_{p,w}}\right)$, $A_a = W_{eq}\frac{H_a}{2}$, $A_d = W_{eq}\delta x,\ A_x = W_{eq}\delta z$, $A_z = W_{eq}\delta x$
$A_{t,a} =$	$\pi r_{1,o}\frac{H_a}{2}$, $A_w = \pi r_{1,i}\left(\frac{H_f}{2} + \frac{H_a}{2} + H_d\right)$, $A_{t,i,tota.} = 2\pi r_{1,i} L_z N_t$
$W_{eq} =$	$\frac{X_l X_t - \pi r_{1,o}^2}{2X_l}$, $\Delta V = W_{eq}\delta x\left(\frac{H_f}{2} + H_d\right)$, $m_t = \rho_t\left(\frac{H_f}{2} + \frac{H_a}{2} + H_d\right)\frac{\pi}{2}\left(r_{1,o}^2 - r_{1,i}^2\right)$
$\rho_a =$	$\rho_{a,dry} + (1 + M_a)$, $c_{p,a} = c_{p,a,dry} + M_a c_{p,v}$
q_{ads} =	$q_{eva}(1 + 0.2843e^{-10.28W})$, $M_d = \frac{0.62188\phi_d}{\frac{P_{atm}}{P_{vs}} - \phi_d}$
$W =$	$1.2402\phi_d^4 - 2.4489\phi_d^3 + 1.0499\phi_d^2 + 0.5404\phi_d + 0.0082$
$P_{vs} =$	$exp\left(23.196 - \frac{3816.44}{T_d + 227.2}\right)$, $m = \sqrt{\frac{2h_a}{k_f H_f}}$, $h_m = \frac{h_a D_a}{k_a}$
$D_{d,a}$ =	$\left(\frac{1}{D_M} + \frac{1}{D_k}\right)^{-1}$, $D_M = \frac{0.00018}{P}(T + 273.15)^{1.685}$, $D_k = 22.86 v_r \sqrt{(T + 273.15)}$
$D_s =$	$1.6 \times 10^{-6} \exp\left(-0.974 \times 10^{-3}\frac{q_{ads}}{(T + 273.15)}\right)$

ANNEX D: Drawing of storage room modeling

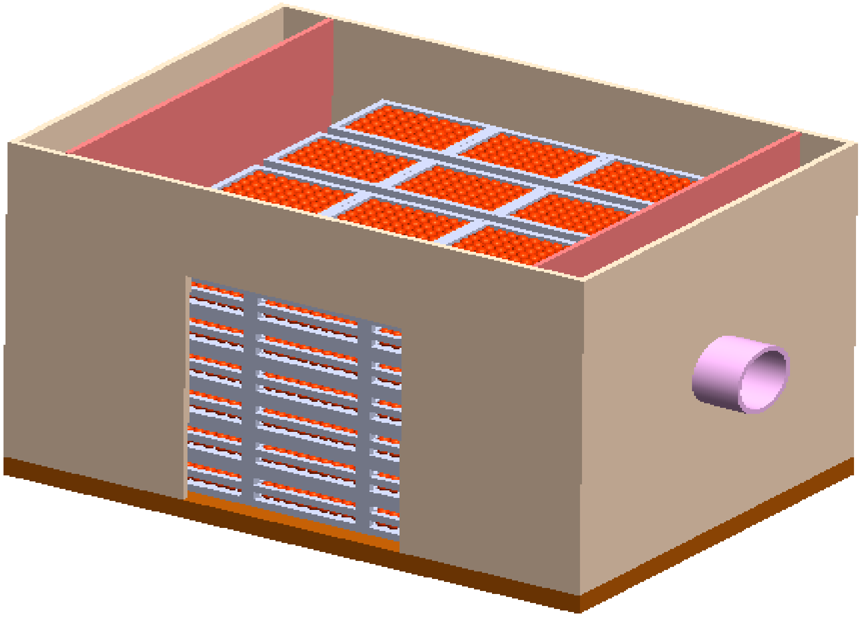

Figure D 1: 3D model of storage room

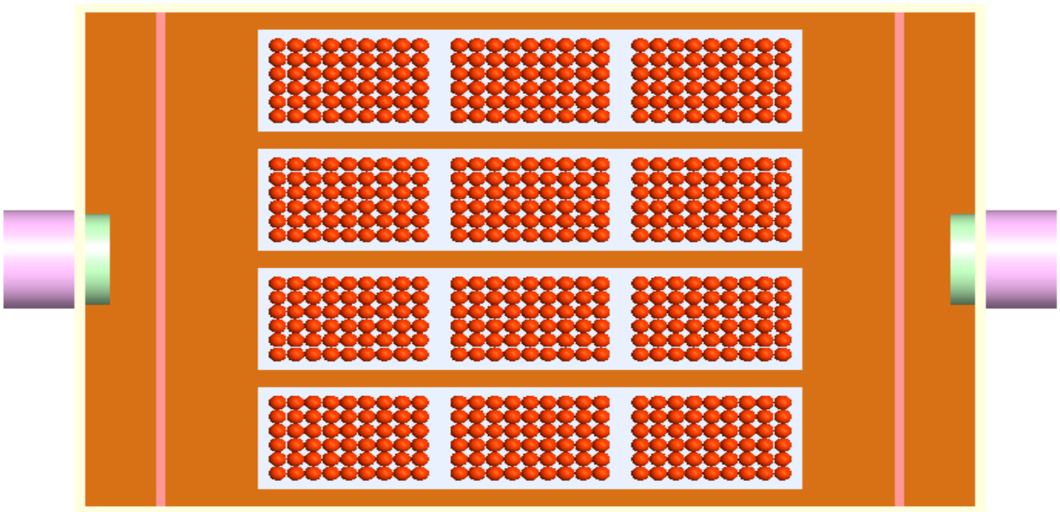

Figure D 2: Top view of 3D modeling

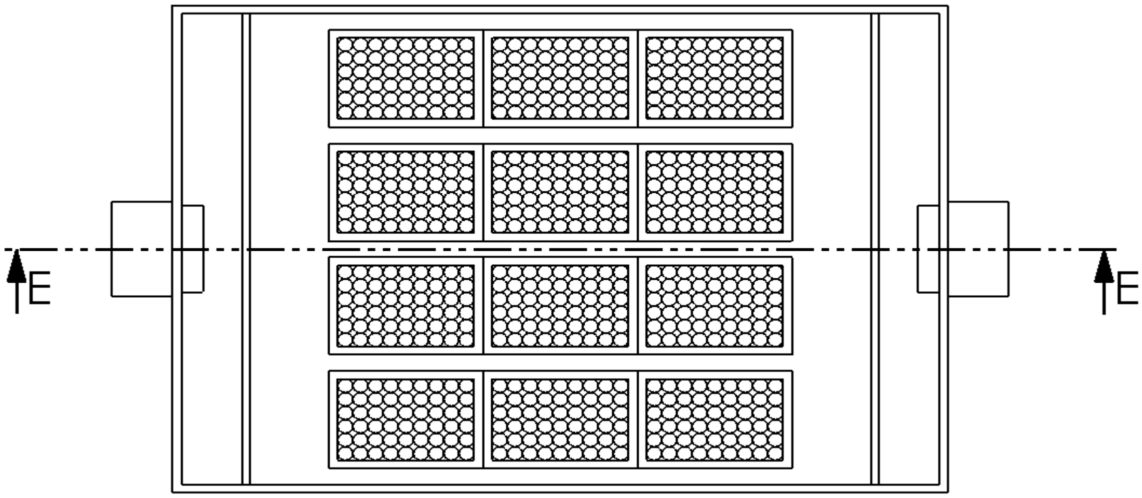

Figure D 3: Sectioning of 3D model along front plane

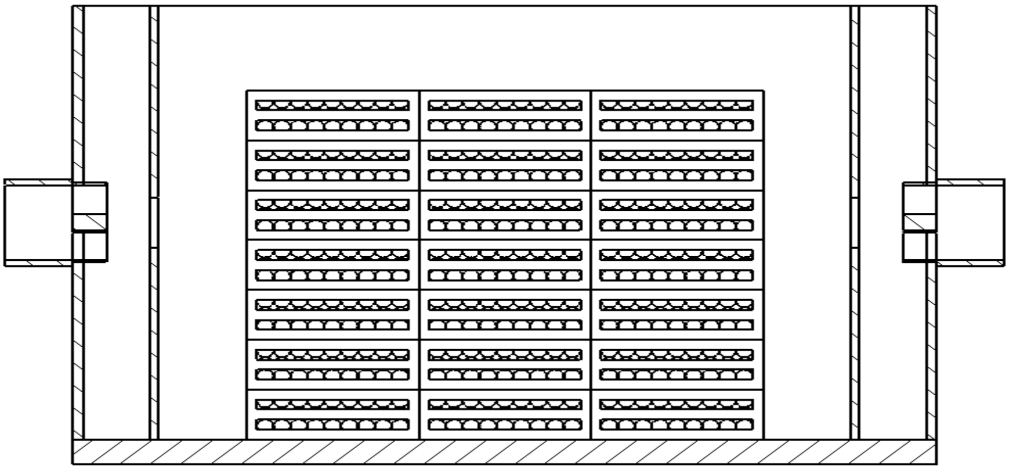

Figure D 4: Front section view of Storage room

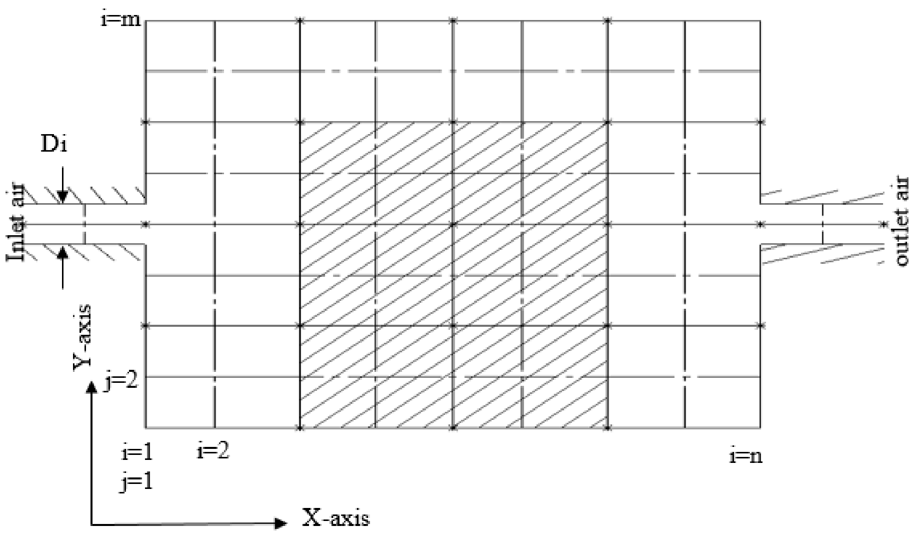

Figure D 5: Computational model of storage room (hatched area represents areas the produce concentrated and internal heat generation considered)

ANNEX E: MATLAB Code

..

Solar radiation Matlab programming

```
%% Constants and initial values
latitude=8.16; Isc=1367; n=17; declination=-20.9; ns=9.39; Tmax=25.5; Tmin=10.5; time_step=180;
stefbolt=5.67E-8; emmisivity_ab=0.1; emmisivity_g=0.85; velocity_w=2;
slope=30; Tconductivity_glycol_liq=1.2; density_glycol_w=988;
gravity=9.81; latent_heat=239E+4; vis=5.58E-3; length_con=0.1;
Dman_i=0.039; density_liq=937.207; density_vap=1.367; Dev=0.0068; Dcon=0.023;
density_g=2600; volume_g=0.00027; specificheat_g=835; Dg=0.058; Dab=0.0466;
A_g=pi*Dg*1.8; transimitivity_g=0.96;
density_ab=2600; volume_ab=0.000221; specificheat_ab=835; A_ab=pi*Dab*1.8; transimitivity_ab=0.96;
absorbance_ab=0.92;
density_ev=8933; volume_ev=0.0000352; specificheat_ev=383; A_ev=pi*Dev*1.6;
density_con=8933; volume_con=0.00000441; specificheat_con=383; A_con=pi*Dcon*0.1;
change_x=0.25; mass_flowrate_w=0.185; specificheat_w=4179;
%% Solar raddiation calculation
Ns=(2/15)*(acosd((0-tand(latitude))*(tand(declination))))
sunset_hour=(acosd((0-tand(latitude))*(tand(declination))))
H_O=(((24*3600*Isc)/pi)*(1+(0.033*cosd(360*n/365)))*((cosd(latitude)*cosd(declination)*sind(sunset_hour))+(((
pi*sunset_hour)/180)*sind(latitude)*sind(declination))))
nr=ns/Ns
a=-0.11+(0.235*cosd(latitude))+(0.323*nr)
b=1.449-(0.533*cosd(latitude))-(0.694*nr)
a1=0.409+(0.502*sind(sunset_hour-60))
b1=0.661-(0.447*sind(sunset_hour-60))
H=H_O*(a+(b*nr))
H_d=H*(0.931-(nr*0.814))

t_step=3600/time_step;
time=0:1/t_step:23;
DH=length(time);
density_g*volume_g*specificheat_g;

hour_angle=15*(time-12);
IG=max(0,((H*(pi/24))*(a1+(b1*cosd(hour_angle))).*(cosd(hour_angle)-
cosd(sunset_hour)))./((sind(sunset_hour))-((pi*sunset_hour/180)*(cosd(sunset_hour)))))%IG=Hourly global
radiation
ID=max(0,((H_d*pi)/(24))*(cosd(hour_angle)-cosd(sunset_hour))./(sind(sunset_hour)-
((pi*sunset_hour/180)*cosd(sunset_hour))));
IB=IG-ID;
plot(time,IG,time,ID,time,IB)
grid on
%% Hourly Ambient Temperature calculation
Tamb=((Tmax+Tmin)/2)+((((Tmax-Tmin)/2)*(cos((2*pi*(time-(15)))./24))));
plot(time,Tamb)
```

Storage room

```
%% Initialization
width=6; %width of the produce storage room
height=6; %height of the produce storage room
nx=5;     %nx is the total grid point along the width of the room
ny=5;     %ny is the total grid point along the height of the room
my=((2*ny+2)/2);
mx=((2*nx+2)/2);
DX=width/(nx-1);
DY=height/(ny-1);
rho=1.225
cv=1.005;
changet=360;
 Ax=DY*ones(2*ny+1,2*nx+1);
Ax([1 2*ny+1],[1:2*nx+1])=DX/2;
Ax(my,1:2)=DX/4;
Ax(my,2*nx:2*nx+1)=DX/4;
Ax
 Ay=DX*ones(2*ny+1,2*nx+1);
Ay([1:2*ny+1],[1 2*nx+1])=DY/2;
Ay
 changex=Ay;
changey=Ax;
 Ps=100000*ones(2*ny+1,2*nx+1);
Ps([1:2*ny+1],[1:2 2*nx:2*nx+1])=0;
Ps([1:2 2*ny:2*ny+1],[1:2*nx+1])=0;
Ps(my,1:2)=200000;
Ps
Pp=zeros(2*ny+1,2*nx+1);
P=Ps
Us=1+(1.5-1).*ones(2*ny+1,2*nx+1);
Us([1:2*ny+1],[1:2 2*nx:2*nx+1])=0;
Us([1:2 2*ny:2*ny+1],[1:2*nx+1])=0;
Us(my,2*nx:2*nx+1)=2;
Us(my,1:2)=2;
Us Up=zeros(2*ny+1,2*nx+1);
U=Us;
 Vs=ones(2*ny+1,2*nx+1);
Vs([1:2*ny+1],[1:2 2*nx:2*nx+1])=0;
Vs([1:2 2*ny:2*ny+1],[1:2*nx+1])=0;
Vs
Vp=zeros(2*ny+1,2*nx+1);
V=Vs;
 Dx=zeros(2*ny+1,2*nx+1);
Dx(3:2*ny-1,3:2*nx-1)=((Ax(3:2*ny-1,3:2*nx-1))./(rho*((Us(3:2*ny-1,3:2*nx-1)).*(Ax(3:2*ny-1,1:2*nx-3)))));
Dy=zeros(2*ny+1,2*nx+1);
Dy(3:2*ny-1,3:2*nx-1)=((Ay(3:2*ny-1,3:2*nx-1))./(rho*((Vs(3:2*ny-1,3:2*nx-1)).*(Ay(1:2*ny-3,3:2*nx-1)))));
 afw=zeros(2*ny+1,2*nx+1);
afw(3:2*ny-1,1:2*nx-3)=rho*(Us(3:2*ny-1,1:2*nx-3).*Ax(3:2*ny-1,1:2*nx-3));
afw
afe=zeros(2*ny+1,2*nx+1);
afe(3:2*ny-1,5:2*nx+1)=rho*(Us(3:2*ny-1,5:2*nx+1).*Ax(3:2*ny-1,5:2*nx+1));
afe
afs=zeros(2*ny+1,2*nx+1);
afs(1:2*ny-3,3:2*nx-1)=rho*(Vs(1:2*ny-3,3:2*nx-1).*Ay(1:2*ny-3,3:2*nx-1));
afs
afn=zeros(2*ny+1,2*nx+1);
```

```
afn(5:2*ny+1,3:2*nx-1)=rho*(Vs(5:2*ny+1,3:2*nx-1).*Ay(5:2*ny+1,3:2*nx-1));
afn agw=zeros(2*ny+1,2*nx+1);
agw(3:2*ny-1,3:2*nx-3)=rho*(Dx(3:2*ny-1,3:2*nx-3).*Ax(3:2*ny-1,4:2*nx-2));
agw
age=zeros(2*ny+1,2*nx+1);
age(3:2*ny-1,5:2*nx-1)=rho*(Dx(3:2*ny-1,5:2*nx-1).*Ax(3:2*ny-1,4:2*nx-2));
age
ags=zeros(2*ny+1,2*nx+1);
ags(3:2*ny-3,3:2*nx-1)=rho*(Dx(3:2*ny-3,3:2*nx-1).*Ay(4:2*ny-2,3:2*nx-1));
ags
agn=zeros(2*ny+1,2*nx+1);
agn(5:2*ny-1,3:2*nx-1)=rho*(Dx(5:2*ny-1,3:2*nx-1).*Ay(4:2*ny-2,3:2*nx-1));
agn,Fgw=zeros(2*ny+1,2*nx+1);
Fgw(3:2*ny-1,3:2*nx-3)=rho*(Us(3:2*ny-1,3:2*nx-3).*Ax(3:2*ny-1,4:2*nx-2));
Fgw
Fge=zeros(2*ny+1,2*nx+1);
Fge(3:2*ny-1,5:2*nx-1)=rho*((Us(3:2*ny-1,5:2*nx-1)).*(Ax(3:2*ny-1,4:2*nx-2)));
Fge
Fgs=zeros(2*ny+1,2*nx+1);
Fgs(3:2*ny-3,3:2*nx-1)=rho*(Vs(3:2*ny-3,3:2*nx-1).*Ay(4:2*ny-2,3:2*nx-1));
Fgs
Fgn=zeros(2*ny+1,2*nx+1);
Fgn(5:2*ny-1,3:2*nx-1)=rho*(Vs(5:2*ny-1,3:2*nx-1).*Ay(4:2*ny-2,3:2*nx-1));
Fgn
for k=1:2000
  for l=1:2000
for j=3:2*nx-1
   for i=3:2*ny-1
  Us(i,j)=(afw(i,j-2).*Us(i,j-2)+afe(i,j+2).*Us(i,j+2)+afs(i-2,j).*Us(i-2,j)+afn(i+2,j).*Us(i+2,j)+Ax(i,j).*(Ps(i,j-1)-Ps(i,j+1)))./(afw(i,j-2)+afe(i,j+2)+afs(i-2,j)+afn(i+2,j));  % where ae=an=0
   end
end
end
Us;
for l=1:2000
for i=3:(2*ny-1)
   for j=3:(2*nx-1)
  Vs(i,j)=(afw(i,j-2).*Vs(i,j-2)+afe(i,j+2).*Vs(i,j+2)+afs(i-2,j).*Vs(i-2,j)+afn(i+2,j).*Vs(i+2,j)+Ay(i,j).*(Ps(i-1,j)-Ps(i+1,j)))./(afw(i,j-2)+afe(i,j+2)+afs(i-2,j)+afn(i+2,j));
   end
end
end
Vs;
 Dx=zeros(2*ny+1,2*nx+1);
Dx(3:2*ny-1,3:2*nx-1)=((Ax(3:2*ny-1,3:2*nx-1))./(rho*((Us(3:2*ny-1,3:2*nx-1)).*(Ax(3:2*ny-1,1:2*nx-3)))));
Dy=zeros(2*ny+1,2*nx+1);
Dy(3:2*ny-1,3:2*nx-1)=((Ay(3:2*ny-1,3:2*nx-1))./(rho*((Vs(3:2*ny-1,3:2*nx-1)).*(Ay(1:2*ny-3,3:2*nx-1)))));
 agw=zeros(2*ny+1,2*nx+1);
agw(3:2*ny-1,3:2*nx-3)=rho*(Dx(3:2*ny-1,3:2*nx-3).*Ax(3:2*ny-1,4:2*nx-2));
agw;
age=zeros(2*ny+1,2*nx+1);
age(3:2*ny-1,5:2*nx-1)=rho*(Dx(3:2*ny-1,5:2*nx-1).*Ax(3:2*ny-1,4:2*nx-2));
age;
ags=zeros(2*ny+1,2*nx+1);
ags(3:2*ny-3,3:2*nx-1)=rho*(Dx(3:2*ny-3,3:2*nx-1).*Ay(4:2*ny-2,3:2*nx-1));
ags;
agn=zeros(2*ny+1,2*nx+1)
```

```
agn(5:2*ny-1,3:2*nx-1)=rho*(Dx(5:2*ny-1,3:2*nx-1).*Ay(4:2*ny-2,3:2*nx-1));
agn;
 Fgw=zeros(2*ny+1,2*nx+1);
Fgw(3:2*ny-1,3:2*nx-3)=rho*(Us(3:2*ny-1,3:2*nx-3).*Ax(3:2*ny-1,4:2*nx-2));
Fgw;
Fge=zeros(2*ny+1,2*nx+1);
Fge(3:2*ny-1,5:2*nx-1)=rho*((Us(3:2*ny-1,5:2*nx-1)).*(Ax(3:2*ny-1,4:2*nx-2)));
Fge;
Fgs=zeros(2*ny+1,2*nx+1);
Fgs(3:2*ny-3,3:2*nx-1)=rho*(Vs(3:2*ny-3,3:2*nx-1).*Ay(4:2*ny-2,3:2*nx-1));
Fgs;
Fgn=zeros(2*ny+1,2*nx+1);
Fgn(5:2*ny-1,3:2*nx-1)=rho*(Vs(5:2*ny-1,3:2*nx-1).*Ay(4:2*ny-2,3:2*nx-1));
Fgn;

 for l=1:2000
     Ppri=Pp;
    for j=4:2*nx-2
        for i=4:2*ny-2
        Pp(i,j)=((agw(i,j-1)*Ppri(i,j-2))+(age(i,j+1).*Ppri(i,j+2))+(ags(i-1,j).*Ppri(i-
2,j))+(agn(i+1,j).*Ppri(i+2,j))+(Fgw(i,j-1)-Fge(i,j+1))+(Fgs(i-1,j)-Fgn(i+1,j)))./(agw(i,j-1)+age(i,j+1)+ags(i-
1,j)+agn(i+1,j));
        end
    end
        Pp;
 end
 Pp;
 for j=3:2*nx-1
     for i=3:2*ny-1
         Up(i,j)=Dx(i,j)*(Pp(i,j-1)-Pp(i,j+1));
     end
 end
 Up;
  for j=3:2*nx-1
     for i=3:2*ny-1
         Vp(i,j)=Dy(i,j)*(Pp(i-1,j)-Pp(i+1,j));
     end
 end
 Vp;

 U(i,j)=Us(i,j)+Up(i,j);
 V(i,j)=Vs(i,j)+Vp(i,j);
 P(i,j)=Ps(i,j)+Pp(i,j);
  Us=U;
 Vs=V;
 afw=zeros(2*ny+1,2*nx+1);
afw(3:2*ny-1,1:2*nx-3)=rho*(Us(3:2*ny-1,1:2*nx-3).*Ax(3:2*ny-1,1:2*nx-3));
afw;
afe=zeros(2*ny+1,2*nx+1);
afe(3:2*ny-1,5:2*nx+1)=rho*(Us(3:2*ny-1,5:2*nx+1).*Ax(3:2*ny-1,5:2*nx+1));
afe;
afs=zeros(2*ny+1,2*nx+1);
afs(1:2*ny-3,3:2*nx-1)=rho*(Vs(1:2*ny-3,3:2*nx-1).*Ay(1:2*ny-3,3:2*nx-1));
afs;
afn=zeros(2*ny+1,2*nx+1);
afn(5:2*ny+1,3:2*nx-1)=rho*(Vs(5:2*ny+1,3:2*nx-1).*Ay(5:2*ny+1,3:2*nx-1));
afn
```

```
end
U(2*ny-1,2*nx-1)=U(2*ny-1,2*nx-2);
U
V
P
 afw=zeros(2*ny+1,2*nx+1);
afw(3:2*ny-1,1:2*nx-3)=rho*(Us(3:2*ny-1,1:2*nx-3).*Ax(3:2*ny-1,1:2*nx-3));
afw;
afe=zeros(2*ny+1,2*nx+1);
afe(3:2*ny-1,5:2*nx+1)=rho*(Us(3:2*ny-1,5:2*nx+1).*Ax(3:2*ny-1,5:2*nx+1));
afe;
afs=zeros(2*ny+1,2*nx+1);
afs(1:2*ny-3,3:2*nx-1)=rho*(Vs(1:2*ny-3,3:2*nx-1).*Ay(1:2*ny-3,3:2*nx-1));
afs;
afn=zeros(2*ny+1,2*nx+1);
afn(5:2*ny+1,3:2*nx-1)=rho*(Vs(5:2*ny+1,3:2*nx-1).*Ay(5:2*ny+1,3:2*nx-1));
afn;
i=1:nx

%% Temperature distribution calculation


To=12*ones(2*ny+1,2*nx+1);
To(my,1:3)=8;


Fw=zeros(2*ny+1,2*nx+1);
Fw=cv*afw;
Fe=zeros(2*ny+1,2*nx+1);


Fe=cv*afe;
Fs=zeros(2*ny+1,2*nx+1);


Fs=cv*afs;
Fn=zeros(2*ny+1,2*nx+1);


Fn=cv*afn;


Dw=(k*Ax)./(changex);
De=Dw;


Ds=(k*Ay)./(changey);
Dn=Ds;


PPw=Fw./Dw;
PPe=Fe./De;
PPs=Fs./Ds;
PPn=Fn./Dn;
 atw=((Dw)).*(max(0,((1-0.1*abs(PPw)).^5)))+(max(Fw,0));
ate=((De).*(max(0,((1-0.1*abs(PPe)).^5))))+(max(-Fe,0));
ats=((Ds).*(max(0,((1-0.1*abs(PPs)).^5))))+(max(Fs,0));
atn=((Dn).*(max(0,((1-0.1*abs(PPn)).^5))))+(max(-Fn,0));


Tnot=8*ones(2*ny+1,2*nx+1);
load('gong.mat')
q=Q
```

```
hour=input('insert operation duration in hour')
q(hour)
q=q(hour)

bb=zeros(2*ny+1,2*nx+1);
bb(2:2*ny,[2:4,2*nx-2:2*nx])=q;
bb(2:4,2:2*nx)=bb(2:4,2:2*nx)+q;
bb
Qgeneration=2000;
b=zeros(2*ny+1,2*nx+1);
b(3:2*ny-1,3:2*nx-1)=Qgeneration;

B=((rho*cv/changet).*(changex.*changey)).*Tnot+b+bb;
B
for n=1:36000
    T=To;



    for k=1:20


        for j=4:2*ny-2
           for i=4:2*nx-2
                 T(i,j)=((atw(i-1,j)*T(i-2,j))+(ate(i+1,j).*T(i+2,j))+(ats(i,j-1).*T(i,j-2))+(atn(i,j+1).*T(i,j+2))+B(i,j))./(atw(i-
1,j)+ate(i+1,j)+ats(i,j-1)+atn(i,j+1));
           end
        end
    end

T(2*ny-2,2*nx-2)=T(2*ny-2,2*nx-3);
To=T;
end

T;
i=1:nx;
TT=T([2*i],[2*i])
colormap(jet);
contourf(TT);
c=colorbar;
c = colorbar;
c.Label.String = 'Temperature in (ºC)';
```